Some Geometrical and Topological Aspects of Dimensionality Reduction in Signal Analysis

Dissertation
zur Erlangung des Doktorgrades
der Fakultät Mathematik,
Informatik und Naturwissenschaften
der Universität Hamburg

vorgelegt
im Fachbereich Mathematik
von

Mijail Guillemard

aus Moskau

Hamburg 2012

Als Dissertation angenommen vom Fachbereich Mathematik der
Universität Hamburg

Auf Grund der Gutachten von:

	Prof. Dr. Armin Iske	(Universität Hamburg)
und	Prof. Dr. Gerlind Plonka-Hoch	(Universität Göttingen)

Tag der Dispulation: Hamburg, den 10.11.2011

Prof. Dr. Ingenium Gasser
Leiter des Fachbereiches Mathematik

Contents

1 Introduction and Overview

Signals and measurements are basic tools for studying interactions of complex phenomena, and a basic example is a polyphonic audio signal $f = \sum_\ell f_\ell$ composed of various sounds f_ℓ originated from different simultaneuous events. In realistic scenarios, using f to extract the components f_ℓ can be a challenging task, and a plain usage of modern tools in harmonic analysis as wavelet methods or frame theory can be insufficient. In this project, we consider the problem of studying f using geometrical and topological properties of a set $X_f = \{x_i\}_i$ defined by collecting local information of f as in the context of time-frequency analysis. As depicted in Fig. 1.1 our work is constructed on top of the recent developments in dimensionality reduction and manifold learning, together with new tools from persistent homology. In the last few years, a major activity of these areas has been motivated by modern problems in data analysis. Our long term goal is to use these new developments in applied geometry and topology in combination with modern tools in harmonic analysis.

Background Topics

Following the Fig. 1.1, we now shortly discuss an overview of the main topics presented in our work, together with their interactions. We begin with background topics including time-frequency analysis, dimensionality reduction and manifold learning, as well as basic modern engineering strategies for signal detection. Additionally, we describe the role of persistent homology as a recent development in computational topology. Using these building blocks, we discuss our contributions in the following section, where we present a particular interaction of time-frequency analysis with modern application tools from geometry and topology.

Over the last decades new tools in pure and applied mathematics have emerged for the analysis of complex geometrical and topological structures. In particular, in application and engineering fields, there has been an important emergence of new strategies for the analysis of datasets $X = \{x_i\}_{i=1}^m \subset \mathbb{R}^n$. On the one hand, new algorithms have been proposed for manifold learning and dimensionality reduction by combining concepts of differential geometry with spectral decompositions. On the other hand, from a topological perspective, a dataset X can now be analyzed with novel tools from persistent homology which has emerged as an important subfield of computational topology.

In a different setting, the groundbreaking developments of noncommutative geometry are currently investigating new type of geometric objects that correspond to noncommutative C^*-algebras. These ideas are extensions of original concepts in noncommutative topology, which is on itself a field based on the celebrated Gelfand-Naimark theory. We argue that this modern view of geometry can be a useful source of ideas for application oriented problems in signal processing and data analysis.

Our objective in this project is to study a particular type of interactions of these topics in the setting of time-frequency analysis. Our motivation is based on the construction of datasets $X = \{x_i\}_{i=1}^m$ arising from a time-frequency representation of a signal f. In particular, the question arises on how to construct new invariants inspired from geometrical and topological properties for designing more accurate methods for signal analysis.

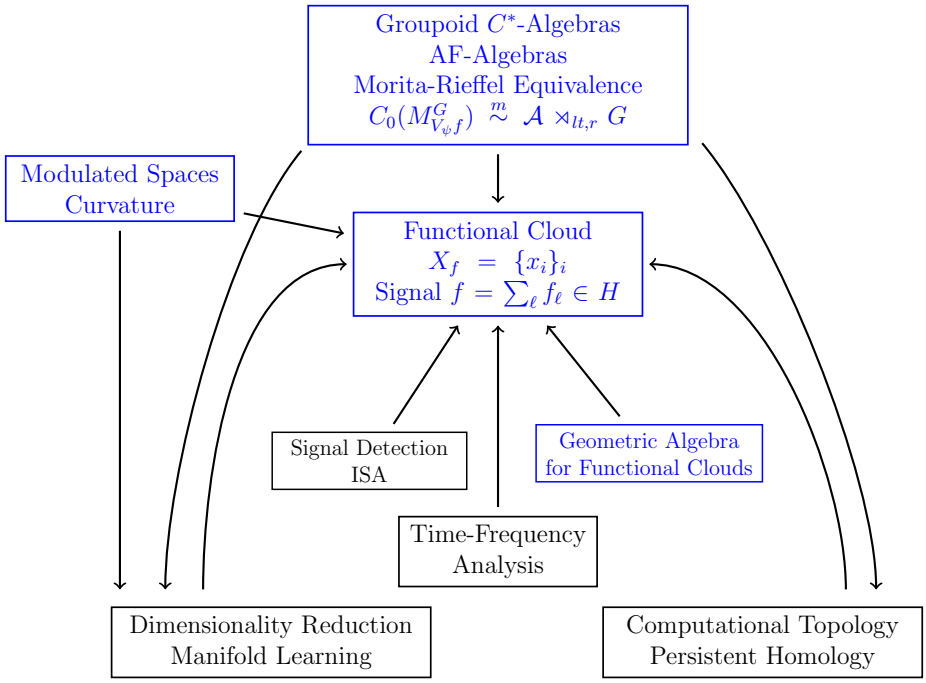

Figure 1.1: Main topics and their interactions

In **dimensionality reduction and manifold learning**, the objective is to study a *point cloud data* (or *dataset*), defined as a finite family of vectors $X = \{x_i\}_{i=1}^m \subset \mathbb{R}^n$ in a n-dimensional Euclidean space. The basic assumption is that X is sampled from $\mathcal{M}$, a (low dimensional) *space*, considered as a submanifold of $\mathbb{R}^n$ or, more generally, we can see $\mathcal{M}$ as the geometrical realization of a topological space (simplicial complex, CW-complex, etc) in $\mathbb{R}^n$. We have therefore, $X \subset \mathcal{M} \subset \mathbb{R}^n$ with $p := \dim(\mathcal{M}) < n$. An additional key concept is the consideration of a simplified model of $\mathcal{M}$, denoted by Ω, embedded in a low dimensional space $\mathbb{R}^d$ (with $d < n$), together with a homeomorphism (or ideally an isometry) $\mathcal{A} : \Omega \to \mathcal{M} \subset \mathbb{R}^n$, $\Omega \subset \mathbb{R}^d$. The space Ω is then a homeomorphic version of $\mathcal{M}$ that could be used for efficient analysis purposes in a low-dimensional environment. For instance, in the case of $\mathcal{M}$ being the well-know Swiss roll dataset, the space Ω is a rectangle. However, in practice we can only try to approximate Ω with a dimensionality reduction map $P : \mathcal{M} \to \Omega' \subset \mathbb{R}^d$, where Ω' is a homeomorphic copy of Ω. Standard methods for dimensionality reduction are Principal Component Analysis (PCA) or Multidimensional Scaling (MDS), but modern nonlinear strategies are important research topics (e.g. Isomap, Local Tangent Space Alignment (LTSA), Laplacian Eigenmaps, etc [4, 9, 58, 81, 87]). We also remark that recent related developments in learning and sampling theory have been achieved as in the work of Niyogi, Smale and Weinberger [75], which provides some conditions under which a dataset $X = \{x_i\}_{i=1}^m$ can be used to recover the topology of $\mathcal{M}$.

Persistent Homology is an a recent development in **computational topology**, and it provides an important strategy for computing topological features of a dataset $X = \{x_i\}_{i=1}^m$. In the context of topological analysis, homology theories are basic tools,

and these can be described as functors from an adequate category of spaces (e.g. topological spaces, CW complexes, smooth manifolds, etc) to a given category of algebraic structures (e.g. abelian groups). Among these theories, one of the simplest is *simplicial homology*, where the concept of *abstract simplicial complex* is the basic object to study. A major problem when considering this strategy for the analysis of a dataset $X = \{x_i\}_{i=1}^m \subset \mathbb{R}^n$, is the fact that there is no simplicial complex structure at hand. Persistent homology [14,27,95] delivers a useful strategy for this problem by efficiently constructing a multiscale topological overview of a point cloud data. The fundamental idea is to construct a family of simplicial complexes by considering the spaces $\mathbb{X}_\epsilon = \cup_{i=1}^m B(x_i, \epsilon)$, where a ball $B(x_i, \epsilon)$ of radius $\epsilon > 0$ is centered around each point of the dataset X. Various well-known structures (e.g. Vietoris Rips complexes) are available for studying homological information of $\mathbb{X}_\epsilon$. There are two crucial remarks for implementing these ideas in an efficient computational framework. First, even though we consider a continuous parameter $\epsilon > 0$, it can be verified that for a given finite dataset X, there are only a finite number of non-homeomorphic simplicial complexes $K_1 \subset K_2 \subset \cdots \subset K_r$ characterizing the set $\{\mathbb{X}_\epsilon, \epsilon > 0\}$. Another fundamental property is an efficient computational procedure (based on variants of the Smith normal form of boundary matrices [27]) for fast calculations of homological information of the family $K_1 \subset K_2 \subset \cdots \subset K_r$ (see [14] for details). These ideas are the result of the work of different research communities in the last two decades (see [14,27]), illustrating an important development combining concepts from pure mathematics with concrete applications problems.

In **Time-frequency analysis** a signal f is analyzed by considering its local bahaviour using a partitioning in segments $x_b = fg_b$, for g a window function, and $g_b(t) = g(t-b)$. In more abstract settings, we can describe this procedure using a locally compact group $\mathcal{G}$ acting in a Hilbert space $\mathcal{H}$. We assume this action to be an irreducible, square integrable group representation, $\pi : G \to \mathcal{U}(\mathcal{H})$, defined as a homomorphism between G and $\mathcal{U}(\mathcal{H})$, the unitary operators in $\mathcal{H}$. With this representation, the *voice transform* is constructed as $V_\psi : \mathcal{H} \to L^2(\mathcal{G})$, with $V_\psi f(x) = \langle f, \pi(x)(\psi)\rangle$ for $f \in \mathcal{H}, x \in G$, and ψ a particular (so called admissible) element of $\mathcal{H}$. Gabor and wavelet transforms are typical examples where ψ corresponds to a Gaussian window function and a wavelet respectively [32–34]. Wavelet analysis, Gabor transforms, frame theory, and a large number of related concepts have been investigated over the last decades, illustrating the importance of the time-frequency philosophy. However, despite the success of these developments, modern engineering problems are demanding more accurate and flexible tools for dealing with the ever increasing complexity of dynamical systems, signals, and datasets arising in many applications.

The basic objective in our program is to study geometrical and topological properties of $X_f = \{x_b\}_b$, in order to analyze the function f. Notice that in the particular case of Gabor analysis, the voice transform is defined as $V_g f(b, w) = \int_{\mathbb{R}} f(t)g(t-b)e^{-2\pi i t w}dt$, and due to the orthogonality property of the Fourier transform, the geometrical and topological characteristics of $X_f = \{x_b\}_b$, are the same as the ones of $X_{V_g f} = \{V_g f(b, .)\}_b$ (i.e. X_f and $X_{V_g f}$ are isometric). But it is important to notice that $X_{V_g f}$ undergoes highly nontrivial geometrical and topological changes when applying time-frequency operations to the function f (e.g. convolution filters). The interplay between the geometric and topological properties of $X_{V_g f}$ and the time-frequency characteristics of f is a main topic in our research.

Signal detection and separation are major areas of signal processing, and recent strategies have appeared in the engineering literature combining dimensionality reduction and time-frequency analysis. For instance, a basic method for extracting the components f_ℓ from a polyphonic single-channel signal $f = \sum_\ell f_\ell$ is the so called *independent subspace analysis* (ISA). Here, the strategy is to apply a dimensionality reduction map to the time-frequency data of f and, subsequently, use *independent component analysis* (ICA) for recovering features of the vectors f_ℓ. These engineering algorithms are concerned with the usability and quality of the separation process, and the mathematical understanding of the resulting tools is not a major concern. A noticeable feature of these engineering strategies is to combine mathematical concepts in original ways for resolving practical problems. We remark that this interaction between engineering solutions and mathematical concepts is a mutually beneficial process, as the resulting algorithms reveal new challenging phenomena from a conceptual (purely mathematical) point of view. One objective in this project is to use these engineering ideas as a motivation to explore new ways of extending tools from time-frequency analysis. The results obtained with the basic strategy in ISA, constructed on top of dimensionality reduction methods, is a motivation towards more geometrically based separation methods. In our notation, ISA can be described as the manipulation of $X_{V_g f}$ using dimensionality reduction maps and ICA in order to extract the components f_ℓ. In our project, we take further steps from a conceptual point of view by studying the interaction of geometrical properties of $X_{V_g f}$ with the different components f_ℓ.

Contributions

The concept of a **functional cloud** of a signal f (or a **cloud** of f for short) considers the segmentation of f in small fragments or chunks x_i assembled in a set $X_f = \{x_i\}$ whose geometrical and topological properties can be used for studying f. As explained in the previous remarks, the construction of X_f is motivated from time-frequency analysis where we fragment a signal f in pieces $x_b = fg_b$, using a window function g, and $g_b(t) = g(t-b)$. A more general construction defines $X_{V_g f}$ using the graph of the voice transform $V_\psi : \mathcal{H} \to L^2(\mathcal{G})$, $V_\psi f(x) = \langle f, \pi(x)(\psi)\rangle$. Remember that for the particular case of Gabor analysis we consider $X_{V_g f} = \{V_g f(b, .)\}_b$ for $V_g f(b, w) = \int_{\mathbb{R}} f(t)g(t-b)e^{-2\pi i t w}dt$ and for concrete engineering applications we obtain a finite point cloud data $X_{V_g f} = \{x_i\}_{i=1}^k$. A basic goal of the concept of functional cloud is to describe mechanisms for decomposing the signal $f = \sum_\ell f_\ell$ using geometrical and topological properties of X_f.

Our results present three types of contributions whose objectives are to manipulate, decompose, and analyze X_f in order to understand f. First, we introduce the concept of a modulated space which is closely related to the idea of a functional cloud, but it explicitly uses a homeomorphism between a space of parameters Ω, and a space of signals $\mathcal{M}$. Here, the basic result is an empirical observation relating the effectiveness of a dimensionality reduction map applied to a space $\mathcal{M}$ with the spectral properties of the elements of $\mathcal{M}$. Secondly, we present a procedure for manipulating a point cloud data using geometric algebra, as defined in the setting of Clifford algebras. A simple application of this procedure is to help identify or classify signals using a high dimensional Möbius transformation by geometrically compressing regions in the space of signals. Finally, we present an analysis framework based on noncommutative C^*-algebras for studying the interaction of the components f_ℓ for $f = \sum_\ell f_\ell$ using the properties of $X_{V_g f}$.

The concept of a **modulated space** $\mathcal{M}$ is closely related to the idea of a functional cloud, but in a modulated space we construct a family $\mathcal{M}$ of signals by explicitly considering a homeomorphism $\mathcal{A} : \Omega \to \mathcal{M}$ between a set of parameters Ω and a space of signals $\mathcal{M} \subset \mathcal{H}$, where $\mathcal{H}$ is an Euclidean space. We think of Ω as a topological space (a simplicial complex or CW-complex), and we assume that it has a low dimension in comparison with the dimension of the Euclidean space $\mathcal{H}$. For constructing $\mathcal{A}$, we use $\{\phi_k\}_{k=1}^d \subset \mathcal{H}$ as a set of dictionary vectors, and $\{s_k : \Omega \to \mathcal{C}_{\mathcal{H}}(\mathcal{H})\}_{k=1}^d$ a family of continuous maps from Ω to the space $\mathcal{C}_{\mathcal{H}}(\mathcal{H})$ of continuous functions from $\mathcal{H}$ to $\mathcal{H}$. We require the homeomorphism $\mathcal{A}$ (we call it a *modulation map*) to be of the form $\mathcal{A}(\alpha) = \sum_{k=1}^d s_k(\alpha)\phi_k$, for $\alpha \in \Omega$. A functional cloud is an important particular case of this situation, but in a modulated space $\mathcal{M}$ the emphasis is placed on the low dimensional parametrization space Ω for encoding a signal, while the concept of a functional cloud stresses the segmentation of a signal f in a set X_f of small chunks useful in the analysis of f. The crucial motivation for the concept of a modulated space is to underline a decomposition of a signal using a low-dimensional structure Ω instead of a traditional frame or basis decomposition. The usefulness of the concept of a modulated space is that it integrates basic features of dimensionality reduction with standard function decomposition and spectral analysis. The fundamental contribution is an empirical observation specifying how distortions in the geometry and curvature of $\mathcal{M}$, and of the dimensionality reduction space $\Omega' = P(\mathcal{M})$, are related to the spectral decomposition of the elements of $\mathcal{M}$. We are not providing in this work a rigorous explanation of these empirical observations, instead, we focus our work in developing new conceptual tools that might eventually help for understanding these numerical phenomena.

The usage of **geometrical algebra** for manipulating **functional clouds** is another component of our work. Geometrical algebra is a research area constructed on top of Clifford algebras for describing geometric manipulations used in some subfields of physics and computer science. In our setting, we are given a point cloud data $X = \cup X_\ell \subset \mathbb{R}^n$ composed of clusters X_ℓ, and our objective is to geometrically manipulate X in such a way that a particular cluster X_ℓ can be contracted to a smaller region in $\mathbb{R}^n$. These geometrical manipulations are implemented with Möbius transformations which provide invertible nonlinear maps with useful geometrical properties. Here, a basic problem is to generalize Möbius transformations, as defined in the field of complex numbers $\mathbb{C}$, to higher dimensional environments. This task can be achieved using Clifford algebras, which provide a convenient way to generalize properties of the complex numbers to higher dimensional spaces. A basic application of these ideas is to support signal classification procedures, where the problem is to decide whether a given point belongs to a cluster X_ℓ of a point cloud data $X_f = \cup_\ell X_\ell \subset \mathbb{R}^n$. The concept is to design a Möbis transformation, with an attractive fixed point $u \in \mathbb{R}^n$, that can be used to geometrically compress or attract a cluster X_{f_ℓ} to a smaller region centered in $u \in \mathbb{R}^n$. When the cluster X_ℓ has complex geometrical properties, our procedure can be used to transform X_ℓ to a smaller object and simpler classification algorithms can be considered.

The vast contributions of **noncommutative geometry** have provided over the last decades powerful concepts for studying difficult geometrical and topological spaces X using algebraic structures based on C^*-algebras. These ideas are an extension of the foundational Gelfand-Naimark theorems, and they have delivered useful tools in many areas of mathematics. A fundamental component in this framework is the concept of

noncommutative quotients, which is based on noncommutative C^*-algebras for studying "bad" quotients spaces, defined as structures $X = Y/\sim$, for an equivalence relation $\sim$ in Y, and where X looses important properties of the space Y (manifold structure, Hausdorff property, etc). In the general framework of noncommutative geometry, this example using an equivalence relation $\sim$ is extended by considering groupoid theory, which is a far reaching and powerful generalization which includes the notions of equivalence relations, groups, group actions, etc. In our work, we use basic ideas of this framework in order to analyze functional clouds X_f related to a signal f.

The strategy is to consider a functional cloud $X_f = \{x_i\}_{i=1}^k$ (that we also denote by $M_f = \{x_i\}_i$ for non necessarily discrete cases) as a quotient space in the setting of time-frequency analysis. We define the quotient space $M_{V_\psi f}^G = F_{V_\psi f}/G$ for $F_{V_\psi f}$ the graph of $V_\psi f|_{\text{supp}V_\psi f}$, a time-frequency transform of f (wavelet, Gabor, etc), and G a groupoid. When considering a functional cloud $M_{V_\psi f}^G$ as a quotient space, we can study its structure in the framework of noncommutative topology. A main result of our work is to illustrate how noncommutative C^*-algebras, and the concept of Morita equivalence, can be applied as a new type of analysis layer in signal processing. The basic idea can be summarized as (Theorem 5.1.6):

$$\text{for a signal} \quad f = \textstyle\sum_{i=1}^k f_i \quad \text{we have} \quad C_0(M_{V_\psi f}^G) \overset{\text{m}}{\sim} \mathcal{A} \rtimes_{lt,r} G,$$

with $\mathcal{A} = \left\{[h_{ij}] \in M_k(C_0(F_{V_\psi f})), h_{ij} \in C_0(F_{V_\psi f_i} \cap F_{V_\psi f_j})\right\}$ a noncommutative C^*-algebra. In this situation, we consider the signal $f \in \mathcal{H}$, as an element of a Hilbert space $\mathcal{H}$, and its time-frequency representation is described abstractly as a voice transform $V_\psi f$. The functional cloud $M_{V_\psi f}^G = F_{V_\psi f}/G$ for $F_{V_\psi f} = \text{graph}(V_\psi f|_{\text{supp}V_\psi f})$, is constructed with a groupoid G acting on $F_{V_\psi f}$, and we are interested in the analysis of the C^*-algebra $C_0(M_{V_\psi f}^G)$, the space of continuous functions vanishing at infinity on $M_{V_\psi f}^G$. As it turns out, $C_0(M_{V_\psi f}^G)$ is Morita equivalent (denoted by $\overset{\text{m}}{\sim}$) to $\mathcal{A} \rtimes_{lt,r} G$. The C^*-algebra $\mathcal{A} \rtimes_{lt,r} G$ is a crossed product encoding the groupoid C^*-dynamical system represented by the action of the groupoid G on $C_0(F_{V_\psi f})$. A great advantage of the noncommutative C^*-algebra $\mathcal{A} \rtimes_{lt,r} G$, is that it expose and reveals information on the time-frequency dynamics of the mixing process $f = \sum_{i=1}^k f_i$, contrary to the C^*-algebra $C_0(M_{V_\psi f}^G)$ which completely ignores this information. Here, the crucial noncommutativity structure of $\mathcal{A} \rtimes_{lt,r} G$ reveals also how to understand the time-frequency interferences between the different signal components f_i, $i = 1, \ldots, k$. Our results are based on new developments in operator algebras and groupoid theory. In particular, we use a recent generalization by J.H. Brown [10, 11] of the work of P. Green [42] and M. Rieffel [80], together with the Renault's equivalence theorem as explained by P.S. Muhly, J. Renault, and D. Williams in [73, 74]. Also, a description of noncommutative C^*-algebras on open coverings of a manifold, as explained by A. Connes in [21, 22], plays a basic role in our setting.

Another aspect of our work is motivated by the need to implement and apply, in computationally feasible algorithms, the concepts we have just developed for signal analysis via C^*-algebras. Here, our proposal (Section 5.1.4) is to use the framework of persistent homology, designed to analyze topological properties of finite datasets $X = \{x_i\}_{i=1}^k$. For this task, we use AF-algebras as an important family of C^*-algebras, particularly useful for studying finite structures, as required in applications of signal processing and data analysis. The core idea of our proposal is to construct an AF-algebra for each simplicial

complex present in a filtration arising in the persistent homology algorithm. Here, we follow the large body of work prepared, in the setting of noncommutative geometry, on the analysis of AF-algebras, poset structures and Bratteli diagrams, as explained by G. Landi and his collaborators [3, 29, 30, 56]. The basic question is to investigate the feasibility of combining these tools with the framework of persistent homology for the analysis of geometrical and topological features of finite datasets.

To explain more precisely our strategy, we recall that, given a point cloud data $X = \{x_i\}_{i=1}^m$, and its corresponding sequence of Vietoris Rips complexes $K_0 \subset K_1 \subset \cdots \subset K_r$, the success of persistent homology lies in the efficient computation of *stable and unstable* holes of X. This information is encoded in a *persistent diagram*, denoted by $\mathrm{dgm}_n(X)$, that represents, for each n-homology level, the lifespan of each (stable and unstable) n-dimensional hole of X. The first conceptual step in this algorithm is to consider a *persistent complex* $\{(C_*^i, \partial_*^i)\}_{i=0}^r$ where each (C_*^i, ∂_*^i) is a chain complex constructed for each simplicial complex K_i. The information of stable and unstable holes of X is encoded in the *persistent homology classes*, defined as $\mathrm{Im} f_n^{ij}$, for an homomorphism $f_n^{ij} : H_n(K_i) \to H_n(K_{i+j})$ induced by the inclusion $K_i \subset K_{i+j}$. In these constructions, we consider several functors that can be described, in the setting of singular homology, as homology functors $H_n : \mathbf{Top} \to \mathbf{Ab}$ from the category of topological spaces **Top** to the category of abelian groups **Ab**. A crucial property of these functors is to remove information of a topological space $X \in \mathrm{Ob}(\mathbf{Top})$ by constructing an object in **Ab**, an homology group, for capturing special topological properties. This crucial procedure is an important characteristic of homology theory, but other type of functorial mechanisms are also available for encoding topological features of X. For instance, the framework of noncommutative geometry provides functors based on the construction of C^*-algebras that can be used for computing geometrical and topological properties of X.

These considerations leads us to ask about persistent analysis mechanisms using tools from noncommutative geometry. The functorial properties of constructions based on C^*-algebras could be of interest as a additional strategy in the persistent homology toolbox. Recall that, when considering compact topological spaces, the functor C that takes a compact space X to the C^*-algebra of continuous complex-valued functions on X is a contravariant functor that allows to define an equivalence between the category of locally compact Hausdorff spaces and the category of (commutative) C^*-algebras [89]. This provides a powerful machinery translating topological features into algebraic information without loss of information. In order to consider these ideas in the case of finite structures, as required in applications and engineering problems, we need a method for studying simplicial complexes with C^*-algebra constructions. One possible strategy is to use the large body of work, prepared in the setting of noncommutative geometry, for studying the interaction of AF-algebras with poset structures [3, 29, 30]. Our proposal is to investigate the feasibility of combining these tools with the framework of persistent homology for the analysis of geometrical and topological features of finite datasets. We remark that posets are truly noncommutative spaces [56] and, therefore, the framework we propose is an attempt to produce a preliminary step for using noncommutative geometry in data and signal analysis. We finally remark that new results have being recently achieved in the setting of AF-algebras and *spectral triples*, which is a fundamental tool for accessing geometrical data using C^*-algebras (see [21] for the concept of spectral triples, and [17] for its interaction with AF-algebras).

The results of this work have been announced in a series of publications and preprints released during the three year period of this project. The introductory material on persistent homology in Chapter 3 has been presented in [40]. The results discussed in Chapter 4 have been announced in the following references: the material of the Sections 4.2 and 4.3 are described in [43], and the Section 4.4 refers to [45] and [46]. The application of groupoid C^*-algebras we consider in the Chapter 5 has been presented in the preprint [44]. Finally, the Chapter 6 contains material discussed in the references [47] and [48].

Acknowledgments

I own a great debt of gratitude to Prof. Armin Iske for his continuous encouragement, and the financial support under the DFG-SPP 1324 project. I'm particularly greatly indebted for the academic freedom and patience he provided me during these three years. I also thank Prof. Gerlind Plonka-Hoch for accepting to be a referee, her support, and for inviting me to visit her research group.

I thank Prof. Udo Zölzer at the Helmut-Schmidt University for his support in the early stages of my return to the academic world. Prof. Bodo Werner helped me in my initial contacts with the University of Hamburg. I thank Prof. Birgit Richter who informed me on two useful conferences, to Prof. Christoph Schweigert for hints on bibliographic references, and to Dr. Frank Klinker for discussions on algebra. I thank Prof. Joseph Várilly for inspiring lectures in my undergraduate times. Prof. Jesús Gonzáles helped me to improve my understanding of algebraic topology during our joint work for an overview paper. Finally, I would also like to thank Prof. Hans G. Feichtinger for his support in the late phase of this work.

A very special thanks goes to Claudia Albrecht for the memories of many special years.

I dedicate this work to my parents: to my mother Nina Yablonskaya and to the memory of my father Jean Guillemard.

2 Dimensionality Reduction and Time-Frequency Analysis

During the last decade, many concepts in *nonlinear dimensionality reduction* (NDR) have received significant attention due to the increasing complexity of many modern problems in data and signal analysis. For designing some of these tools, special emphasis is placed on geometrical aspects, where concepts from differential geometry and algebraic topology play an important role [12, 14, 61, 62, 94, 96]. The geometry-based approach of NDR can be viewed as a complementary strategy to statistical oriented methods from machine learning and data mining [58]. In this Chapter, we shortly describe the basic setting of dimensionality reduction and manifold learning, and we quickly recall elementary conceptual in time-frequency analysis. We conclude by explaining a setting and motivations, where it is of interest to combine these modern tools of signal and data analysis.

2.1 Manifold Learning and Dimensionality Reduction

In dimensionality reduction [58], we study a *point cloud data* defined as a finite family of vectors

$$X = \{x_i\}_{i=1}^m \subset \mathbb{R}^n$$

embedded in an n-dimensional Euclidean space. The fundamental assumption is that X lies in $\mathcal{M}$, a (low dimensional) *space* (manifold or topological space i.e. CW-complex, simplicial complex) embedded in $\mathbb{R}^n$. We have therefore, $X \subset \mathcal{M} \subset \mathbb{R}^n$ with $p := \dim(\mathcal{M}) < n$. An additional key concept is the consideration of an *ideal model* representing $\mathcal{M}$, and denoted by Ω, embedded in a low dimensional space $\mathbb{R}^d$ (with $d < n$), together with a homeomorphism (diffeomorphism)

$$\mathcal{A} : \Omega \to \mathcal{M} \subset \mathbb{R}^n,\ \Omega \subset \mathbb{R}^d.$$

The space Ω represents an ideal representation of $\mathcal{M}$ that could be used for analysis procedures in a low-dimensional environment. For instance, in the case of $\mathcal{M}$ being the well-know Swiss roll dataset, the space Ω is a rectangle. However, in practice, we can only try to approximate Ω with a dimensionality reduction map

$$P : \mathcal{M} \to \Omega' \subset \mathbb{R}^d,\ \mathcal{M} \subset \mathbb{R}^n,$$

where Ω' is an homeomorphic copy of Ω.

A Schematic Explanation

In Figure 2.2, we present a schematic view of the main task in dimensionality reduction, where the input data is the point cloud data $X = \{x_i\}_{i=1}^m \subset \mathcal{M} \subset \mathbb{R}^n$, with the hypothesis that $\mathcal{M}$ is a manifold or topological space (CW, simplicial complex) such that $\dim(\mathcal{M}) = p < n$. Additionally, we have $\mathbb{R}^d \supset \Omega \xrightarrow{\mathcal{A}} \mathcal{M} \subset \mathbb{R}^n$ an homeomorphism with $d < n$. The fundamental objective is to construct $Y = \{y_i\}_{i=1}^m \subset \Omega' \subset \mathbb{R}^d$, $d < n$ using a dimensionality reduction map P seing as an homeomorphism (diffeomorphism) $\mathbb{R}^n \supset \mathcal{M} \xrightarrow{P} \Omega' \subset \mathbb{R}^d$.

Input: Point Cloud Data $X = \{x_i\}_{i=1}^m \subset \mathcal{M} \subset \mathbb{R}^n$

Hypothesis:

$\mathcal{M}$ manifold, topological space (CW, simplicial complex)

$\dim(\mathcal{M}) = p < n$

$\mathbb{R}^d \supset \Omega \xrightarrow{\mathcal{A}} \mathcal{M} \subset \mathbb{R}^n$ homeomorphism, $d < n$.

Objectives:

Construct $Y = \{y_i\}_{i=1}^m \subset \Omega' \subset \mathbb{R}^d$, $d < n$

$\mathbb{R}^n \supset \mathcal{M} \xrightarrow{P} \Omega' \subset \mathbb{R}^d$ homeomorphism (diffeomorphism)

Figure 2.1: Basic tasks and hypothesis in dimensionality reduction

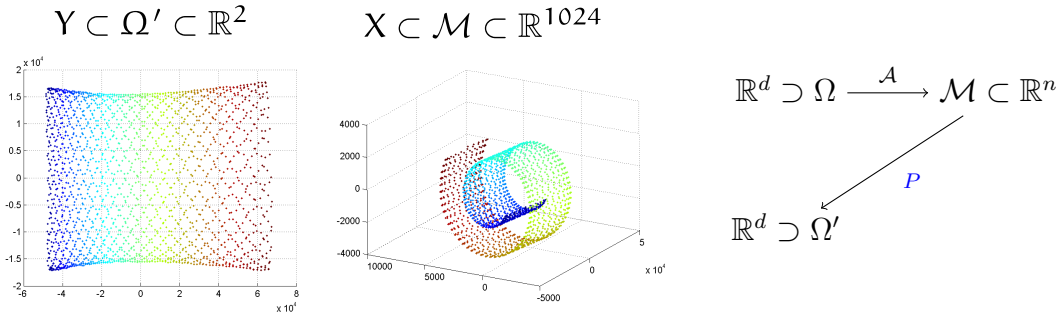

Figure 2.2: Schematic view of the dimensionality reduction task

Manifold Reconstruction from Discrete Data

A crucial requirement in manifold learning is to ensure conditions under which the finite sampling $X = \{x_i\}_{i=1}^m$ is dense enough for recovering geometrical and topological properties of $\mathcal{M}$. In the case of topological conditions, new properties have been investigated over the last years [75]. A main concept is the *condition number* $1/\tau$ of the manifold which encodes local and global curvature properties of $\mathcal{M}$. The condition number can be related to the *medial axis* of $\mathcal{M}$, which is defined as the closure of the set

$$G = \{x \in \mathbb{R}^n : \exists\, p, q \in \mathcal{M}, p \neq q, \text{ with } d(x, \mathcal{M}) = \|x - p\|_{\mathbb{R}^n} = \|x - q\|_{\mathbb{R}^n}\}.$$

By using the medial axis of the manifold, we have

$$\tau = \inf_{p \in \mathcal{M}} d(p, \overline{G}).$$

We also recall that a *deformation retract* between topological spaces U and X, $X \subset U$, is a family of continuous maps $r_t : X \to X, t \in [0, 1]$ with $r_0 = 1_X$, $r_1(X) = U$, and $r_t|_U = 1$ for all t. [49]. Using these concepts, the following result [75] relates the sampling of the manifold with its homological reconstruction.

Proposition 2.1.1 (Niyogi, Smale, Weinberger, 2008)**.** *Let $\mathcal{M}$ be a compact Riemannian submanifold of $\mathbb{R}^n$ and $X = \{x_i\}_{i=1}^m \subset \mathbb{R}^n$ a finite $\epsilon/2$-dense collection in $\mathcal{M}$, i.e., for each $p \in \mathcal{M}$, there is an $x \in X$ satisfying $\|p - x\|_{\mathbb{R}^n} < \epsilon/2$. Then for any $\epsilon < \sqrt{3/5}\tau$, we have that $U = \bigcup_{x \in X} B_\epsilon(x)$ deformation retracts to $\mathcal{M}$, and therefore the homology of U equals the homology of $\mathcal{M}$.*

This proposition describes requirements for the discretization of a manifold when reconstructing the homology as a basic topological invariant. But in order to recover geometrical information, we need to consider differential geometric data. Sampling and discretization aspects in differential geometry are emergent and very active research topics. Basic concepts in this field are the angle defect [7,16] and the usage of the Laplacian operator when computing the mean and Gaussian curvatures [5, 8, 50, 71]. A series of additional important developments for manifold sampling have also been developed over the last years [82,83]. Other important topics are generalizations of the curvature concept in Alexandrov spaces or cell-complexes, as discussed in [38, 76].

2.2 Time-Frequency Analysis

A main drawback of classical harmonic analysis is the difficulty to analyze the time evolution of frequency components in a signal. In the first half of the 20th century, D. Gabor and his collaborators proposed a fundamental strategy for this problem, in what is known today as the Gabor transform. The basic idea consists of partitioning the signal in consecutive segments, and consider a Gauss function as a transformation window. In the second step of this procedure, these segments are analyzed with the Fourier transform, and a time evolution of the frequency components can be obtained. This procedure can be generalized using other types of windows functions, and the resulting mechanism is the well known *Short term Fourier Transform* (STFT). The scheme is a fundamental example of time-frequency analysis, and provides both *analysis* and *synthesis* stages, as a basic philosophy of harmonic analysis.

The STFT is a basic tool for many problems where simultaneous time-frequency information is required. However, this method has several limitations, as the time-frequency tiling design has a fixed resolution, providing an inconvenient scheme for some applications.

Wavelet theory offers an alternative strategy by considering a special type of window, the so called *wavelet functions* that are localized both in the time and the frequency domains. This property allows a more flexibly construction that builds a tiling of time-frequency plane consisting of high resolution for high frequencies and low resolution for low frequencies [19, 51].

Definition 2.2.1 (Wavelet Transform *analysis*)**.** The wavelet transform in $L^2(\mathbb{R})$ is defined as a map $W : L^2(\mathbb{R}) \to L^2(\mathbb{R} \times \mathbb{R}^*)$ with

$$W_\psi f(b,a) := \langle f, \psi_{b,a} \rangle = \int_{\mathbb{R}} f(t)\overline{\psi_{b,a}(t)}\,|a|^{-1/2}\,dt, \quad \psi_{b,a}(t) := \psi\left(\frac{t-b}{a}\right),$$

where we require $\psi \in L^2(\mathbb{R})$ to be an "admissible" function, that is:

$$C_\psi := \int_{\mathbb{R}} \frac{|\hat{\psi}(\omega)|^2}{|\omega|}\,d\omega < \infty.$$

As in the case of the short term Fourier transform, the crucial component that relates the analysis procedure with the synthesis mechanism is an isometry property.

Theorem 2.2.1 (Isometry of the Wavelet transform)**.** *If ψ is a basic wavelet, we have:*

$$\begin{aligned} C_\psi \langle f_2, f_2 \rangle &= \langle W_\psi f_1, W_\psi f_2 \rangle \\ &= \int_{\mathbb{R}^*} \int_{\mathbb{R}} (W_\psi f_1)(b,a) \overline{(W_\psi f_2)(b,a)} \, \frac{da}{a^2} \, db. \qquad \forall f_1, f_2 \in L^2(\mathbb{R}). \end{aligned}$$

We can also derive a reconstruction formula for the wavelet transform, with an alternative construction for a translation mechanism between a function f and its transform $W_\psi f$:

Corollary 2.2.2 (Reconstruction with wavelet transforms *Synthesis*)**.** With the hypothesis of the Theorem 2.2.1, we have for any $t \in \mathbb{R}$ where f is continuous:

$$f(t) = \frac{1}{C_\psi} \int_{\mathbb{R}^*} \int_{\mathbb{R}} W_\psi f(b,a) \psi_{b,a}(t) \, \frac{da}{a^2} \, db.$$

Remark 2.2.1 (Admissibility condition)**.** We notice that the admissibility condition is clearly necessary in the reconstruction formula, and this requirement provides also an intuitive explanation for the term "wavelet" ("small wave"). We remark that $C_\psi < \infty$ implies $\hat{\psi}(0) = 0$, which in turn implies the following property, intuitively related to the idea of a "small wave" localized over time:

$$\int_{\mathbb{R}} \psi(t) \, dt = 0.$$

A conceptual view

The basic mechanism behind many time-frequency transformations such as wavelet or STFT is based on the action of a locally compact group $\mathcal{G}$ in a Hilbert space of functions $\mathcal{H}$. This action is an irreducible and unitary group representation $\pi : \mathcal{G} \to \mathcal{U}(\mathcal{H})$ that fulfills square integrable conditions (here π is a group homomorphism, and $\mathcal{U}(\mathcal{H})$ is the space of unitary operators in the Hilbert space $\mathcal{H}$). With this representation, the voice transform is constructed by setting

$$V_\psi : \mathcal{H} \to L^2(\mathcal{G}), \quad \text{with} \quad V_\psi(f)(x) := \langle f, \pi(x)(\psi) \rangle.$$

These transforms represent an interplay between $\mathcal{H}$ and $L^2(\mathcal{G})$, that allows to analyze the function f, by porting its information to a setting defined by $\mathcal{G}$. One can say that the transformation V_ψ "unfolds" data present in f, using $\mathcal{G}$ as an analysis environment. In the case of the STFT transform, the Weyl-Heisenberg group represents the time-frequency setting to which information from f is translated. In wavelet analysis, the affine group is responsible for providing a time-scale representation of the function. In these situations, a fundamental objective is to understand the components of f, using $\mathcal{G}$ and V_ψ as observation tools.

A crucial property of the voice transform is the orthogonality relation. In this situation, for a square integrable representation π, a unique self-adjoint positive operator C on $\mathcal{H}$, such that for $f_1, f_2 \in \mathcal{H}$ and $\psi_1, \psi_2 \in \operatorname{dom} C$, we have:

$$\int_{\mathcal{G}} \langle f_1, \pi(x)\psi_1 \rangle \, \langle \pi(x)\psi_2, f_2 \rangle d\mu(x) = \langle f_1, f_2 \rangle \, \langle C\psi_1, C\psi_2 \rangle.$$

These relationships imply that the transform V_ψ is an isometry from $\mathcal{H}$ into $L^2(\mathcal{G})$. Another way to express this idea is that the energy of f is conserved by V_ψ. It will then be possible, by restricting to the range of the transform, to build inversion formulas. The second crucial concept of the voice transform is the characterization of its range. Here, we notice that $V_\psi(\mathcal{H}) \subseteq L^2(\mathcal{G})$ is a reproducing kernel Hilbert space, meaning that a reproducing formula is valid:

$$V_\psi(f) = V_\psi(f) * V_\psi(\psi), \ \forall f \in \mathcal{H}.$$

This reproducing formula can be rephrased by saying that a function $F \in L^2(\mathcal{G})$ belongs to $V_\psi(\mathcal{H})$, if and only if $F = F * V_\psi(\psi)$.

2.3 Dimensionality Reduction and Signal Transforms

Our main interest is to understand a particular type of interaction between dimensionality reduction tools and signal transformations. Recall that a basic characteristic of short term Fourier analysis is the high dimensionality of the Euclidean space where the time-frequency data is embedded. In this context, for many applications, a combination with dimensionality reduction methods could be useful for improving the quality of the data analysis. Our motivation examples in time-frequency analysis can be naturally related to the dimensionality reduction framework by considering X_f to be a subset of $\mathcal{M}$, a (low dimensional) space, embedded in the high dimensional Euclidean space $\mathbb{R}^n$. We have therefore, $X_f \subset \mathcal{M} \subset \mathbb{R}^n$ with $p := \dim(\mathcal{M}) < n$. We recall that there is a well-known framework for studying properties of sets X_f in the context of nonlinear time series and dynamical systems (see e.g. [53]). But in our situation, we are additionally considering a close interaction with signal processing transforms T, together with dimensionality reduction techniques P (Principal component analysis, Isomap, LTSA, etc). The construction of time-frequency data can be described as the application of a map $T : \mathcal{M} \supset X_f \to T(X_f) \subset \mathcal{M}_T$, where $\mathcal{M}_T := T(\mathcal{M})$, and $T(x_i)$ is the signal transformation of x_i (Fourier transform, wavelet, etc). The following diagram shows the basic situation:

$$\begin{array}{ccc} \mathbb{R}^d \supset \Omega & \xrightarrow{\mathcal{A}} & \mathcal{M} \supset X_f \subset \mathbb{R}^n \\ & & \Big\downarrow T \\ \mathbb{R}^d \supset \Omega' & \xleftarrow[P]{} & \mathcal{M}_T \supset T(X_f) \subset \mathbb{R}^n \end{array}$$

2.4 Motivations and Objectives

A basic motivation in our environment are time-frequency representations where a signal f is analyzed by considering a partition in chunks $x_b = fg_b$, using $g_b(t) = g(t-b)$ for a window function g, This is typical scenario in the short term Fourier transform (STFT), where a signal $f \in L^2(\mathbb{R})$ is analyzed using

$$V_g f(b,\omega) = \langle f, g_{b,\omega} \rangle = \int f(t)\overline{g_{b,\omega}(t)}\, dt \quad \text{where} \quad g_{b,\omega}(t) = g(t-b)e^{2\pi i \omega t}.$$

In the last decades, this fundamental procedure has been generalized to a large framework including wavelet theory and modern discrete methods of frame decompositions. However, despite the voluminous research activity in this area, many signals in modern applications fields remain difficult to analyze. Just to mention one example, an accurate separation or characterization of polyphonic acoustic signals in speech or music analysis still remains a very challenging task. Part of the problem lies in the fact that it is still difficult to cleanly characterize (e.g. with a few amount of wavelet coefficients) many realistic signals with modern frame decomposition methods. In our setting, we consider each signal (or family of signals) as an entity that can be analyzed with a combination of standard time-frequency transforms with geometrical and topological invariants.

The procedure we follow is to consider the dataset of chunks X_f, constructed with the time-frequency segmentation, as a main object of study. For instance, in the case of finite signals we have a finite set of the form

$$X_f = \{x_i\}_{i=1}^m \qquad \text{for} \qquad x_i = (f(t_{k(i-1)+j}))_{j=0}^{n-1} \in \mathbb{R}^n$$

for $k \in \mathbb{N}$ being a fixed *hop-size*. Here, the regular sampling grid $\{t_\ell\}_{\ell=0}^{km-k+n-1} \subset [0,1]$ is constructed with considering the Nyquist-Shannon theorem for f. Notice that X_f may be embedded in a very high-dimensional ambient space $\mathbb{R}^n$, even though the dimension of X_f itself may be small. For instance, in audio analysis, for 44kHz signals, $n = 1024$ is commonly used, and therefore, in the case of signals whose time-frequency representations are not sparse, the usage of dimensionality reduction methods could be of interest. With this particular scheme, the STFT of f can be interpreted as a transformation of the set X_f by taking the (windowed) Fourier transform of each x_i.

A second family of examples (similar in spirit to time-frequency analysis) arises in image processing. One strategy would be to consider a dataset $X_f = \{x_i\}_{i=1}^m$ constructed from a grayscale image $f : [0,1]^2 \to [0,1]$, along with a finite covering of small squares (each containing n pixels) $\{O_i \subset [0,1]^2\}_{i=1}^m$, centered at pixels positions $\{k_i\}_{i=1}^m \subset [0,1]^2$. As in the previous situation, when considering band-limited images, the domain $[0,1]^2$ can be sampled uniformly and the dataset can then be defined as

$$X_f = \{f(O_i) \in \mathbb{R}^n\}_{i=1}^m,$$

where n is the size of the squares O_i, and m denotes the number of pixels k_i. As before, our aim is to analyze the geometry of the image data X_f to gain useful information about the properties of the image f. For instance, we consider a grayscale image $f : [0,1]^2 \to [0,1]$ using a covering with small squares, or patches, $\{O_i \subset [0,1]^2\}_{i=1}^m$, each containing n pixels. In this toy example we assume that the corresponding point cloud data $X_f = \{f(O_i) \in \mathbb{R}^n\}_{i=1}^m$ lies in some manifold $\mathcal{M} \subset \mathbb{R}^n$. If an image f is composed of an homogeneous texture, the dataset X_f is a cluster whose elements have similar geometrical characteristics. In a simplified scenario, the idea would be to use a representative patch $\phi \in \mathbb{R}^n$ in order to generate all elements of X_f. The main task is to find a family of transformations (the *modulation maps*) $s(\alpha) : \mathbb{R}^n \to \mathbb{R}^n$, parametrized by a low dimensional space Ω, such that for any patch $y \in X_f$, there is some $\alpha \in \Omega$ with $y = s(\alpha)\phi$. We remark that several methods in image processing have recently been proposed with a loosely related philosophy (see e.g. the *patch-based texture analysis* as part of classical *texture synthesis* methods [55]).

3 Basics on Persistent Homology

In this Chapter, we present a short introduction to the basic ideas of persistent homology, which is an important algorithmic and theoretical tool developed over the last decade as a topic of computational topology. First, we present basic concepts on persistent homology as an important new development in computational topology for extracting qualitative information from a point cloud data $X = \{x_i\}$. As we discuss in Chapter 2, our interest lies mostly on datasets arising from time frequency analysis and signal processing problems. With the concepts of functional clouds, piles, and modulation maps we can formalize a framework for this signal processing setting (see Chapter 5). As we will further explain in the next chapters, a strategy we want to analyze for studying these geometrical objects is the setting of C^*-algebras, and noncommutative topology. In order to implement these ideas in a computational framework we need to adapt the tools of persistent homology using the framework of C^*-algebras. We use, in Chapter 5, the theory of posets and AF-algebras for the implementation, in the context of persistent homology, a framework for point cloud data analysis with C^*-algebras.

3.1 Simplicial and persistent homology

We first recall elementary concepts on simplicial homology as a basic homology theory used for constructing algebraic data from topological spaces (see [40] for similar material).

Remark 3.1.1 (Simplicial complexes)**.** A basic component in this context is a (finite) *abstract simplicial complex* which is a nonempty family of subsets K of a vertex set $V = \{v_i\}_{i=1}^m$ such that $V \subseteq K$ (here we simplify the notation and we identify the vertex v with the set $\{v\}$) and if $\alpha \in K, \beta \subseteq \alpha$, then $\beta \in K$. The elements of K are denominated *faces*, and their *dimension* is defined as their cardinality minus one. Faces of dimension zero and one are called vertices and edges, respectively. A *simplicial map* between simplicial complexes is a function respecting their structural content by mapping faces in one structure to faces in the other. These concepts represent combinatorial structures capturing the topological properties of many geometrical constructions. Given an abstract simplicial complex K, an explicit topological space is defined by considering the associated *geometric realization* or *polyhedron*, denoted by $|K|$. These are constructed by thinking of faces as higher dimensional versions of triangles or tetrahedrons in a large dimensional Euclidean spaces and gluing them according to the combinatorial information in K.

Remark 3.1.2 (Homology groups)**.** A basic analysis tool of a simplicial complex K, is the construction of algebraic structures for computing topological invariants, which are properties of $|K|$ that do not change under homeomorphisms and even continuous deformations. From an algorithmic point of view, we compute topological invariants of K by translating its combinatorial structure in the language of linear algebra. For this task, a basic scenario is to consider the following three steps. First, we construct the *groups of k-chains* C_k, defined as the formal linear combinations of k-dimensional faces of K with coefficients in a commutative ring R (with e.g. $R = \mathbb{Z}$, or $R = \mathbb{Z}_p$). We then consider linear maps between the group of k-chains by constructing the *boundary operators* ∂_k, defined as the linear transformation which maps a face $\sigma = [p_0, \cdots p_n] \in C_n$ into C_{n-1} by

$\partial_n \sigma = \sum_{k=0}^{n} (-1)^k [p_0, \cdots, p_{k-1}, p_{k+1}, \cdots p_n]$. As a third step, we construct the *homology groups* defined as the quotient $H_k := \ker(\partial_k)/\mathrm{im}(\partial_{k+1})$. Finally, the concept of *number of k-dimensional holes* are defined using the rank of the homology groups, $\beta_k = \mathrm{rank}(H_k)$ (Betti numbers). For instance, in a sphere we have zero 1-dimensional holes, and one 2-dimensional hole. In the case of a torus, there are two 1-dimensional holes, and one 2-dimensional hole.

3.2 Basics on Persistent Homology

In many application problems a main objective is to analyze experimental datasets $X = \{x_i\}_{i=1}^m \subset \mathbb{R}^n$ and understand their content by computing qualitative information. Topological invariants are important characteristics of geometrical objects, and their properties would be fundamental tools for understanding experimental datasets. The major problem when computing topological invariants of datasets are their finite characteristics and the corresponding inherent instability when computing homological information. Indeed, minor variations (e.g. noise and error in measurements) on how topological structures are constructed from X, could produce major changes on the resulting homological information. Persistent homology [14, 27, 28] is an important computational and theoretical strategy developed over the last decade for computing topological invariants of finite structures. We now describe its motivations, main principles, and theoretical background.

Motivations

A major problem when using tools from simplicial homology for studying a dataset $X = \{x_i\}_{i=1}^m \subset \mathbb{R}^n$ is the fact that we do not have a simplicial complex structure at hand. If we assume that X is sampled from a manifold (e.g. $X \subset \mathcal{M}$, with $\mathcal{M}$ being a submanifold of $\mathbb{R}^n$), a main objective would be to compute homological information of $\mathcal{M}$ using only the dataset X. We remark that more generalized settings, where $\mathcal{M}$ is not necessarily a manifold, are fundamental cases for many applications and experimental scenarios. But we can discuss, for illustration purposes, the simplified situation of $\mathcal{M}$ being a manifold. We also notice that the crucial problem of finding density conditions for X to be a meaningful sampling set of a manifold $\mathcal{M}$ has been recently addressed in [75], and we discuss these issues later in this report.

Attempting to construct a simplicial complex structure from X can be a very difficult problem. A simple strategy would be to consider the homology of the spaces

$$\mathbb{X}_\epsilon = \cup_{i=1}^m B(x_i, \epsilon)$$

where a ball $B(x_i, \epsilon)$ of radius ϵ is centered around each point of X. A naive approach would be to try to find an optimal ϵ_o such that the homology of $\mathbb{X}_{\epsilon_o}$ corresponds to the homology of $\mathcal{M}$. But this approach is highly unstable, as different homological values might be obtained when considering small perturbations of ϵ_o.

The proposal in *persistent homology* is to consider topological information for all $\epsilon > 0$ simultaneously, and not just a single value ϵ_o. The key concept is that a general homological overview for all values $\epsilon > 0$ is a useful tool when studying the topology of finite datasets. From a computational point of view, estimating homological data for all

continuous values $\epsilon > 0$ might sound unreasonable, but there are two crucial remarks for implementing these ideas in an efficient computational framework. On the one hand, despite the fact that we are considering a continuous parameter $\epsilon > 0$, it can be verified that for a given dataset X, there is actually only a finite number of non-homeomorphic simplicial complexes

$$K_1 \subset K_2 \subset \cdots \subset K_r$$

(which is the concept of a *filtration* to be explicitly defined later on) that can be constructed from $\{\mathbb{X}_\epsilon, \epsilon > 0\}$. On the other hand, another crucial property is that the persistent homology framework includes efficient computational procedures for calculating homological information of the whole family $K_1 \subset K_2 \subset \cdots \subset K_r$, [96].

We also remark that, given a parameter ϵ with corresponding set $\mathbb{X}_\epsilon$, there are various topological structures useful for studying homological information of X. In particular, an efficient computational construction is given by the *Vietoris-Rips complexes* $R_\epsilon(X)$, defined with X as the vertex set, and setting the vertices $\sigma = \{x_0, \ldots, x_k\}$ to span a k-simplex of $R_\epsilon(X)$ if $d(x_i, x_j) \leq \epsilon$ for all $x_i, x_j \in \sigma$. For a given ϵ_k the Vietoris-Rips complex $R_{\epsilon_k}(X)$ provides an element of the filtration $K_1 \subset K_2 \subset \cdots \subset K_r$, with $K_k = R_{\epsilon_k}(X)$. In conclusion, there is only a finite set of positive values $\{\epsilon_i\}_{i=1}^r$, that describe homological characteristics of X, each of which generate a Vietoris Rips complex $\{K_i\}_{i=1}^m$ representing the topological features of the family $\{\mathbb{X}_\epsilon, \epsilon > 0\}$. Therefore, the topological analysis of a point cloud data X boils down to the analysis of a filtration $K_1 \subset K_2 \subset \cdots \subset K_r$, which is the main object of study in persistent homology. We now describe the main conceptual ingredients in this framework.

3.2.1 Conceptual setting

The input in the persistent homology framework is a *filtration* of a simplicial complex K, defined as a nested sequence of subcomplexes $\emptyset = K_0 \subset K_1 \subset K_2 \subset \cdots \subset K_r = K$. Given a simplicial complex K, we recall that the boundary operators ∂_k connect the chain groups C_k, and define a *chain complex*, denoted by C_*, and depicted with the diagram:

$$\ldots C_{k+1} \xrightarrow{\partial_{k+1}} C_k \xrightarrow{\partial_k} C_{k-1} \to \ldots .$$

Recall that given a chain complex C_* one defines the k-cycle groups and the k-boundary groups as $Z_k = \ker \partial_k$, and $B_k = \mathrm{im}\partial_{k+1}$, respectively. As we have nested subgroups $B_k \subseteq Z_k \subseteq C_k$, the k-homology group $H_k = Z_k/B_k$ is well defined.

There are several basic definitions required for the setting of persistent homology. A *persistent complex* is defined as a family of chain complexes $\{C_*^i\}_{i\geq 0}$ over a commutative ring R, together with maps

$$f^i : C_*^i \to C_*^{i+1} \quad \text{related as} \quad C_*^0 \xrightarrow{f_0} C_*^1 \xrightarrow{f_1} C_*^2 \xrightarrow{f_2} \ldots ,$$

or more explicitly, described with the following diagram

$$\begin{array}{ccccccc}
\vdots & & \vdots & & \vdots & & \\
\downarrow{\scriptstyle \partial_3} & & \downarrow{\scriptstyle \partial_3} & & \downarrow{\scriptstyle \partial_3} & & \\
C_2^0 & \xrightarrow{f^0} & C_2^1 & \xrightarrow{f^1} & C_2^2 & \xrightarrow{f^2} & \dots \\
\downarrow{\scriptstyle \partial_2} & & \downarrow{\scriptstyle \partial_2} & & \downarrow{\scriptstyle \partial_2} & & \\
C_1^0 & \xrightarrow{f^0} & C_1^1 & \xrightarrow{f^1} & C_1^2 & \xrightarrow{f^2} & \dots \\
\downarrow{\scriptstyle \partial_1} & & \downarrow{\scriptstyle \partial_1} & & \downarrow{\scriptstyle \partial_1} & & \\
C_0^0 & \xrightarrow{f^0} & C_0^1 & \xrightarrow{f^1} & C_0^2 & \xrightarrow{f^2} & \dots \\
\downarrow{\scriptstyle \partial_0} & & \downarrow{\scriptstyle \partial_0} & & \downarrow{\scriptstyle \partial_0} & & \\
0 & \xrightarrow{f^0} & 0 & \xrightarrow{f^1} & 0 & \xrightarrow{f^2} & \dots
\end{array}$$

We remark that, due to the applications we have in mind, we will assume that chain complexes are trivial in negative dimensions. Given a filtration of a simplicial complex K, a basic example of a persistent complex is given by considering the functions f^i as the inclusion maps between each simplicial complex in the nested sequence $\emptyset = K_0 \subset K_1 \subset K_2 \subset \cdots \subset K_r = K$. Another fundamental concept is a *persistent module*, defined as a family of R-modules M^i and homomorphisms $\phi^i : M^i \to M^{i+1}$. We say that the persistent module is of *finite type* if each M^i is finitely generated, and the maps ϕ^i are isomorphisms for $i \geq k$ and some integer k. The basic example of a persistent module is given by the homology of the simplicial complexes of a filtration. We now define the *p-persistent homology group* of K_i as the group

$$H_k^{i,p} = Z_k^i / (B_k^{i+p} \cap Z_k^i),$$

where Z_k^i and B_k^i stand respectively for the k-cycles and k-boundaries groups in C^i. This group can also be described in terms of the inclusions $K^i \subset K^{i+p}$, their induced homomorphisms $f_k^{i,p} : H_k^i \to H_k^{i+p}$, and the corresponding relation

$$\mathrm{im}(f_k^{i,p}) \cong H_k^{i,p}.$$

These persistent homology groups contain homology classes that are stable in the interval i to $i+p$: they are born before the "time" index i and are still alive at $i+p$. Persistent homology classes alive for large values of p, are stable topological features of X, while classes alive only for small values of p are unstable or noise-like topological components. We will see, in the following paragraphs, alternative views for explaining generalized versions of persistent objects as functors between special categories.

The output of the persistent homology algorithm are representations of the evolution, with respect to the parameter $\epsilon > 0$, of the topological features of X. These representations are depicted with *persistent diagrams* indicating, for each homology level k, the amount and stability of the different k-dimensional holes of the point cloud X. We now present a more precise explanation of the concepts related to persistent diagrams and some of its properties.

The main task we now describe is the analysis of persistent homology groups by capturing their properties in a single algebraic entity represented by a finitely generated

module. Recall that a main objective of persistent homology is to construct a summary of the evolution (with respect to ϵ) of the topological features of X using the sets $\{\mathbb{X}_\epsilon, \epsilon > 0\}$. This property is analyzed when constructing, with the homology groups of the complexes K_i, a module over the polynomial ring $R = \mathbb{F}[t]$ with a field $\mathbb{F}$. The general setting for this procedure is to consider a persistent module $M = \{M^i, \phi_i\}_{i\geq 0}$ and construct the graded module $\alpha(M) = \bigoplus_{i\geq 0} M^i$ over the graded polynomial ring $\mathbb{F}[t]$, defined with the action of t given by the shift $t\cdot(m^0, m^1, \dots) = (0, \phi^0(m^0), \phi^1(m^1), \dots)$. The crucial property of this construction is that α is a functor that defines an equivalence of categories between the category of persistent modules of finite type over $\mathbb{F}$, and the category of finitely generated non-negatively graded modules over $\mathbb{F}[t]$. In the case of a filtration of complexes K_0 to K_r, this characterization of persistent modules provides the finitely generated $\mathbb{F}[t]$ module:

$$\alpha(M) = H_p(K_0) \oplus H_p(K_1) \oplus \cdots \oplus H_p(K_r).$$

These modules are now used in a crucial step that defines and characterizes the output of persistent homology. The main tool is the well-know structure theorem characterizing finitely generated modules over principle ideal domains (this is why we need $\mathbb{F}$ to be a field). This property considers a finitely generated non-negatively graded module $\mathfrak{M}$, and ensures that there are integers $\{i_1, \dots, i_m\}$, $\{j_1, \dots, j_n\}$, $\{l_1, \dots, l_n\}$, and an isomorphism:

$$\mathfrak{M} \cong \bigoplus_{s=1}^{m} \mathbb{F}[t](i_s) \oplus \bigoplus_{r=1}^{n} (\mathbb{F}[t]/(t^{l_r}))(j_r).$$

This decomposition is unique up to permutation of factors, and the notation $\mathbb{F}[t](i_s)$ denotes an i_s shift upward in grading. The relation with persistent homology is given by the fact that when a persistent homology class τ is born at K_i and dies at K_j it generates a torsion module of the form $\mathbb{F}[t]\tau/t^{j-i}(\tau)$. When a class τ is born at K_i but does not die, it generates a free module of the form $\mathbb{F}[t]\tau$.

We can now explain the concept of persistent diagrams using an additional characterization of $\mathbb{F}[t]$-modules. We first define a P-interval as an ordered pair (i, j) where $0 \leq i < j$ for $i, j \in \mathbb{Z} \cup \{\infty\}$. We now construct the function Q mapping a P-interval as $Q(i, j) = (\mathbb{F}[t]/t^{j-i})(i)$, $Q(i, \infty) = \mathbb{F}[t](i)$, and for a set of P-intervals $S = \{(i_1, j_1), \dots, (i_n, j_n)\}$, we have the $\mathbb{F}[t]$-module

$$Q(S) = \bigoplus_{\ell=1}^{n} Q(i_\ell, j_\ell).$$

This map Q turns out to be a bijection between the sets of finite families of P-intervals and the set of finitely generated graded modules over $\mathbb{F}[t]$.

Now, we can recap all these results by noticing that the concept of persistent diagrams can be described as the corresponding set of P-intervals associated to the finitely generated graded module over $\mathbb{F}[t]$, constructed with the functor α from a given filtration $\emptyset = K_0 \subset K_1 \subset K_2 \subset \cdots \subset K_r = K$. There are several graphical representations for persistent diagrams, and two well known examples are the so called barcodes, and triangular regions of index-persistent planes.

Remark 3.2.1 (Stability of persistent diagrams)**.** A crucial property in persistent homology is the concept of *stability of persistent diagrams*. We recall that for a topological

space X, and a map $h : X \to \mathbb{R}$, we say that h is *tame* if the homology properties of $\{X_\epsilon, \epsilon > 0\}$, for $X_\epsilon = h^{-1}(]-\infty, \epsilon[)$, can be completely described with a finite family of sets $X_{a_0} \subset X_{a_1}, \subset \cdots \subset X_{a_r}$, where the positive values $\{a_i\}_{i=0}^r$ are *homology critical points*. If we denote the *persistent diagram* for X and $h : X \to \mathbb{R}$, as $\mathrm{dgm}_n(h)$, we have a summary of the *stable and unstable* holes generated by the filtration

$$X_{a_0} \subset X_{a_1}, \subset \cdots \subset X_{a_r}$$

(see [27]). With these concepts, the *stability of persistent diagrams* is a property indicating that small changes in the persistent diagram $\mathrm{dgm}_n(h)$ can be controlled with small changes in the tame function $h : X \to \mathbb{R}$ (see [20] for details on the stability properties of persistent diagrams).

An important theoretical and engineering problem to investigate is the sensibility of the persistent homology features of X_f when applying signal transformations to f. This is in relation to the question of finding useful signal invariants using the persistent diagram of X_f. For instance, in the case of audio analysis, a crucial task is to understand the effects in the persistent diagram of X_f when applying audio transformations to f as, for instance, delay filters or convolution transforms (e.g room simulations). This task requires both theoretical analysis and numerical experiments. For a conceptual analysis, a possible strategy is to consider these recent theorems explaining the stability of persistent diagrams.

3.2.2 Generalizations with functorial properties

In order to design useful generalizations of persistent homology, it is important to understand its setting in a deeper conceptual level. A recent formulation, providing the core features of persistent homology, has been presented in [14], and describes this concept as a functor between well chosen categories. Indeed, a crucial aspect of persistent homology is the association from an index set to a sequence of homology groups constructed from a filtration $\emptyset = K_0 \subset K_1 \subset K_2 \subset \cdots \subset K_r = K$. An important generalization of this construction considers a general partially ordered set P as an index set which we associate to a family of objects in a given category $\mathbf{C}$. Notice that we can consider the partially ordered set P as a category $\mathbf{P}$, whose objects are P, and a morphism from x to y is defined whenever $x \leq y$. With this setting, a P-persistent object in $\mathbf{C}$ is defined as a functor $\Phi : \mathbf{P} \to \mathbf{C}$, described also as a family of objects $\{c_x\}_{x \in P}$ in $\mathbf{C}$, and morphisms $\phi_{xy} : c_x \to c_y$, when $x \leq y$.

These concepts are of fundamental importance for extending the main ideas of persistent homology in more general situations. Notice that in standard persistent homology we use the partial ordered sets $P = \mathbb{N}$ or $P = \mathbb{R}$, but important extensions have been recently developed in the context of multidimensional persistence. Here, we consider multidimensional situations where the partial ordered sets are, for instance, $P = \mathbb{N}^k$ or $P = \mathbb{R}^k$, $k > 1$. These developments are motivated by multiple practical considerations, such as the analysis of point cloud using both density estimations and the Vietoris Rips Complex construction.

A Schematic explanation

In the following two diagrams, we present a particularly simple way to see the strategy of persistent homology. The algorithmic input is a point cloud data X, or more generally, the distance relations between its elements. Note that no topological structures are given, therefore, the basic task is to construct simplicial complexes in order to estimate topological information. By considering Vietoris-Rips complex structures, we can study the set $\mathbb{X}_\epsilon = \cup_{i=1}^{m} B(x_i, \epsilon)$. As we previously explained, it is difficult to try to find and define a optimum ϵ that is meaningful for the dataset X at hand (see Fig. 3.1). The strategy of persistent homology is to consider a multiscale process that takes into account all possible values ϵ using efficient algorithmic strategies. The resulting output of the persistent homology algorithm is an overview of the "stable" and "unstable" holes related to the dataset X (see Fig. 3.2).

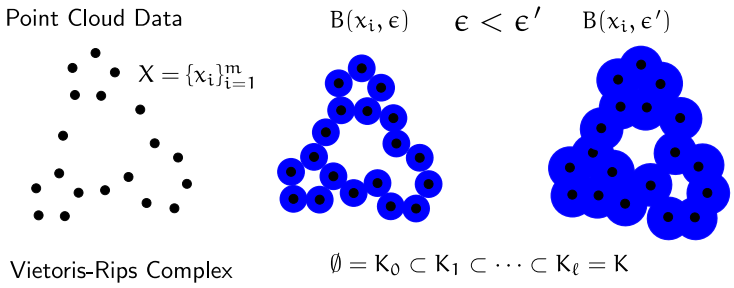

Figure 3.1: Illustrating the difficulty of finding a meaningful ϵ for a point cloud data X as an input for the persistent homology algorithm

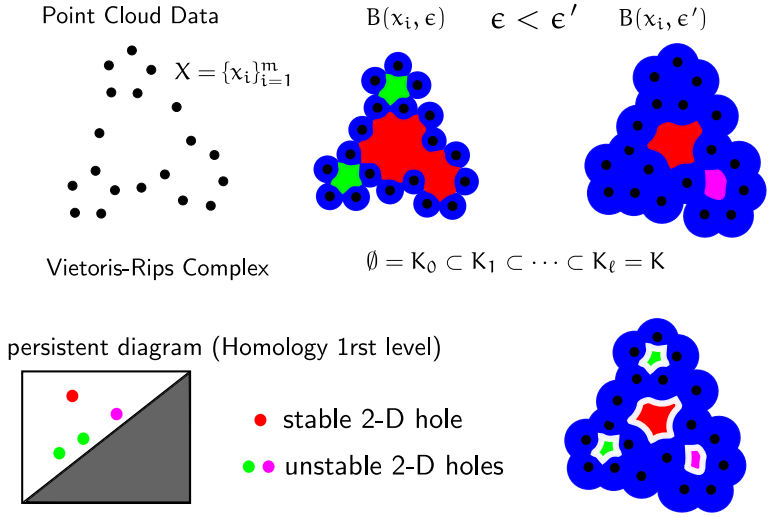

Figure 3.2: Schematic explanation of the persistent homology diagram, and the lifetime of the stable and unstable holes

4 Numerical Curvature Analysis of Modulated Spaces

In this Chapter, we propose the concepts of modulation maps and modulated spaces for the construction of particular datasets relevant in signal processing and nonlinear dimensionality reduction (NDR). We consider numerical methods for analyzing geometrical properties of the modulated manifolds, with a particular focus on their scalar and mean curvature. In our numerical examples, we apply the resulting geometry-based analysis to simple test cases, where we present geometrical and topological effects of relevance in manifold learning.

4.1 Introduction

We briefly recall the basic problem of NDR and manifold learning, suppose we are given a dataset $X = \{x_i\}_{i=1}^m \subset \mathbb{R}^n$ lying in a high-dimensional Euclidean space, where X is assumed to be sampled from a submanifold $\mathcal{M}$ of $\mathbb{R}^n$, i.e., $X \subset \mathcal{M} \subset \mathbb{R}^n$. Moreover, we assume that the dimension of $\mathcal{M}$ is much smaller than the dimension of the ambient space, i.e., $\dim(\mathcal{M}) \ll n$. The primary objective of manifold learning is to construct a low-dimensional representation of X which can be used to efficiently visualize and analyze its geometrical properties.

For many examples of datasets $X = \{x_i\}_{i=1}^m \subset \mathbb{R}^n$, each element $x_i \in X$ can be considered as a signal that may be analyzed through a transformation map T, defined via convolution transforms, Fourier analysis, or wavelet functions. Therefore, from a manifold learning perspective, a relevant question is the analysis of the geometrical changes that X goes through when deformed with T resulting in the set $T(X) = \{T(x_i)\}_{i=1}^m$ and, in particular, to study the composition $P \circ T$ of a NDR map P with a signal transform T.

To analyze these problems, we construct a particular class of datasets X sampled from manifolds $\mathcal{M}$ generated by *modulation maps*. The idea of modulation maps is inspired by concepts in frequency modulation techniques from signal transmission in engineering domains. Here, our main interest is to consider these signal processing concepts from a geometrical perspective. To gain further insight into their geometrical properties, we use numerical approximations to construct basic geometric data such as metric and curvature tensors. With these modulated manifolds we can design examples of low-dimensional datasets embedded in high dimensional spaces, which are relevant both in signal processing and dimensionality reduction. A main characteristic of these constructions is that they provide examples (in the same spirit as the Swiss role dataset) of test cases where classical linear projections, such as principal component analysis (PCA) are outperformed by more recent nonlinear methods, such as isomap , Riemannian normal coordinates (RNC), etc [58, 62, 94].

The contributions of this chapter can be summarized as follows. We introduce modulation maps and modulated manifolds as a relevant concept in dimensionality reduction. We provide conditions that justify the terminology used for these objects (as diffeomorphism and manifolds). We consider numerical procedures for computing geometrical quantities, such as metric tensors, Gaussian and mean curvatures. In our numerical examples, we illustrate relevant phenomena of modulated manifolds in the context of dimensionality reduction.

The outline of this chapter is as follows. In Section 4.2, the concept of modulated man-

ifolds is explained, where a concrete example is presented under the setting of frequency modulation. In Section 4.2.2 we present a discussion on measuring geometric deformations of modulated manifolds using metric and curvature tensors, and the Laplace-Beltrami operator for computing the mean curvature. In Section 4.3, numerical examples are provided, where the geometric distortion of selected manifolds (sphere and torus surfaces) is illustrated by combining modulation maps and dimensionality reduction methods. In the numerical examples, we also compare standard PCA techniques with modern (nonlinear) dimensionality reduction strategies. We also present in Section 4.3.3 various geometrical and topological effects that are relevant from both a dimensionality reduction and signal processing viewpoint.

4.2 Modulation Maps and Curvature Distortion

This section is devoted to a particular construction of manifolds $\mathcal{M}$ and diffeomorphisms $\mathcal{A}$ based on modulation maps. Modulation techniques are well-known engineering and telecommunication procedures used to transmit information by varying the frequency of a carrier signal ϕ. A main property of these techniques is the simultaneous transmission of different information by using different frequency bands that can be conveniently separated with special convolution filters. Motivated by these ideas, we want to analyze, from a geometrical point of view, a frequency modulation map $\mathcal{A} : \Omega \to \mathcal{M}$, where $\mathcal{M}$ represents the carrier signals modulated by Ω, which is the information content to be transmitted. Rather than analyzing a specific engineering modulation method, our goal is to use and generalize these concepts in order to construct manifolds and datasets with relevant properties in dimensionality reduction and signal analysis. In our particular situation, the domain Ω is a manifold and so its structural content, transmitted via $\mathcal{A}$, needs to be extracted from $\mathcal{M}$.

4.2.1 Modulation Maps and Modulated Spaces

We now define the concept of modulation maps and modulated manifolds. Additionally, we provide basic examples together with some properties where these ideas can formally be described. We start with an intuitive explanation and a short motivation using an image processing example. Our current focus on smooth manifolds is an important conceptual step before one may address more general situations (e.g. simplicial complexes, CW-complexes, Alexandrov spaces, etc) that are crucial for many engineering applications.

In the following, we assume $\mathcal{M}$ to be a submanifold of a high dimensional Euclidean space $\mathcal{H}$, $\mathcal{M} \subset \mathcal{H}$, and Ω to be a parameter space considered as a submanifold of a low dimensional Euclidean space. The intuition behind the concept of a *modulated manifold* $\mathcal{M}$ is to generate the elements of $\mathcal{M}$ by a family of signal transforms $\{s(\alpha) : \mathcal{H} \to \mathcal{H}\}_{\alpha\in\Omega}$ and a vector $\phi \in \mathcal{H}$ such that for each $y \in \mathcal{M}$, we have $y = s(\alpha)\phi$ for some $\alpha \in \Omega$. This concept extends the classical notion of modulation by considering maps $s(\alpha) : \mathcal{H} \to \mathcal{H}$ in order to transform (or *modulate*) a function ϕ for generating the elements of $\mathcal{M}$. A straightforward generalization is to consider a family of vectors $\{\phi_k\}_{k=1}^d \subset \mathcal{H}$ together with a corresponding family of signal transforms $\{s_k(\alpha) : \mathcal{H} \to \mathcal{H}\}_{k=1,\,\alpha\in\Omega}^d$, such that for

any $y \in \mathcal{M}$ there is one unique $\alpha \in \Omega$ satisfying

$$y = \sum_{k=1}^{d} s_k(\alpha)\phi_k.$$

To further explain our motivation, let us return to the analysis of a grayscale image $f : [0,1]^2 \to [0,1]$ using a covering of small squares, or patches, $\{O_i \subset [0,1]^2\}_{i=1}^m$, each containing n pixels. In this toy example we assume that the corresponding point cloud data $X_f = \{f(O_i) \in \mathbb{R}^n\}_{i=1}^m$ lies in some manifold $\mathcal{M} \subset \mathbb{R}^n$. If an image f is composed of an homogeneous texture, the dataset X_f is a cluster whose elements have similar geometrical characteristics. In a simplified scenario, the idea would be to use a representative patch $\phi \in \mathbb{R}^n$ in order to generate all elements of X_f. The main task is to find a family of transformations (the *modulation maps*) $s(\alpha) : \mathbb{R}^n \to \mathbb{R}^n$, parametrized by a low dimensional space Ω, such that for any patch $y \in X_f$, there is some $\alpha \in \Omega$ with $y = s(\alpha)\phi$. We remark that several methods in image processing have recently been proposed with a loosely related philosophy (see e.g. the *patch-based texture analysis* as part of classical *texture synthesis* methods [55]).

Definition 4.2.1 (Modulation maps and modulated spaces)**.** Let $\{\phi_k\}_{k=1}^d \subset \mathcal{H}$ be a set of vectors in an Euclidean space $\mathcal{H}$, and $\{s_k : \Omega \to \mathcal{C}_{\mathcal{H}}(\mathcal{H})\}_{k=1}^d$ a family of continuous maps from a space (e.g. manifold, topological space) Ω to $\mathcal{C}_{\mathcal{H}}(\mathcal{H})$ (the continuous functions from $\mathcal{H}$ into $\mathcal{H}$). We say that a space $\mathcal{M} \subset \mathcal{H}$ is a $\{\phi_k\}_{k=1}^d$-*modulated space* if

$$\mathcal{M} = \left\{ \sum_{k=1}^{d} s_k(\alpha)\phi_k,\ \alpha \in \Omega \right\}.$$

In this case, the map $\mathcal{A} : \Omega \to \mathcal{M}$, $\alpha \mapsto \sum_{k=1}^d s_k(\alpha)\phi_k$, is called *modulation map*. We frequently will consider the situations where Ω and $\mathcal{M}$ are manifolds.

This concept can also be described using the language of vector bundles. Recall that a vector bundle (E, Ω, π, F) is defined for a manifold E as a surjective map $\pi : E \to \Omega$, with a vector space F as a *fiber*, and a manifold *base* Ω such that $\pi^{-1}(\alpha)$ is isomorphic to F for each $\alpha \in \Omega$. Locally, E is homeomorphic to $\Omega \times F$, where E may have a non-trivial global structure. Two typical examples for a vector bundle are the tangent bundle of a manifold and the Möbius band E, whose base Ω is a circle and whose fiber F is a line. *Sections* of a vector bundle $\pi : E \to \Omega$ are smooth maps $s : \Omega \to E$ such that $\pi(s(\alpha)) = \alpha$, and their prototypical examples are vector fields on Ω. In our Definition 4.2.1 we currently use a trivial vector bundle $\pi : E \to \Omega$ for $E = \Omega \times \mathcal{C}_{\mathcal{H}}(\mathcal{H})$, a fiber $\mathcal{C}_{\mathcal{H}}(\mathcal{H})$, and smooth sections $\{s_k : \Omega \to E\}_{k=1}^d$.

Example 4.2.1 (Frequency and scale modulation)**.** A basic example of a modulation map for a manifold $\Omega \subset \mathbb{R}^d$ is a map $\mathcal{A} : \Omega \subset \mathbb{R}^d \to \mathbb{R}^n$ of the form

$$\mathcal{A}_\alpha(t_i) = \sum_{k=1}^{d} \phi_k(\alpha_k t_i), \quad \alpha = (\alpha_1, \ldots, \alpha_d) \in \Omega, \quad \{t_i\}_{i=1}^n \subset [0,1],$$

for a finite set of smooth band-limited functions $\{\phi_k \in \mathcal{C}^\infty([0,1]) \cap \mathcal{B}_{f_s},\}_{k=1}^d$, with $\mathcal{B}_{f_s} = \{f \in L^2([0,1]),\ \mathrm{supp}(\hat{f}) \subseteq [-f_s, f_s]\}$, and a given fixed sampling rate f_s. We use a

uniformly spaced finite sampling set $\{t_i\}_{i=1}^n \subset [0,1]$ (as justified by the Nyquist-Shannon sampling theorem), by considering band-limited functions $\{\phi_k\}_{k=1}^d$. Note that we use the same notation for the band-limited functions ϕ_k and the vector of sampling values $\{\phi_k(t_i)\}_{i=1}^n$, as justified by the *Whittaker-Shannon interpolation formula*. More precisely, as the support of our functions ϕ_k is located in $[0,1]$, and due to their band-limited property, the interpolation formula allows us to reconstruct each ϕ_k with the finite sampling set $(\phi_k(t_i))_{i=1}^n \in \mathbb{R}^n$, which unambiguously identifies the function $\phi_k : [0,1] \to \mathbb{R}$ with a vector $\phi_k \in \mathbb{R}^n$. Note that the maps $s_k(\alpha)$ of Definition 4.2.1 are in this example given by $s_k(\alpha)\phi_k(t_i) = \phi_k(\alpha_k t_i)$. In other words, we use the (continuous) map $s_k(\alpha) : \mathcal{C}^\infty([0,1]) \to \mathcal{C}^\infty([0,1])$, $f(t) \mapsto f(\alpha_k t)$, as the scaling by factor α_k, the k-th coordinate of vector $\alpha \in \Omega \subset \mathbb{R}^d$. We now consider additional properties to ensure a meaningful definition of frequency modulation, as required in Proposition 4.2.1.

The first property is the *band separation* for Ω, defined as $B_k \cap B_j = \emptyset$, for all $k \neq j$, with $B_k = \{\alpha_k \in \mathbb{R},\ \alpha = (\alpha_1, \ldots, \alpha_{k-1},\ \alpha_k, \alpha_{k+1}, \ldots, \alpha_d) \in \Omega\}$. The intuition behind this assumption is that the coordinates of the manifold Ω are ranged in different and non overlapping regions. This is actually a standard condition in telecommunication engineering, where different non-overlapping frequency bands are used for the transmission of different signals. This property will help ensure the injectivity of $\mathcal{A}$, as required in Proposition 4.2.1.

The second property is a *sufficiently dense sampling set* for $\{\phi_k : [0,1] \to \mathbb{R}\}_{k=1}^d$ and $\Omega \subset \mathbb{R}^d$, defined as a set $\{t_i\}_{i=1}^n \subset [0,1]$ that is dense enough for reconstructing each function in $\{\phi_k\}_{k=1}^d$ using the Whittaker-Shannon interpolation formula. Note that these conditions restrict the range of values for Ω, but more general situations could be considered when using different domains for the functions ϕ_k.

Now the following proposition justifies the motivation of Definition 4.2.1 and the terminology used in the above example.

Proposition 4.2.1 (Manifold structure of $\mathcal{M}$ and diffeomorphism property of $\mathcal{A}$)**.** *Suppose that Ω is a submanifold of $\mathbb{R}^d$ with separated bands. Moreover, let $\{t_i\}_{i=1}^n \subset [0,1]$ be a sufficiently dense sampling compact set for Ω and a family of smooth band-limited functions ϕ_k with essential support in $[0,1]$, $\{\phi_k : [0,1] \to \mathbb{R}\}_{k=1}^d$. If for any element $\alpha = (\alpha_1, \ldots, \alpha_d) \in \Omega$ the $d \times d$ matrix $\mathfrak{J}_{\mathcal{A}}(\alpha)$ with entries*

$$\mathfrak{J}_{\mathcal{A}}(\alpha)_{ks} = \sum_{i=1}^n t_i^2 \phi_k'(\alpha_k t_i)\phi_s'(\alpha_s t_i), \quad 1 \leq k, s \leq d, \tag{4.1}$$

is invertible, then $\mathcal{M} = \left\{\left(\sum_{k=1}^d \phi_k(\alpha_k t_i)\right)_{i=1}^n, \alpha = (\alpha_1, \ldots, \alpha_d) \in \Omega\right\}$ is a submanifold of $\mathbb{R}^n$, and the map $\mathcal{A} : \Omega \to \mathcal{M}$, $\mathcal{A}_\alpha(t_i) = \sum_{k=1}^d \phi_k(\alpha_k t_i)$, is a diffeomorphism.

Proof. This follows as a straightforward application of the rank theorem for manifolds. The first step is to verify that the map $\mathcal{A} : \Omega \to \mathbb{R}^n$, $\mathcal{A}_\alpha(t_i) = \sum_{k=1}^d \phi_k(\alpha_k t_i)$ is an injective immersion. Since Ω is compact we can then conclude that $\mathcal{A}$ is also a smooth embedding (see [60, Proposition 7.4]). With this property, $\mathcal{A} : \Omega \to \mathbb{R}^n$ is a homeomorphism onto its image $\mathcal{M} = \mathcal{A}(\Omega)$.

The injectivity of $\mathcal{A}$ can be ensured with the *band separation* property of Ω. In order to verify that $\mathcal{A}$ is an immersion, we compute the rank of $\mathcal{A}$ at $\alpha \in \Omega$, defined as the rank

of the linear map $\mathcal{A}_* : T_\alpha\Omega \to T_{\mathcal{A}(\alpha)}\mathbb{R}^n$ (the differential of $\mathcal{A}$ with the tangent spaces $T_\alpha\Omega$ and $T_{\mathcal{A}(\alpha)}\mathbb{R}^n$ at α and $\mathcal{A}(\alpha)$, respectively) For this task, we consider a smooth chart (U, χ), with $\alpha \in U \subset \Omega$ and $\chi : U \subset \Omega \to \tilde{U} \subset \mathbb{R}^p$ a smooth map, where $p = \dim(\Omega)$. Now, the derivative $\mathcal{A}_*$ (or pushforward) of $\mathcal{A}$ at $\alpha \in \Omega$ can be described in local coordinates as the Jacobian matrix of $\hat{\mathcal{A}} = \psi \circ \mathcal{A} \circ \chi^{-1} : \chi(U) = \tilde{U} \subset \mathbb{R}^p \to \psi(\mathbb{R}^n) = \mathbb{R}^n$, at $\chi(\alpha)$ for $\psi = \mathrm{Id}_{\mathbb{R}^n} : \mathbb{R}^n \to \mathbb{R}^n$, the identity using $(\mathbb{R}^n, \mathrm{Id}_{\mathbb{R}^n})$ as a single chart of the smooth manifold $\mathbb{R}^n$. The Jacobian matrix of $\hat{\mathcal{A}}$ is the $n \times p$ matrix $J_{\hat{\mathcal{A}}} = J_\psi \, J_{\mathcal{A}} \, J_{\chi^{-1}}$, i.e., a product of the $n \times n$ matrix J_ψ, the $n \times d$ matrix $J_{\mathcal{A}}$, and the $d \times p$ matrix $J_{\chi^{-1}}$. As J_ψ is the identity matrix, we have $\mathrm{rank}(J_{\hat{\mathcal{A}}}) = \mathrm{rank}(J_{\mathcal{A}} \, J_{\chi^{-1}})$, and since $\chi^{-1} : \tilde{U} \subset \mathbb{R}^p \to U \subset \Omega \subset \mathbb{R}^d$ is a diffeomorphism, we have $\mathrm{rank}(J_{\chi^{-1}}) = p$. Now, if we assume that $\mathrm{rank}(J_{\mathcal{A}}) = d$, with the Sylvester rank inequality we have $\mathrm{rank}(J_{\mathcal{A}}) + \mathrm{rank}(J_{\chi^{-1}}) - d \leq \mathrm{rank}(J_{\mathcal{A}} \; J_{\chi^{-1}})$. Therefore, due to our assumption $\mathrm{rank}(J_{\mathcal{A}}) = d$, we obtain $\mathrm{rank}(J_{\hat{\mathcal{A}}}) = p$, so that $\mathcal{A} : \Omega \to \mathbb{R}^n$ is an immersion, since $\mathrm{rank}(\mathcal{A}) = \mathrm{rank}(\mathcal{A}_*) = \dim(\Omega)$. Our assumption $\mathrm{rank}(J_{\mathcal{A}}) = d$ is equivalent to $\det(J_{\mathcal{A}}^T(\alpha) \, J_{\mathcal{A}}(\alpha)) \neq 0$, for each $\alpha \in \Omega$ and $d \times d$ matrices $J_{\mathcal{A}}^T(\alpha) \, J_{\mathcal{A}}(\alpha)$. Therefore, for $\mathfrak{J}_{\mathcal{A}}(\alpha) = J_{\mathcal{A}}^T(\alpha) \, J_{\mathcal{A}}(\alpha)$, we obtain the representation (4.1).

Using the previous argument we can guarantee that $\mathcal{M} = \mathcal{A}(\Omega)$ is a submanifold of $\mathbb{R}^n$, if $\mathfrak{J}_{\mathcal{A}}(\alpha)$ is invertible for each $\alpha \in \Omega$. Therefore, the map $\mathcal{A} : \Omega \to \mathcal{M}$ is a surjective smooth constant-rank map. Finally, we now use an important consequence of the rank theorem for manifolds (see [60, Theorem 7.15]) to conclude that $\mathcal{A}$ is a diffeomorphism between the manifolds Ω and $\mathcal{M}$, and therefore $\dim(\mathcal{M}) = \dim(\Omega) = p$. ■

Example 4.2.2 (An explicit case of a frequency modulation map)**.** We now continue the analysis for Example 4.2.1, using Proposition 4.2.1, to construct a *frequency modulation map*. A prototypical case is given by trigonometric functions, $\phi(t) = \sin(t)$, where the corresponding modulation map $\mathcal{A} : \Omega \to \mathbb{R}^n$, with Ω a submanifold of $\mathbb{R}^d$, is called *frequency modulation map*. A concrete construction is given by $\mathcal{A}^\gamma : \Omega \to \mathbb{R}^n$ with

$$\mathcal{A}_\alpha^\gamma(t_i) = \sum_{k=1}^{d} \sin((\alpha_k^0 + \gamma\alpha_k)t_i), \quad \{t_i\}_{i=1}^n \subset [0, 1], \tag{4.2}$$

for a fixed *bandwidth* parameter $\gamma > 0$, *center frequencies* $\alpha^0 = (\alpha_1^0, \ldots, \alpha_d^0) \in \mathbb{R}^d$, and *separated* bands B_k, i.e., $B_k \cap B_j = \emptyset$ for all $k \neq j$, where

$$B_k = \{\alpha_k^0 + \gamma\alpha_k \in \mathbb{R}, \; \alpha = (\alpha_1, \ldots, \alpha_{k-1}, \; \alpha_k, \alpha_{k+1}, \ldots, \alpha_d) \in \Omega\}.$$

This construction can be viewed as the application of an affine transform to the manifold $\Omega \subset \mathbb{R}^d$, with shift α^0 and bandwidth γ, so that the coordinates of the vectors in the resulting set $\alpha^0 + \gamma\Omega = \{\alpha^0 + \gamma\alpha, \alpha \in \Omega\}$ will not share common values. In this case, the frequency content introduced by each coordinate $\alpha \in \Omega$ will not overlap.

Now we need to verify that $\mathcal{A}^\gamma$ in (4.2) is a diffeomorphism for specific parameters γ and α^0, and the following lemma provides a particular situation.

Lemma 4.2.1 (Diffeomorphism property of frequency modulated maps)**.** *Suppose that Ω is a submanifold of $\mathbb{R}^d$ with $\Omega \subset [-1,1]^d$, and let $\alpha^0 \in \mathbb{R}^d$ be a vector, such that $\Omega_{\alpha^0} = \alpha^0 + \Omega = \{\alpha^0 + \gamma\alpha, \alpha \in \Omega\}$ has separated bands. If the $d \times d$ matrix $\mathfrak{J}(\alpha^0)$ is invertible for $\{t_i = i/n\}_{i=1}^n \subset [0,1]$, and*

$$\mathfrak{J}(\alpha^0)_{ks} = \sum_{i=1}^{n} t_i^2 \cos(\alpha_k^0 t_i)\cos(\alpha_s^0 t_i), \qquad 1 \leq k, s \leq d,$$

then there exist a bandwidth parameter $\gamma > 0$, such that the matrix $\mathfrak{J}(\beta)_{ks}$ is regular for all $\beta \in \Omega_{\alpha^0}^{\gamma} = \alpha^0 + \gamma\Omega$.

Proof. This follows from a straightforward application of the Gershgorin circle theorem, where we compare the locations of the eigenvalues of $\mathfrak{J}(\beta)$ with those of the eigenvalues of $\mathfrak{J}(\alpha^0)$. Using the mean value theorem for $\cos(\beta_k t_i)$, with $\beta_k = \alpha_k^0 + \gamma\alpha_k$, we have $\cos((\alpha_k^0 + \gamma\alpha_k)t_i) = \cos(\alpha_k^0 t_i) + \gamma\alpha_k t_i \cos(\eta)$ for $\alpha_k^0 t_i < \eta < \alpha_k^0 t_i + \gamma\alpha_k t_i$. This implies

$$\begin{aligned}
\mathfrak{J}(\beta)_{ks} &= \sum_{i=1}^{n} t_i^2 \cos((\alpha_k^0 + \gamma\alpha_k)t_i)\cos((\alpha_s^0 + \gamma\alpha_s)t_i) \\
&= \sum_{i=1}^{n} t_i^2 \cos(\alpha_k^0 t_i)\cos(\alpha_s^0 t_i) + \gamma\tau_{ks}\sum_{i=1}^{n} t_i^2 \\
&= \mathfrak{J}(\alpha^0)_{ks} + \gamma\tau_{ks}\frac{(n+1)(2n+1)}{6n},
\end{aligned}$$

with $t_i = i/n$ and $\tau_{ks} \in \mathbb{R}$ satisfying $|\tau_{ks}| \leq 1$. Using the triangle inequality, we obtain

$$\mathfrak{J}(\beta)_{kk} - \sum_{k\neq s} |\mathfrak{J}(\beta)_{ks}| \geq \mathfrak{J}(\alpha^0)_{kk} - \sum_{k\neq s} |\mathfrak{J}(\alpha^0)_{ks}| - \sum_{i=1}^{d-1} \gamma\frac{(n+1)(2n+1)}{6n}.$$

Therefore, due to the Gershgorin circle theorem, the regularity of the matrices $\mathfrak{J}(\beta)$, for $\beta \in \Omega_{\alpha^0}^{\gamma}$, can be guaranteed, if $\mathfrak{J}(\alpha^0)_{kk} - \sum_{k\neq s} |\mathfrak{J}(\alpha^0)_{ks}| > \sum_{i=1}^{d-1} \gamma\frac{(n+1)(2n+1)}{6n}$. In particular, this property can be fulfilled for any $\gamma \geq 0$ satisfying

$$\gamma < \gamma_{\max} = \frac{6n \min\limits_{1\leq i\leq d}\left(\mathfrak{J}(\alpha^0)_{ii} - \sum_{j\neq i} |\mathfrak{J}(\alpha^0)_{ij}|\right)}{(d-1)(n+1)(2n+1)}. \tag{4.3}$$

■

Assuming the hypothesis of the above lemma in combination with Proposition 4.2.1, we can conclude that $\mathcal{M} = \left\{\left(\sum_{k=1}^{d} \sin((\alpha^0 + \gamma\alpha)t_i)\right)_{i=1}^{n} \in \mathbb{R}^n, \alpha \in \Omega\right\}$ is a submanifold of $\mathbb{R}^n$, and the map $\mathcal{A}^{\gamma} : \Omega \to \mathcal{M}$, $\mathcal{A}_{\alpha}^{\gamma}(t_i) = \sum_{k=1}^{d} \sin((\alpha_k^0 + \gamma\alpha_k)t_i)$, is the corresponding diffeomorphism. We remark that it is also straightforward to justify this lemma by using the continuity of the determinant of $\mathfrak{J}(\alpha^0)$. But the bound on γ in (4.3) allows us to provide a concrete range for the bandwidth parameter γ, where we can ensure the desired diffeomorphism and manifold properties for $\mathcal{A}$ and $\mathcal{M}$. As a concrete example, consider a sampling rate $n = 256$Hz, and center frequencies $\alpha^0 = (40\text{Hz}, 60\text{Hz}, 80\text{Hz})$. In this case, the matrix $\mathfrak{J}(\alpha^0)$ is regular for any bandwidth parameter $\gamma < \gamma_{\max}$ with $\gamma_{max} \approx 0.2454$Hz. We remark that our numerical simulations suggest that the range for γ, allowing diffeomorphism and manifold properties for $\mathcal{A}$ and $\mathcal{M}$, is much larger than in the estimate (4.3). A more detailed analysis on these properties, however, is beyond the aim of the present chapter.

4.2.2 Geometric Deformation with Curvature Measurements

Now we analyze the geometrical deformation between Ω, $\mathcal{M}$ and Ω', as incurred by the modulation map $\mathcal{A} : \Omega \to \mathcal{M}$ and the dimensionality reduction transform $P : \mathcal{M} \to \Omega'$. In order to analyze the geometrical deformation we consider basic curvature concepts, including Gaussian and mean curvature. On the one hand, we first present a very general procedure for computing the scalar curvature using the Riemannian metric as main input. On the other hand, we describe a discrete scheme for computing the mean curvature by using the Laplace-Beltrami operator.

We first recall basic ingredients for computing the scalar curvature of a p-dimensional manifold $\mathcal{M}$, and refer to [59,92] for further details. The fundamental tool for describing the geometry of $\mathcal{M}$ is a metric tensor field $g : \mathcal{M} \to \mathbb{R}^{p\times p}$, defined for local coordinates $(x_1, \ldots, x_p)$ as

$$g_{ij}(x) = \langle \partial_i, \partial_j \rangle \qquad \text{for } x \in \mathcal{M} \text{ and } 1 \leq i, j \leq p.$$

Here, the partial derivatives ∂_i represent the tangent vectors at each $x \in \mathcal{M}$, and the notation $g_{ij}(x)$ is occasionally used for $g(x)$. With this fundamental building block, all other required structures for defining the scalar curvature are defined, including the Christoffel symbols and curvature tensors. The Christoffel symbols can be described as

$$\Gamma_{ij}^{k} = \frac{1}{2} \sum_{\ell=1}^{p} \left(\frac{\partial g_{j\ell}}{\partial x_i} + \frac{\partial g_{i\ell}}{\partial x_j} - \frac{\partial g_{ij}}{\partial x_\ell} \right) g^{\ell k}. \tag{4.4}$$

Here, the expression g^{ij} denotes the inverse matrix of g_{ij}. An explicit formula for the curvature tensor is given in terms of the Christoffel symbols (the 1,3 curvature tensor) as

$$R^{\ell}{}_{ijk} = \sum_{h=1}^{p} (\Gamma_{jk}^{h} \Gamma_{ih}^{\ell} - \Gamma_{ik}^{h} \Gamma_{jh}^{\ell}) + \frac{\partial \Gamma_{jk}^{\ell}}{\partial x_i} - \frac{\partial \Gamma_{ik}^{\ell}}{\partial x_j}. \tag{4.5}$$

We use the tensor contractions

$$R_{ijk\ell} = \sum_{h=1}^{p} R_{ijk}^{h} g_{\ell h} \qquad \text{and} \qquad R_{ij} = \sum_{k,\ell=1}^{p} g^{k\ell} R_{kij\ell} = \sum_{k=1}^{p} R_{kij}^{k} \tag{4.6}$$

for intermediate computations. The scalar curvature is computed together with Gaussian curvature, which for the case of two dimensional manifolds differs by a factor 2, as

$$S = \sum_{i,j=1}^{p} g^{ij} R_{ij}. \tag{4.7}$$

In our particular situation, we are considering manifolds embedded in linear spaces (i.e., $\Omega \subset \mathbb{R}^d$ and $\mathcal{M} \subset \mathbb{R}^n$). Our strategy for introducing the concept of curvature distortion is to compare the geometries of Ω and $\mathcal{M}$ generated by their corresponding first fundamental forms, which are particular metrics induced by their ambient space.

The usage of these concepts in discrete settings as meshes for manifolds is a highly nontrivial task, and there are relatively simple situations where convergence properties cannot be guaranteed. A typical example is the *Schwarz lantern* which is a simple mesh discretization of a cylinder with very poor approximation properties [50]. With this

warning in mind, we consider a straightforward discretization scheme for computing the Gaussian curvature in (4.7), cf. Algorithm 4.2.1. But on the other hand, we also consider a rigorous discretization procedure, with good convergence properties, for computing the mean curvature as described in the following paragraph.

Another strategy to analyze the curvature distortion is to compute the mean curvature using the Laplacian-Beltrami operator $\Delta_{\mathcal{M}} f = \operatorname{div}(\nabla_{\mathcal{M}} f)$, where f are the coordinates of the embedded manifold $\mathcal{M} \subset \mathbb{R}^n$. The Laplace-Beltrami operator is also defined with the metric tensor g_{ij}, its inverse matrix g^{ij}, and its determinant $|g_{ij}|$:

$$\Delta_{\mathcal{M}} f(x) = \frac{1}{\sqrt{|g_{ij}(x)|}} \sum_{k,\ell=1}^{p} \partial_k \Big(\sqrt{|g_{ij}(x)|} g^{ij}(x) \partial_\ell f(x) \Big) \qquad \text{for } x \in \mathcal{M}.$$

Designing accurate and robust methods for discretizing the operator Δ is a very active research topic. A recent method [5] for doing so provides an efficient strategy by using

$$L_K^h f(w) = \frac{1}{4\pi h^2} \sum_{t \in K} \frac{\text{Area(t)}}{\#(t)} \sum_{p \in V(t)} e^{-\frac{||p-w||^2}{4h}} (f(p) - f(w)). \tag{4.8}$$

Here, K is a mesh in $\mathbb{R}^3$, the set of vertices is denoted by V, and $f : V \to \mathbb{R}$. For a face $t \in K$, the number of vertices in t is denoted by $\#(t)$, and $V(t)$ is the set of vertices of t. The parameter h is a positive quantity representing the size of the mesh at each point. As we consider two dimensional manifolds, the mesh $K_{\epsilon,\eta}$ can be described with two variables ϵ, η for controlling the parameter h. We finally remark that the discretization scheme in (4.8) convergences w.r.t. $\|\cdot\|_\infty$ (see [5] for details), i.e.,

$$\lim_{\epsilon,\eta \to 0} \sup_{K_{\epsilon,\eta}} \| L_{K_{\epsilon,\eta}}^{h(\epsilon,\eta)} f - \Delta_{\mathcal{M}} f \|_\infty = 0.$$

4.2.3 Metric Tensor for Frequency Modulated Manifolds

We now compute a metric tensor in $\mathcal{M}$ in order to analyze the geometrical deformation of Ω as incurred by the application of a modulation map $\mathcal{A} : \Omega \subset \mathbb{R}^d \to \mathcal{M} \subset \mathbb{R}^n$. The resulting metric tensor can then be used for computing the curvature tensor and the corresponding scalar curvature, which will be used as a measure for the geometric deformation. Our strategy is to consider a parametrization of Ω and to compute the metric tensor generated from the ambient space $\mathbb{R}^n$. In particular, we use the first fundamental form with respect to the given parametrization. The resulting formula (4.9) follows by direct computation, as explained in the following proposition, where we compute the first fundamental form of a modulated manifold $\mathcal{M}$.

Proposition 4.2.2. *Let $\mathcal{M}$ be a manifold constructed from a diffeomorphic modulation map $\mathcal{A} : \Omega \subset \mathbb{R}^d \to \mathcal{M} \subset \mathbb{R}^n$,*

$$\mathcal{A}_\alpha(t_i) = \sum_{k=1}^{d} \phi_k(\alpha_k t_i) \qquad \textit{where } \alpha = (\alpha_1, \ldots, \alpha_d) \in \Omega \textit{ and } \{t_i\}_{i=1}^n \subset [0,1],$$

and $\{\alpha_j(\theta_1,\ldots,\theta_p)\}_{j=1}^d$ *be a parametrization of* Ω *with* $p = \dim(\mathcal{M}) = \dim(\Omega)$*. Then, the first fundamental form of* $\mathcal{M}$ *constructed from this parametrization is given by*

$$g_{sr} = \sum_{\ell=1}^{n} t_\ell^2 \sum_{r,q=1}^{d} \left(\frac{d\phi_r}{dt}(\alpha_r t_\ell) \frac{d\phi_q}{dt}(\alpha_q t_\ell) \frac{\partial \alpha_r}{\partial \theta_s} \frac{\partial \alpha_q}{\partial \theta_r} \right). \tag{4.9}$$

Proof. This follows as a direct computation of the Jacobian of the composition $\mathcal{A} \circ \alpha$. The Jacobian with respect to parametrization $\alpha_j(\theta_1,\ldots,\theta_d)$ of Ω is given by

$$J_{\mathcal{A}} = \left(\frac{\partial \mathcal{A}_\ell}{\partial \theta_i} \right)_{\ell,i} \qquad \text{where} \qquad \frac{\partial \mathcal{A}_\ell}{\partial \theta_i} = \frac{\partial}{\partial \theta_i} \left(\sum_{j=1}^{d} \phi_j(\alpha_j t_\ell) \right) = \sum_{j=1}^{d} \frac{d\phi_j}{dt}(\alpha_j t_\ell) t_\ell \frac{\partial \alpha_j}{\partial \theta_i}.$$

The first fundamental form (metric tensor) of $\mathcal{M}$ is given by

$$\begin{aligned}
\left(J_{\mathcal{A}}^T J_{\mathcal{A}}\right)_{s,r} &= \sum_{\ell=1}^{n} \left(\sum_{j=1}^{d} \frac{\partial \phi_j}{\partial t}(\alpha_j t_\ell) t_\ell \frac{\partial \alpha_j}{\partial \theta_s} \right) \left(\sum_{j=1}^{d} \frac{\partial \phi_j}{\partial t}(\alpha_j t_\ell) t_\ell \frac{\partial \alpha_j}{\partial \theta_r} \right) \\
&= \sum_{\ell=1}^{n} \sum_{r,q=1}^{d} \left(\frac{d\phi_r}{dt}(\alpha_r t_\ell) t_\ell \frac{\partial \alpha_r}{\partial \theta_s} \frac{d\phi_q}{dt}(\alpha_q t_\ell) t_\ell \frac{\partial \alpha_q}{\partial \theta_r} \right) \\
&= \sum_{\ell=1}^{n} t_\ell^2 \sum_{r,q=1}^{d} \left(\frac{d\phi_p}{dt}(\alpha_r t_\ell) \frac{d\phi_q}{dt}(\alpha_q t_\ell) \frac{\partial \alpha_r}{\partial \theta_s} \frac{\partial \alpha_q}{\partial \theta_r} \right)
\end{aligned}$$

As g_{sr} is given by $\left(J_{\mathcal{A}}^T J_{\mathcal{A}}\right)_{s,r}$, we obtain the resulting equation (4.9). ∎

The expression in equation (4.9) will play an important role in our following discussion. However, due to its complexity (even for rather simple examples as a sphere or a torus), we prefer to work with a numerical framework for illustrating its properties through the relevant curvature tensors. Moreover, the numerical approach taken provides a flexible scheme that can handle arbitrary two-dimensional frequency modulated manifolds $\mathcal{M}$ that are defined by a finite scattered dataset $X = \{x_i\}_{i=1}^m \subset \mathcal{M}$.

4.2.4 Numerical Computation of Curvature Tensors

Now we combine the representation (4.9) with the curvature tensors in (4.6) and (4.7) for describing how Ω is geometrically deformed under the mapping $\mathcal{A} : \Omega \to \mathcal{M}$. In the following computations, we focus on the particular case of two-dimensional manifolds embedded in a three-dimensional space, i.e., $d = 3$, $\dim(\Omega) = 2$, with $\Omega \subset \mathbb{R}^3$. In our computation of the metric tensor in (4.9), the main inputs are the functions $\{\phi_j\}_{j=1}^3$ and the parametrization $\{\alpha_j(\theta_1,\theta_2)\}_{j=1}^3$ of Ω, which is used to construct the Jacobian components $\frac{\partial \alpha_p}{\partial \theta_s}$ and $\frac{\partial \alpha_q}{\partial \theta_r}$. The following algorithm describes the basic steps for computing the scalar curvature S and the metric tensors g_{ij} of the modulated manifold $\mathcal{M}$.

Algorithm 4.2.1. (Curvature and metric tensors of manifolds.)

Input:
(a) *Parametrization* $\alpha = (\alpha_j(\theta_1, \theta_2))_{j=1}^3$ *of* Ω*;*
(b) *Functions* $\{\phi_j\}_{j=1}^3$ *generating the map* $\mathcal{A}$*.*

(1) *Compute the Jacobian matrices* J_α*;*

(2) *Compute the metric tensor* g_{ij} *via equation (4.9);*

(3) *Compute the Christoffel symbols* Γ_{ij}^k *via equation (4.4);*

(4) *Compute the tensors* $R_{ijk\ell}$*,* R_{ij} *via equations (4.6);*

(5) *Compute the scalar curvature* S *via equation (4.7).*

Output: *Scalar curvature* S *of* $\mathcal{M}$*.*

4.3 Computational Experiments

We now apply Algorithm 4.2.1 and the discretization in (4.8) to compute the Gaussian and mean curvature of frequency modulated manifolds for two different toy examples. The corresponding Matlab code is available at `www.math.uni-hamburg.de/home/guillemard/`. In these test cases we use the sphere $\Omega = \mathbb{S}^2$ and the torus $\Omega = \mathbb{T}^2$ to illustrate how the curvature is modified under modulation maps and dimensionality reduction projections.

4.3.1 Frequency Modulation for a Sphere

In this first numerical example, we use the unit sphere for the parameter space i.e., $\Omega = \mathbb{S}^2 \subset \mathbb{R}^3$, and the modulation map $\mathcal{A} : \mathbb{S}^2 \subset \mathbb{R}^3 \to \mathcal{M} \subset \mathbb{R}^{256}$ is defined as $\mathcal{A}_\alpha(t_i) = \sum_{k=1}^3 \sin((\alpha_k^0 + \gamma\alpha_k)t_i)$, where

$$\begin{aligned} \alpha_1(u, v) &= \cos(v)\cos(u), \\ \alpha_2(u, v) &= \cos(v)\sin(u), \\ \alpha_3(u, v) &= \sin(v). \end{aligned}$$

Here, we use a finite and regular distribution of values $u \in [0, 2\pi]$, $v \in [0, \pi]$, and $\{t_i\}_{i=1}^{256} \subset [0, 1]$. We apply shifting and scaling to the manifold $\mathbb{S}^2$, so that the frequency positions are given by the coordinates $(\alpha_0^1, \alpha_0^2, \alpha_0^3)$ and the scaling factor γ. We use these parameters to obtain a separation of the frequency bands as described in Subsection 4.2.1. The scaling factor γ gives the spreading of each frequency band (bandwidth). A main observation of the following experiments is that the geometrical deformation depends primarily on the parameter γ. A graphical display of the manifolds $\mathbb{S}^2$ and $\mathcal{M}$ is presented in Figure 4.1, where the sphere $\mathbb{S}^2$ is compared with a three dimensional PCA projection of $\mathcal{M}$ (denoted as $P(\mathcal{M})$). The PCA projection $P(\mathcal{M})$ of $\mathcal{M} \subset \mathbb{R}^n$, $n = 256$, produces a significant geometrical deformation. One objective of the following analysis is to measure this distortion. It can be observed experimentally that an increase in the scale factor γ corresponds to a more pronounced cubic shape deformation, as shown in Figure 4.1 **(b)**.

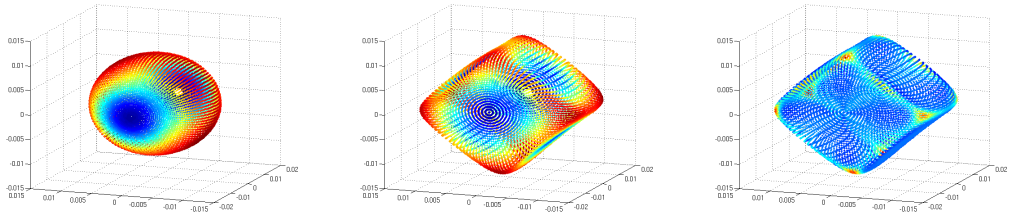

(a) **(b)** **(c)**

Figure 4.1: PCA projections of a modulated sphere $\mathcal{M} = \mathcal{A}^{\gamma}(\Omega) \subset \mathbb{R}^n$, for $\Omega = \mathbb{S}^2 \subset [-1,1]^3$, with sample frequency $n = 256$, center frequencies $\alpha^0 = (40\text{Hz}, 60\text{Hz}, 80\text{Hz})$, and bandwidth parameter $\gamma = 0.4\text{Hz}$ **(a)** The sphere $\mathbb{S}^2 \subset \mathbb{R}^3$ with the mean curvature of $\mathcal{M}$ as color code; **(b)** PCA projection $P_{\text{PCA}}(\mathcal{M}) \subset \mathbb{R}^3$ with its mean curvature in the color code; **(c)** PCA projection $P_{\text{PCA}}(\mathcal{M}) \subset \mathbb{R}^3$ with its Gaussian curvature in the color code.

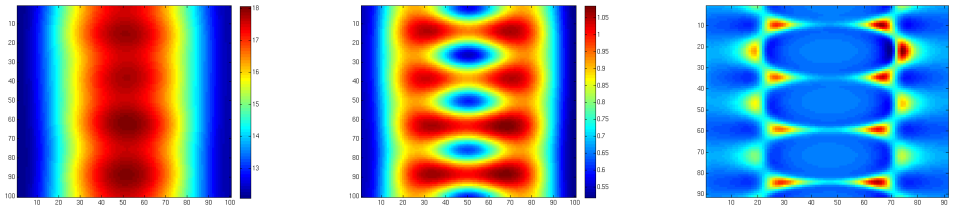

(a) **(b)** **(c)**

Figure 4.2: Curvatures of the modulated sphere $\mathcal{M} = \mathcal{A}(\Omega)$ and its projection $P_{\text{PCA}}(\mathcal{M})$ (see Figure 4.1). **(a)** The mean curvature of $\mathcal{M} \subset \mathbb{R}^{256}$; **(b)** the mean curvature of $P(\mathcal{M}) \subset \mathbb{R}^3$; **(c)** the Gaussian curvature of $P(\mathcal{M}) \subset \mathbb{R}^3$.

The objective of these examples is to illustrate the geometrical deformation when applying the frequency modulation map $\mathcal{A}$ to Ω. We notice a cubic type deformation as soon as the bandwith parameter increases with several isolated points where the curvature reaches high values.

In order to measure this geometric deformation, we compute the scalar and mean curvature of $\mathcal{M} \subset \mathbb{R}^{256}$ and that of its three-dimensional PCA projection $P(\mathcal{M})$. Figure 4.2 **(a)** shows the mean curvature of the manifold $\mathcal{M}$ and the Gaussian curvature of its projection $P(\mathcal{M})$ is displayed in Figure 4.2 **(c)**. Note that the mean curvature of $\mathcal{M}$ shows some small variations over its surface, indicating only a small deformation of the spherical geometry via the frequency modulation map $\mathcal{A}$. In contrast, the PCA projection of $\mathcal{M}$ shows significant curvature variations, as presented in Figure 4.1 **(c)**. Note that there are two sets of four maximal scalar curvature values, corresponding to the corners of the cubic shaped surface shown in Figure 4.1 **(c)**.

4.3.2 Frequency Modulation for a Torus

In this second numerical example, we use the torus surface $\Omega = \mathbb{T}^2 \subset \mathbb{R}^3$ in combination with the modulation map $\mathcal{A}_\alpha(t_i) = \sum_{k=1}^{3} \sin((\alpha_k^0 + \gamma\alpha_k)t_i)$, and the parametrization

$$\begin{aligned} \alpha_1(u,v) &= (R + r\cos(v))\cos(u), \\ \alpha_2(u,v) &= (R + r\cos(v))\sin(u), \\ \alpha_3(u,v) &= r\sin(v). \end{aligned}$$

We use a regular distribution of values $u \in [0, 2\pi]$, $v \in [0, 2\pi]$, and $\{t_i\}_{i=1}^{256} \subset [0, 1]$. As in the previous example, the parameter γ plays a key role in the cubic deformation, cf. Figure 4.3 **(c)**.

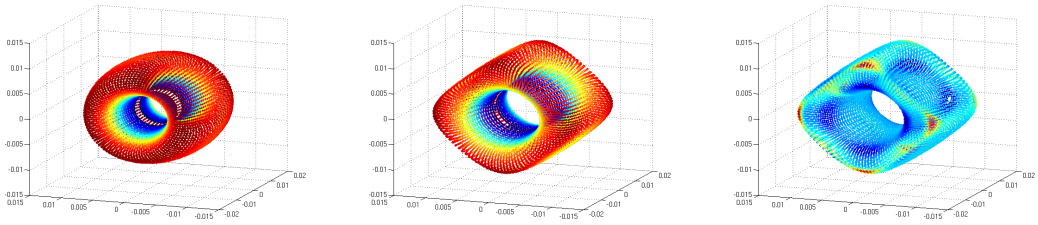

(a) **(b)** **(c)**

Figure 4.3: PCA projections of a modulated torus $\mathcal{M} = \mathcal{A}^\gamma(\Omega) \subset \mathbb{R}^n$, for $\Omega = \mathbb{T}^2 \subset [-1, 1]^3$, with sample frequency $n = 256$, center frequencies $\alpha^0 = (40\text{Hz}, 60\text{Hz}, 80\text{Hz})$, and bandwidth parameter $\gamma = 0.3\text{Hz}$ **(a)** The torus $\mathbb{T}^2 \subset \mathbb{R}^3$ with the mean curvature of $\mathcal{M}$ as color code; **(b)** PCA projection $P_{\text{PCA}}(\mathcal{M}) \subset \mathbb{R}^3$ with its mean curvature in the color code; **(c)** PCA projection $P_{\text{PCA}}(\mathcal{M}) \subset \mathbb{R}^3$ with its Gaussian curvature in the color code.

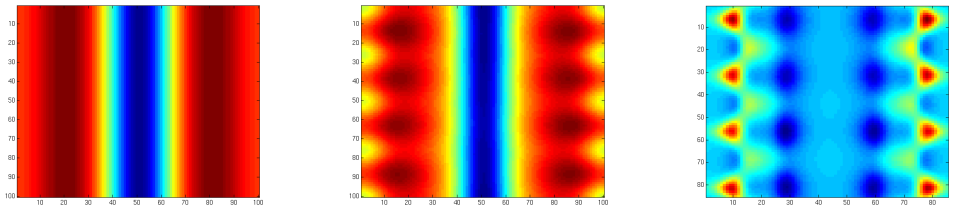

(a) **(b)** **(c)**

Figure 4.4: Curvatures of the modulated torus $\mathcal{M} = \mathcal{A}(\Omega)$ and its projection $P_{\text{PCA}}(\mathcal{M})$ (see Figure 4.3). **(a)** The mean curvature of $\mathcal{M} \subset \mathbb{R}^{256}$; **(b)** the mean curvature of $P_{\text{PCA}}(\mathcal{M}) \subset \mathbb{R}^3$; **(c)** the Gaussian curvature of $P_{\text{PCA}}(\mathcal{M}) \subset \mathbb{R}^3$.

The mean curvature of $\mathcal{M} \subset \mathbb{R}^{256}$ is shown in Figure 4.4 **(a)**. We observe a typical pattern for the torus geometry: a constant value for the mean curvature along the smaller circle of the torus (depicted with the middle vertical line in Figure 4.4 **(a)**), two circles with constant curvature on the top and bottom of the torus (depicted with two vertical

lines equidistant to the middle of Figure 4.4 **(a)**), and another circle with constant mean curvature along the larger circle of the torus (depicted with the leftmost and rightmost vertical lines of the Figure 4.4 **(a)**).

The Gaussian curvature of the PCA projection $P(\mathcal{M})$, shown in Figure 4.4 **(c)**, illustrates a similar structure, but with a additional geometrical deformations which includes two sets of four points with maximal scalar curvature, representing the corners of the cubic shaped projection $P(\mathcal{M})$ shown in Figure 4.3 **(c)**.

We finally remark that, for these toy examples, the task of estimating the frequencies of each $x \in \mathcal{M}$ (and therefore computing Ω) is not a difficult problem. A straightforward method for doing so is to use the Fourier transform of the signals $x \in \mathcal{M}$, as for instance performed in classical *partial tracking* techniques. But our focus here is to conceptually understand the geometrical effects of dimensionality reduction methods in datasets $\mathcal{M} = \mathcal{A}(\Omega)$. From a signal processing point of view, the problem of estimating Ω becomes much more challenging when considering more complex functions ϕ_k for the modulation map $\mathcal{A}$. In such situations, the presented geometrical framework will be useful for estimating Ω in more complex test case scenarios.

4.3.3 Dimensionality Reduction and Topological Effects from Curvature

In our numerical experiments, we observe that an increase of the bandwidth parameter γ amplifies the geometrical distortion of the modulated manifolds $\mathcal{M} \subset \mathbb{R}^n$. In fact, when increasing the bandwidth parameter γ, standard (linear) projection methods, such as PCA, fail to recover the geometry of the manifold. In contrast, recent nonlinear dimensionality reduction methods, such as isomap, achieve to recover (up to a certain bandwidth γ) the geometry of Ω. For the purpose of further illustration, Figure 4.5 **(b)** shows how the linear PCA projection destroys the geometrical content of the modulated torus $\mathcal{M}$, whereas the nonlinear isomap projection achieves to recover the topological and geometrical features of the torus $\mathbb{T}^2$ reasonably well. This effect is similar as when comparing the isomap and PCA methods for the classical Swiss Roll dataset example. But with our concept we can generate much more challenging datasets from modulated manifolds to evaluate the performance of NDR techniques.

To further investigate the geometrical distortion of modulated manifolds incurred by dimensionality reduction maps, we illustrate how the bandwidth parameter γ affects the topological reconstruction of Ω. To this end, we analyze the evolution of the mean curvature of the manifold $\mathcal{M} = \mathcal{A}^\gamma(\Omega)$ for a range of bandwidth parameters γ (see Figure 4.6). In this case, we compute for values $\gamma \in [0, 4]$ the maximum mean curvature of $\mathcal{M}$. We let $\Omega = \mathbb{T}^2 \subset [-1, 1]^3$, and therefore, if the projection $P(\mathcal{M})$ correctly reconstructs the topology of $\mathcal{M}$, we expect the Betti numbers of $P(\mathcal{M})$ to be $b_0 = 1$ and $b_1 = 2$.

Figure 4.6 **(a)** shows an increase of the maximum mean curvature as the bandwidth parameter is amplified. For small values of γ, a standard (linear) dimensionality reduction method, such as PCA, achieves to reproduce the topology of Ω. This can be verified by the persistent homology of $P(\mathcal{M})$, as depicted in the barcode graph of Figure 4.6 **(b)**, where for $\gamma = 0.2$Hz, the first two Betti numbers agree with that of a torus structure ($b_0 = 1, b_1 = 2$). But for higher values γ, the geometry of $\mathcal{M} = \mathcal{A}^\gamma(\Omega)$ is more difficult to reconstruct. In fact, the topological structure of the dimensionality reduced datasets $P(\mathcal{M})$ are in this case incorrect. This can be seen in Figure 4.6 **(c)**, where the persistent

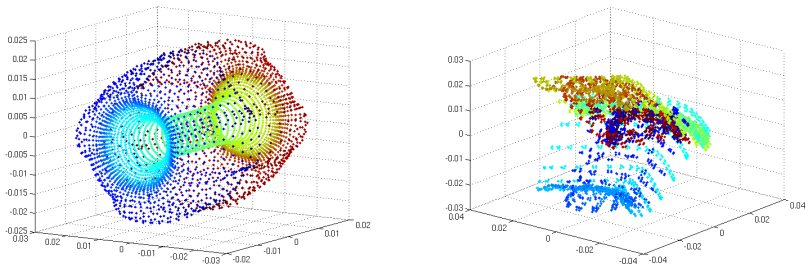

(a) **(b)**

Figure 4.5: Dimensionality reduction of a frequency modulated manifold $\mathcal{M} = \mathcal{A}(\Omega) \subset \mathbb{R}^n$, for a torus $\Omega = \mathbb{T}^2 \subset [-1,1]^3$ using a sampling frequency $n = 256$, with center frequencies $\alpha^0 = (40\text{Hz}, 60\text{Hz}, 80\text{Hz})$, and bandwidth parameter $\gamma = 4\text{Hz}$. **(a)** $P_{\text{Isomap}}(\mathcal{M})$ isomap projection of $\mathcal{M}$; **(b)** $P_{\text{PCA}}(\mathcal{M})$ PCA projection of $\mathcal{M}$.

homology barcode of $P_{\text{PCA}}(\mathcal{M})$ with $\gamma = 4\text{Hz}$, yields incorrect Betti numbers $b_0 = 3$ and $b_1 = 0$. An example of one data set $P_{\text{PCA}}(\mathcal{M})$ is shown in Figure 4.5 **(b)**, where $\gamma = 4\text{Hz}$.

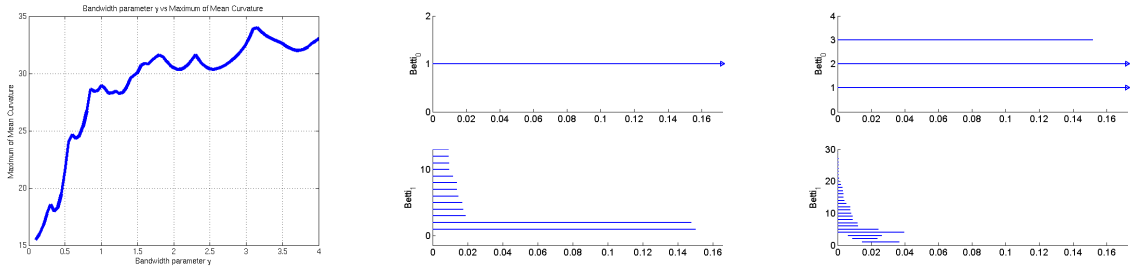

(a) **(b)** **(c)**

Figure 4.6: **(a)** Maximum mean curvature of $\mathcal{M} = \mathcal{A}(\Omega)$ vs bandwidth parameter γ in the interval $[0,4]$, for $\Omega = \mathbb{T}^2 \subset [-1,1]^3$, and center frequencies $\alpha^0 = (40\text{Hz}, 60\text{Hz}, 80\text{Hz})$. **(b)** Betti numbers of $P_{\text{PCA}}(\mathcal{M})$ and bandwidth parameter $\gamma = 0.2\text{Hz}$ ($b_0 = 1, b_1 = 2$), **(c)** Betti numbers of $P_{\text{PCA}}(\mathcal{M})$ and bandwidth parameter $\gamma = 4\text{Hz}$ ($b_0 = 3, b_1 = 0$).

4.4 Filtering Effects

We present here additional numerical experiments illustrating the effect of the curvature distortion when applying filtering procedures. Our main objective is to estimate the curvature distortion in the geometry of the manifold $\mathcal{M}$ when applying a linear transformation $T : \mathcal{M} \to \mathcal{M}_T$, where T represents, for instance, a wavelet or a convolution filter. We first need to evaluate relevant effects on the geometrical deformation of $\mathcal{M}$ under various transformations T.

4.4.1 Sectional Curvature Distortions

In order to estimate the distortion caused by the linear map $T : \mathcal{M} \to \mathcal{M}_T$, we compare the Gaussian curvatures between $\mathcal{M}$ and $\mathcal{M}_T$, denoted respectively $K_{\mathcal{M}}$, and $K_{\mathcal{M}_T}$,

$$D_K^T(p) = K_{\mathcal{M}}(p) - K_{\mathcal{M}_T}(T(p)) \quad \text{for } p \in \mathcal{M}.$$

If T is invertible, then the Gaussian curvature $K_{\mathcal{M}_T}$ in $\mathcal{M}_T$ can be computed as a function of the metric g in $\mathcal{M}$ by using a *pullback* of the curvature tensor R in $\mathcal{M}$ with respect to the inverse map $T^{-1} : \mathcal{M}_T \to \mathcal{M}$, or, equivalently, by using a *pushforward* of the curvature tensor R in $\mathcal{M}$ with respect to $T : \mathcal{M} \to \mathcal{M}_T$. An alternative strategy is to consider the composition of T with a particular system of local coordinates $(x_1, \ldots, x_n)$ of $\mathcal{M}$, along with the metric tensor

$$g_{ij}(p) = g_{ij}(x_1, \ldots, x_m) = \left\langle \frac{\partial}{\partial x_i}, \frac{\partial}{\partial x_j} \right\rangle.$$

When considering the linear transformation T representing the convolution filter, an important case is when T is represented by a Toeplitz matrix, with filter coefficients $H = (h_1, \ldots, h_m)$, i.e.,

$$T = \begin{bmatrix} h_1 & 0 & \ldots & 0 \\ h_2 & h_1 & \ldots & 0 \\ \vdots & \vdots & \ldots & \vdots \\ h_m & h_{m-1} & \ldots & h_1 \\ 0 & h_m & \ldots & h_2 \\ \vdots & \vdots & \ldots & \vdots \\ 0 & 0 & \ldots & h_m \end{bmatrix}.$$

Note that the curvature distortion caused by the map T will be controlled by the singular values of T, which due to the Toeplitz matrix structure, are obtained from the Fourier coefficients of H.

Now, our primary objective is to investigate the influence of the filter coefficients in H on the curvature distortion D_K^T. Moreover, we study filters being required to obtain a given curvature distortion. The latter is particularly useful for the adaptive construction of a low dimensional representation of U.

4.4.2 Curvature Distortions for Curves

As for the special case of a curve $r : I = [t_0, t_1] \to \mathbb{R}^m$, with arc-length parameterization $s(a,t) = \int_a^t \|r'(x)\|\, dx$, recall that the curvature of r is $k(s) = \|r''(s)\|$. For an arbitrary parameterizations of r, its curvature is given by

$$K^2 = \frac{\|\ddot{r}\|^2 \|\dot{r}\|^2 - <\ddot{r}, \dot{r}>^2}{(\|\dot{r}\|^2)^3}.$$

In the remainder of this section, we briefly discuss the curvature distortion under linear maps (e.g. convolution transform) and under smooth maps. To compute the curvature

distortion of a curve $r : I = [t_0, t_1] \to \mathbb{R}^m$ under a linear map T, we consider the curvature of $r_T = \{Tr(t), t \in I\}$, computed as follows.

$$K_T^2 \equiv K_T^2(t) = \frac{\|T\ddot{r}\|^2\|T\dot{r}\|^2 - < T\ddot{r}, T\dot{r} >^2}{(\|T\dot{r}\|^2)^3}. \tag{4.10}$$

As for the general case of smooth maps $F : \mathbb{R}^m \to \mathbb{R}^r$, the curvature distortion can be approximated by using the Jacobian matrix J_F and its singular value decomposition,

$$\begin{aligned} J_F(p) &= \begin{bmatrix} \frac{\partial f_1}{\partial x_1}(p) & \dots & \frac{\partial f_1}{\partial x_m}(p) \\ \vdots & \ddots & \vdots \\ \frac{\partial f_r}{\partial x_1}(p) & \dots & \frac{\partial f_r}{\partial x_m}(p) \end{bmatrix} \\ &= U_F(p) D_F(p) V_F^T(p) \qquad \text{for } p \in \mathcal{M}. \end{aligned}$$

The curvature distortion of a curve $r : [t_0, t_1] \to \mathbb{R}^m$ under F can in this case be analyzed through the expression

$$K_F^2 \equiv K_F^2(p) = \frac{\|J_F\ddot{r}\|^2\|J_F\dot{r}\|^2 - < J_F\ddot{r}, J_F\dot{r} >^2}{(\|J_F\dot{r}\|^2)^3},$$

where, unlike in the linear case (4.10), the Jacobian matrices J_F depend on $p \in \mathcal{M}$.

4.4.3 Numerical Examples

This section presents three different numerical examples to illustrate basic properties of the proposed analysis of high-dimensional signal data. Further details shall be discussed during the conference.

Low-dimensional parameterization of scale modulated signals

In this example, we illustrate the geometrical effect of a convolution transform for a set of functions lying on a curve embedded in a high dimensional space. More precisely, we analyze a scale modulated family of functions $U \subset \mathbb{R}^{64}$, parameterized by three values in $\Omega \subset \mathbb{R}^3$,

$$U = \left\{ f_{\alpha(t)} = \sum_{i=1}^{3} e^{-\alpha_i(t)(\cdot - b_i)^2} : \alpha(t) \in \Omega \right\}.$$

The parameter set for the scale modulation is given by the curve

$$\Omega = \left\{ \alpha(t) = (\alpha_1(t), \alpha_2(t), \alpha_3(t))^T \in \mathbb{R}^3, \ : t \in [t_0, t_1] \right\}.$$

Figure 4.7 (left) shows the parameter domain Ω, a star shaped curve in $\mathbb{R}^3$. A PCA projection in $\mathbb{R}^3$, applied to the set $U \subset \mathbb{R}^{64}$, is also displayed in Figure 4.7 (middle). The projection illustrates the curvature distortion caused by the nonlinear map $A : \Omega \subset \mathbb{R}^3 \to U \subset \mathbb{R}^{64}$, $A(\alpha(t)) = f_{\alpha(t)}$.

Finally, Figure 4.7 (right), shows the resulting data transformation $T(U)$ using a Daubechies wavelet w.r.t. a specific band of the multiresolution analysis, resulting in

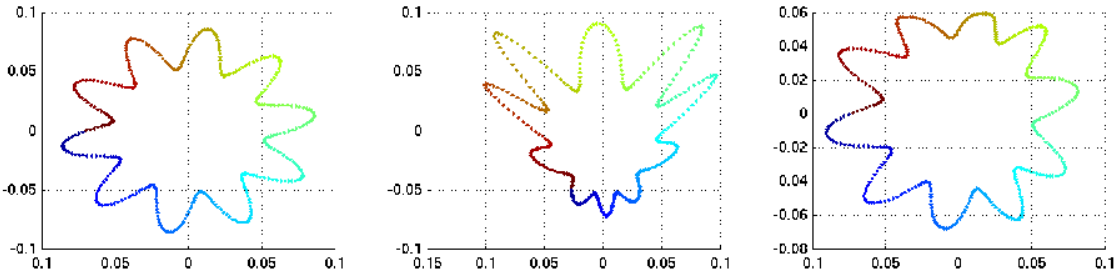

Figure 4.7: Parameter set $\Omega \subset \mathbb{R}^3$, data $U \subset \mathbb{R}^{64}$, and wavelet correction $T(U) \subset \mathbb{R}^{64}$

a filtering process for each element in U. The resulting $T(U)$, presents a curvature correction that recovers the original geometry of Ω up to some degree.

As seen in this example, the resulting curvature effects are related to the singular values and singular vectors of the convolution map T. We remark that the singular values of T can be viewed as scaling factors (stretching or shrinking) along corresponding axis in the (local) embedding of U. Notice also that the spectrum of T depends on the particular filter design.

Low dimensional parameterization of wave equation solutions

In this second example, we regard the one-dimensional wave equation

$$\frac{\partial u}{\partial t} = c^2 \frac{\partial u}{\partial x}, \quad 0 < x < 1, \ t \geq 0, \tag{4.11}$$

with initial conditions

$$u(0,x) = f(x), \ \frac{\partial u}{\partial t}(0,x) = g(x), \quad 0 \leq x \leq 1. \tag{4.12}$$

We make use of the previous example to construct a set of initial values (i.e. functions) parameterized by a star shaped curve $U_0 = U$. Our objective is to investigate the distortion caused by the evolution U_t of the solutions on given initial values U_0. Recall that the evolution of the wave equation is constituted by the set of solutions

$$\begin{aligned} U_t \ = \ & \{u_\alpha \equiv u_\alpha(t,x) : u_\alpha \text{ satisfying (4.11) with} \\ & \text{initial condition } f \equiv f_\alpha \text{ in (4.12) for } \alpha \in \Omega\}. \end{aligned}$$

Now, the solution of the wave equation can numerically be computed by using finite differences, yielding the iteration

$$u^{(j+1)} = Au^{(j)} + b^{(j)},$$

where for $\mu = \gamma \Delta t/(\Delta x)^2$, the iteration matrix is given by

$$A = \begin{bmatrix} 1-2\mu & \mu & & & & \\ \mu & 1-2\mu & \mu & & & \\ & \mu & 1-2\mu & \mu & & \\ & & \ddots & \ddots & \ddots & \\ & & & 0 & \mu & 1-2\mu \end{bmatrix}.$$

Recall that in the convergence analysis of the iteration, which can be rewritten as,

$$\begin{aligned} u^{(j+2)} &= Au^{(j+1)} + b^{(j+1)} \\ &= A(Au^{(j)} + b^{(j)}) + b^{(j+1)} \\ &= A^{(2)}u^{(j)} + Ab^{(j)} + b^{(j+1)}, \end{aligned}$$

the spectrum of the matrices A^k play a key role. Notice that due to the decomposition $A^k = UD^kU^T$, the geometrical distortion in the evolution of U_t depends on the evolution of the eigenvalues of A.

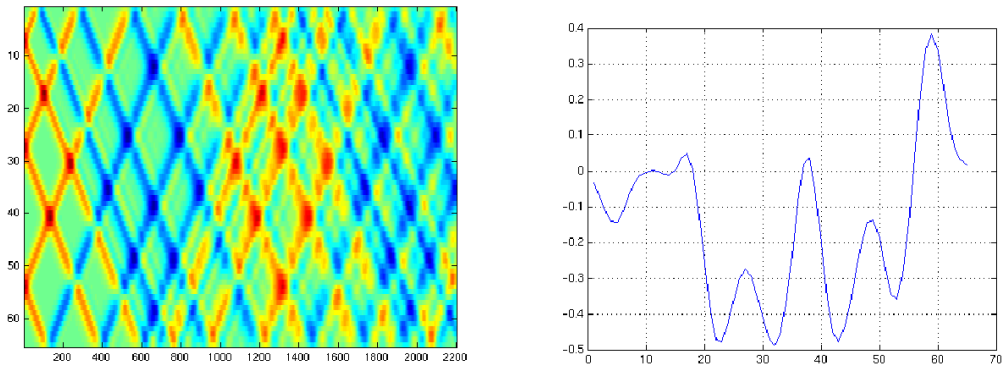

Figure 4.8: One solution of the wave equation $u(t, x)$ and one measurement $u(t_k, x)$, $t_k = 20$

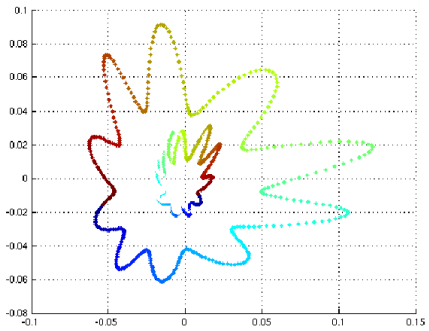

Figure 4.9: Curvature distortion of the initial manifold under the evolution of the wave equation. The outer curve represents the initial conditions U_0 while the inner curve reflects the corresponding solutions U_t for some time t

Topological Distortion and Filtering

In this example, we illustrate a relevant phenomenon concerning the topological distortion that occurs when using a convolution transform. In this test cases, we take a 1-torus $\Omega_1 \subset \mathbb{R}^3$ and one 2-torus $\Omega_2 \subset \mathbb{R}^3$ as parameter space, respectively. As in the previous examples, we generate a corresponding set of scale modulation functions U_1 and U_2 (see

Figure 4.10), using Ω_1 and Ω_2 as parameter domains. This gives, for $j = 1, 2$, two different data sets

$$U_j = \left\{ f_{\alpha^j(t)} = \sum_{i=1}^{3} e^{-\alpha_i^j(t)(\cdot - b_i^j)^2} : \alpha^j(t) \in \Omega_j \right\}.$$

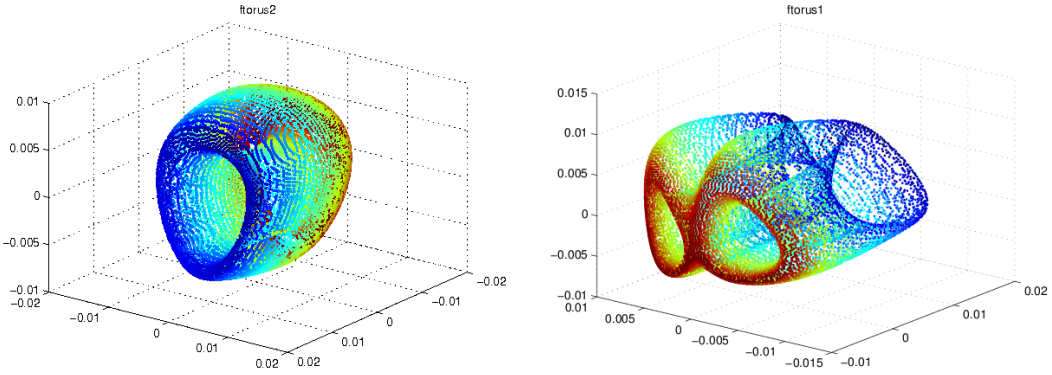

Figure 4.10: PCA projections of $U_1, U_2 \subset \mathbb{R}^{64}$ onto $\mathbb{R}^3$, generated by $\Omega_1, \Omega_2 \subset \mathbb{R}^3$, two tori of genus 1 and 2

Now we combine the set U_1 and U_2 by

$$U = \left\{ f_t = f_{\alpha^1(t)} + f_{\alpha^2(t)} : \alpha^1(t) \in \Omega_1, \alpha^2(t) \in \Omega_2 \right\}.$$

The resulting projection of the data U is shown in Figure 4.11.

For the purpose of illustration, we recover the sets U_1 and U_2 from U. Figure 4.12 shows the reconstruction of the two surfaces U_1 and U_2. Note that the broad geometrical and topological features of U_1 and U_2 are recovered. The reconstruction involves a selection of suitable bands from the corresponding wavelet multiresolution decomposition.

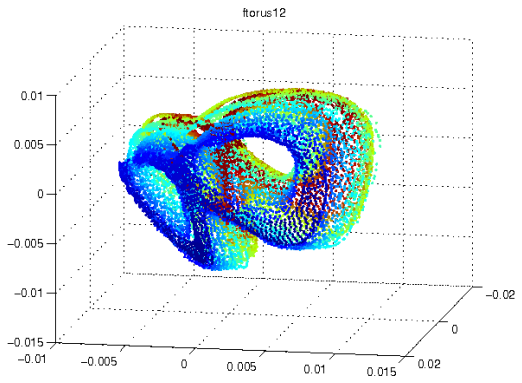

Figure 4.11: PCA projection of $U \subset \mathbb{R}^{64}$ onto $\mathbb{R}^3$

4.5 Conclusion and Future Steps

We have introduced the concept of frequency modulation maps and modulated manifolds as relevant objects in manifold learning and dimensionality reduction. We have developed

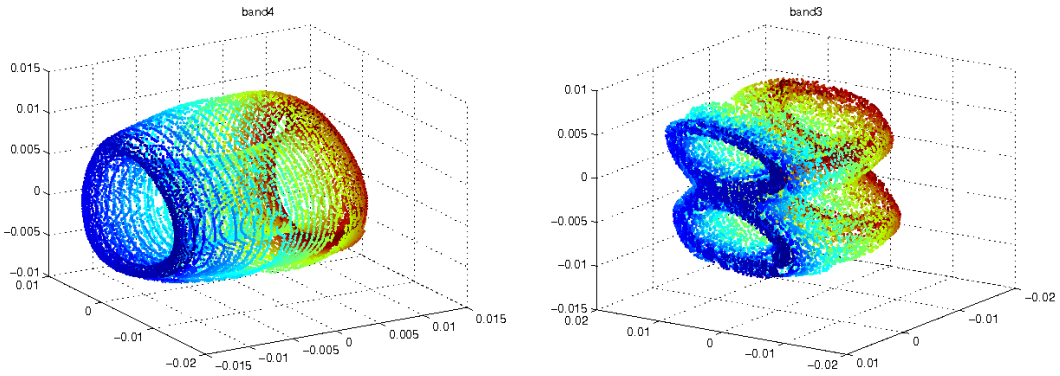

Figure 4.12: Reconstruction of U_1 (left), U_2 (right) from U

a numerical scheme, Algorithm 4.2.1, for computing the scalar curvature of a modulated manifold, along with its metric tensor. We applied the algorithm to two different test cases of frequency modulated manifolds. In one test case, we considered the sphere $\mathbb{S}^2$, and the other example relies on the torus $\mathbb{T}^2$. The numerical examples are illustrating the geometrical distortion incurred by the dimensionality reduction when relying on PCA projections. Moreover, we have shown that the standard linear PCA projection is outperformed by the nonlinear isomap projection, which achieves to recover the geometry of the modulated surface. But the concept of modulated manifold can also be used to construct more challenging datasets for nonlinear dimensionality reduction methods. The results of this chapter provide only a first insight into the nature of frequency modulation maps and modulated manifolds. Weaker structural assumptions on Ω and $\mathcal{M}$ (Alexandrov spaces, cell-complexes, etc) are possible useful extensions to cover a larger variety of engineering applications. To this end, the work on persistent homology, discrete Morse theory, or Alexandrov spaces [37, 38, 76] gives a suitable background.

5 Groupoid C^*-Algebras and Time-Frequency Analysis

We now study some topological aspects in time-frequency analysis in the context of dimensionality reduction using C^*-algebras and noncommutative topology. Our main objective is to propose and analyze new conceptual and algorithmic strategies for computing topological features of datasets arising in time-frequency analysis. The main result of our work is to illustrate how noncommutative C^*-algebras and the concept of Morita equivalence can be applied as a new type of analysis layer in signal processing. From a conceptual point of view, we use groupoid C^*-algebras constructed with time-frequency data in order to study a given signal. From a computational point of view, we consider persistent homology as an algorithmic tool for estimating topological properties in time-frequency analysis. The usage of C^*-algebras in our environment, together with the problem of designing computational algorithms, naturally leads to our proposal of using AF-algebras in the persistent homology setting. Finally, some computational toy examples are presented, illustrating some elementary aspects of our framework.

In this chapter, we present our main machinery for studying signals using tools from noncommutative C^*-algebras as explained in the Introduction 1. The core idea is to exploit the powerful concepts of groupoid theory and Morita equivalence in order to analyze geometrical/topological spaces constructed from signals in a time-frequency setting. The outline of this chapter is as follows. In Section 5.1.1 we present the basic concepts of our framework, together with several examples motivating our definitions. We present an overview of basic concepts in groupoid theory in Section 5.1.2. In Section 5.1.3 we present our basic results illustrating the usage of C^*-algebra structures in signal analysis. In Section 5.1.4 we present our proposal of integrating basic ideas of persistent homology together with AF-algebras technology. Finally, in Section 5.2, we discuss a toy example illustrating a (very) limited set of features of our theoretical developments.

5.1 Functional Clouds and C^*-Algebras

Our objective is to design tools for signal processing using properties of spaces constructed from a signal, in the same spirit as the construction of time-frequency data. As we will also shortly explain, a similar construction occurs also in the setting of nonlinear time series and the Taken's theorem. We present in this section basic definitions, where a core idea is to study the segmentation of a signal f, as classically performed in wavelet or short term Fourier transforms. Two basic concepts are the notions of a functional cloud M_f of a signal f, and its related pile F_f. The information encoded in these structures contains the interplay between local and global properties of f, and our plan is to use geometrical and topological tools for their analysis. The notion of a modulation map as introduced in Definition 4.2.1 provides the interaction with the dimensionality reduction and manifold learning framework. Some basic properties of a functional cloud and a pile are discussed in Section 5.1.3, where we study their topology by applying elementary notions of C^*-algebras and their K-theory. For instance, in Proposition 5.1.3 we consider the case of a signal decomposition $f = \sum f_i$, and a simplified scenario illustrating the topological interaction between the spaces M_f, $\{M_{f_i}\}_i$, and F_f.

5.1.1 Motivating and Defining Functional Clouds

Time-frequency transforms are fundamental tools in modern developments of harmonic analysis. An important task in this field is to construct adequate strategies for decomposing a function in order to study their time-frequency behavior. The basic procedure is to split a signal f in consecutive segments (sometimes denominated patches or chunks) that can be used to perform a global analysis of the function f. We now introduce an abstraction of these ideas by denoting (for lack of better names), a *functional cloud* and a *pile* as our basic objects of study. Given a real function in a locally compact group, we construct a functional cloud as a quotient space of a pile with an adequate equivalence relation. We will also generalize the equivalence relation to a more powerful concept of groupoid in order to use the rich theory readily available in this field, as well as preparing the terrain for new potential application problems.

Definition 5.1.1 (Functional cloud and pile of a function)**.** Given a locally compact group B, and a continuous function $\mathcal{F} : B \to \mathbb{C}$, we define the *functional cloud* for $\mathcal{F}$ and a measurable compact set A with $0 \in A \subset B$, as the set $M_{\mathcal{F},A} \subset L^1(A)$ with

$$M_{\mathcal{F},A} := \bigcup_{x \in B} \{\mathcal{F}_x : A \to \mathbb{C}\},$$

for $\mathcal{F}_x(y) := \mathcal{F}(x+y)$, $\forall\, y \in A$. The related *pile* is defined as the corresponding disjoint union:

$$F_{\mathcal{F},A} := \bigsqcup_{x \in B} \{\mathcal{F}_x : A \to \mathbb{C}\}.$$

We will abuse the notation, and we use also $F_{\mathcal{F},A}$ for the disjoint union of the graphs of the functions $\mathcal{F}_x$:

$$F_{\mathcal{F},A} := \bigsqcup_{x \in B} F_x \subset B \times A \times \mathbb{C}, \quad F_x := \operatorname{graph}(\mathcal{F}_x) = \{(y, \mathcal{F}_x(y)), y \in A\} \subset A \times \mathbb{C}.$$

Remark 5.1.1 (Notational comments)**.** Note that in the set $M_{\mathcal{F},A}$, no repeated elements are taken into account. Namely, only one representative $\mathcal{F}_x$ is used for different elements $x_1 \neq x_2$ where $\mathcal{F}_{x_1}(y) = \mathcal{F}_{x_2}(y)$, $\forall\, y \in A$. In contrast, in the disjoint union $F_{\mathcal{F},A}$ we keep track of repeated elements $\mathcal{F}_x$ for different values $x \in B$. It is clear that we can establish a link between these concepts using an adequate equivalence relation R and a quotient space $M_{\mathcal{F},A} = F_{\mathcal{F},A}/R$. As we will see later on, our main object of study is an important generalization of this construction using $M^G_{\mathcal{F},A} = F_{\mathcal{F},A}/G$ for a groupoid G acting on $F_{\mathcal{F},A}$. To avoid clutter the notation, we denote $M_{\mathcal{F},A}$ by $M_{\mathcal{F}}$ and $F_{\mathcal{F},A}$ by $F_{\mathcal{F}}$ when no confusion arises. We also remark that we use both notations $X_{\mathcal{F}}$ and $M_{\mathcal{F}}$ to denote a functional cloud of $\mathcal{F}$, but $X_{\mathcal{F}}$ is mostly preferred for the case of finite signals.

Remark 5.1.2 (Motivations)**.** The idea of functional cloud captures a basic time-frequency strategy by segmenting a function $f \in L^2(\mathbb{R})$ in chunks f_x, constructed with the translations $A_x = \{x + y, y \in A\}$ of a set A that can be defined as the support of a given window function. For instance, the standard wavelet procedure for computing the product $\langle f, \psi_{a,b} \rangle$, with a wavelet ψ, can be considered as a local analysis of f in a region defined by $\psi_{a,b}$. Remember that the region of influence of $\psi_{a,b}$ is defined by the scale a

and the translation factor b. In the concept of a functional cloud of f, the set A can be related to the support of ψ, but it also plays a generalization role for the scale factor a. The objective is to consider M_f as a set which encodes the local behavior of f (using the set A as a measuring tool) and whose geometrical properties are of interest.

Notice that in this particular concept, we do not take into account different resolution scales, as a single set A is used for constructing M_f. Currently, our main focus is to study a single scale level, and we leave for future work the analysis of geometrical and topological interactions between clouds $M_{f,A}$ with different scales A.

The conceptual motivation of a functional cloud is also in close relation to the concepts of a phase space and attractors in dynamical systems, as seen in the setting of the Taken's theorem (Example 5.1.5). Here, we use the term functional cloud in order to stress the relation to the concept of a point cloud data as used in dimensionality reduction. In the standard philosophy of time series analysis, as seen in dynamical systems, the interactions with classical Fourier analysis are usually not that taken into consideration. Here, we want to consider situations where a combination of these techniques could be of interest. We now present a family of examples where the concept of a cloud plays a significant role.

Example 5.1.1 (Cloud of a discrete 1d signal)**.** A typical example of a finite functional cloud is the point cloud dataset constructed by drawing samples from a signal f. More precisely, we consider, for a bandlimited signal $f \in L^2(\mathbb{R})$, the set of signal patches $X_f = \{x_i\}_{i=1}^m \subset \mathbb{R}^n$, $x_i = (f(t_{k(i-1)+j}))_{j=0}^{n-1} \in \mathbb{R}^n$. The construction of this cloud X_f involves the set of integers $A = \{0, \ldots, n-1\}$, and the identification $C(A, \mathbb{R}) = \mathbb{R}^n$, and we can see A as a subset indexing the values ℓ. Here, the regular sampling grid $\{t_\ell\}_{\ell=0}^{km-k+n-1}$ is constructed when considering the Nyquist-Shannon theorem for f.

Example 5.1.2 (Cloud of an Image)**.** A straightforward generalization of the previous example applies for the case of an image $f : [0,1]^2 \to [0,1]$. Here, the cloud M_f depends on a set of pixels represented by a representative patch A. In this particular example, the usefulness of a topological analysis of M_f lies, for instance, in the study of its connectivity (e.g. clustering aspects) for estimating qualitative as well as quantitative differences between different regions in the image f.

Example 5.1.3 (Cloud of a sinusoid)**.** Let $f : \mathbb{T} \to \mathbb{R}$ with $f(x) = \sin(x), x \in \mathbb{T} = \mathbb{R}/2\pi\mathbb{Z}$ and let $A = \{x \mod (2\pi), -\epsilon < x < \epsilon\}$. If $0 < \epsilon < \pi$ the functional cloud M_f is homeomorphic to a circle. This can be seen by considering the map $\phi : M_f \to \mathbb{T}$, $\phi(f_x) = x$. Notice that $f_x(z) - f_{x+\delta}(z) = \delta \cos(\xi)$, for $\xi \in]z + x, z + x + \delta[$, and we can ensure that ϕ is continuous, with the uniform norm in the space $C(A, \mathbb{R})$ using the estimation $\|f_x - f_{x+\delta}\|_\infty \leq |\delta|$. When considering the inverse function $\phi^{-1}(x) = f_x$, we can use the computation $f_{x+\delta}(z) - f_x(z) = f(z + x + \delta) - f(z + x)$ for $x - \epsilon < z < x + \epsilon$, and as f is continuous, we have $\lim_{\delta \to 0} f_{x+\delta}(z) = f_x(z)$, and as f_x is continuous we have ϕ^{-1} continuous. Finally, notice that ϕ is bijective only for the cases $0 < \epsilon < 2\pi$.

Example 5.1.4 (Cloud of a modulated path)**.** Consider an embedded manifold $\Omega \subset [-1,1]^d$, and a path (i.e. a continuous map) $\phi : [0,1] \to \Omega$. We construct $f : [0,1] \to \mathbb{R}$ as

$$f(x) = \sum_{i=1}^{d} \sin\Big(\int_0^x (\alpha_c^i + \gamma \phi_i(t))\, dt \Big),$$

such that the entries of the vector $\alpha_c = (\alpha_c^i)_{i=1}^d \in \mathbb{R}^d$ are center frequencies where a number of d frequency bands are located, and the value γ plays the role of a *bandwidth parameter*. The notation $\phi_i(x)$ refers to the i-th coordinate of $\phi(x)$. A basic question in this example is, given an open set A, what are the conditions for the path ϕ such that the functional cloud $M_f \subset C(A, \mathbb{R})$ "approximates" an homeomorphic copy of Ω. Here, the meaning of approximation can be considered, for instance, in the context of persistent homology. If the functional cloud of f is a path in $C(A, \mathbb{R})$ the question would be, given an adequate finite sampling of M_f, whether its persistent homology corresponds to the persistent homology of a finite sampling of Ω.

Another point of view for comparing the homology of Ω with a finite sampling of M_f can be expressed with conditions for approximating the homology of submanifolds with high confidence from random samples (see the work of Niyogi, Smale and Weinberger [75]). For this setting, the question would be to ask if a given finite sampling of M_f fulfills the conditions in [75] for reconstructing the homology of an homeomorphic copy of Ω in $C(A, \mathbb{R})$.

Example 5.1.5 (Time series and dynamical systems)**.** In dynamical systems and time series analysis, a similar segmentation procedure for a signal is implemented as in the functional cloud concept. In the framework of the celebrated Taken's theorem [84], we consider a dynamical system $\phi \in \mathrm{Diff}(M)$, defined as a diffeomorphism ϕ of a manifold M, a smooth function $h : M \to \mathbb{R}$, and a *delay coordinate map* $F(h, \phi) : M \to \mathbb{R}^n$, constructed by drawing consecutive samples from a time series:

$$F(h, \phi)(x) := (h(x), h(\phi(x)), h(\phi^2(x)), \ldots, h(\phi^{n-1}(x))), \quad x \in M.$$

The main result is that under suitable conditions, the map $F(h, \phi)$ is an embedding. Given a signal $f(k) = h(\phi^k(x)), k \in \mathbb{Z}$, the Taken's theorem provides a conceptual framework that justifies the estimation of geometrical and topological properties of M using the signal f. The key notion in this construction turns out to be a functional cloud $M_{f,A}$ for A an n-dimensional set.

Example 5.1.6 (Voice transform, wavelets and short term Fourier analysis)**.** In time-frequency analysis and voice transforms, a crucial component is the way a locally compact group $\mathcal{G}$ acts in a Hilbert space of functions $\mathcal{H}$. This action is an irreducible and unitary group representation, $\pi : \mathcal{G} \to \mathcal{U}(\mathcal{H})$, (for $\mathcal{U}(\mathcal{H})$ unitary operators in $\mathcal{H}$) that fulfills square integrable conditions. With this representation the *voice transform* is constructed as [18, Formula 17.3, p387]:

$$V_\psi : \mathcal{H} \to C(\mathcal{G}) \quad \text{with} \quad V_\psi f(x) = \langle f, \pi(x)(\psi) \rangle, \ f, \psi \in \mathcal{H}, x \in \mathcal{G}.$$

The short term Fourier transform (STFT) and wavelet transforms are typical examples where ψ corresponds to a window function for the former and to a wavelet for the latter. These transforms represent an interplay between $\mathcal{H}$ and $C(\mathcal{G})$, that allows to analyze the function f, by porting its information to a setting defined by $\mathcal{G}$. Another way to rephrase this procedure is that the transformation V_ψ "unfolds" data present in f, using $\mathcal{G}$ as an analysis environment. In the case of the STFT transform, the Weyl-Heisenberg group represents the time-frequency background to which information from f is translated. In the case of the wavelet transform, the affine group provides a time-scale representation of

a function. In these situations, a fundamental objective is to understand the components of f, using $\mathcal{G}$ and V_ψ as observation tools. Discretization aspects of these transforms have been designed in the setting of coorbit theory and frames of a Hilbert space $\mathcal{H}$ [32–34]. Recall that a frame of $\mathcal{H}$ is a collection of vectors $F = \{f_i\}_{i\in I} \subset \mathcal{H}$, such that there exist two constants $0 < A \leq B$, with $A\|f\|^2 \leq \sum_{i\in I} |\langle f, f_i\rangle|^2 \leq B\|f\|^2$, for any $f \in \mathcal{H}$.

In the particular case of Gabor analysis, the voice transform is defined as

$$V_g f(b, w) = \int_{\mathbb{R}} f(t)g(t-b)e^{-2\pi i t w} dt,$$

$f \in L^2(\mathbb{R})$ and we can define two basic functional clouds in this setting. The cloud $X_f = \{x_b\}_b$ is defined with chunks $x_b = fg_b$ by splitting the function f, and using $g_b(t) = g(t-b)$ for a window function g. We can also define a cloud of the corresponding spectral view using

$$X_{V_g f} = \{V_g f(b, .)\}_b.$$

Due to the orthogonality property of the Fourier transform, the geometrical and topological properties of $X_f = \{x_b\}_b$, are the same as the ones of the set $X_{V_g f} = \{V_g f(b, .)\}_b$ (i.e. X_f and $X_{V_g f}$ are isometric spaces). But it is crucial to notice that highly nontrivial geometrical and topological changes can occur in $X_{V_g f}$ when applying time-frequency operations to the function f (e.g. filters and convolution operations). The interplay between the geometry of $X_{V_g f}$ and the time-frequency properties of f is a main topic in our research (a toy-example of this interaction will be discussed in Section 5.2, and can also be found in [45] and its corresponding simulation).

Studying M_f with F_f

In order to study the functional cloud M_f, the pile F_f is used for estimating its geometrical and topological properties. The motivation for this strategy is based on standard procedures of noncommutative geometry. A prototypical situation is to study the geometry of a quotient space $X = Y/\sim$ using a C^*-algebra constructed with the equivalence relation $\sim$. The relation between a pile and a function cloud can be interpreted as quotient space using an equivalence relation (and more generally a groupoid). These conceptual interactions will be the main topic we will investigate.

The basic idea of a pile F_f is to study each segment f_x of the function f, by keeping track their relationship with respect to the parameter $x \in B$. This is in contrast with the construction of a functional cloud M_f, where we study the interactions between the vectors f_x, irrespectively of their positions x. Basic standard procedures in time-frequency analysis are related to this concept. For instance, when studying the time-frequency representation of a signal f, an important objective is to keep track to the time evolution of different frequency components of f. For example, the topic of *partial tracking* is a classical signal processing task which keeps track of harmonic information in a signal. Speech analysis is a typical example, where vocal information is represented in the time-frequency plane by varying harmonical components. The time-frequency data in this context is obtained by considering the Fourier transform of each segment f_x in the pile. We now describe an important particular scenario that justifies the terminology *pile*.

Proposition 5.1.1 (Pile as a foliated manifold)**.** *Let F_f be a pile for a continuous function $f : B \to \mathbb{R}$, where B is a finite dimensional Hilbert space, and A an open set with $0 \in A \subset B$. The set F_f is a manifold of dimension $2\dim(B)$, and it has a foliation structure of dimension $\dim(B)$.*

Proof. This easily follows by considering the graph of the function $\phi : B \times A \to \mathbb{R}$, $\phi(x, y) = f_x(y)$. As f is continuous and $f_x(y) = f(x + y)$, ϕ is a continuous function. The graph of ϕ can be identified with $\{(x, y, f_x(y), (x, y) \in B \times A\}$, and therefore it is also identified with the pile F_f. The map ϕ exhibits a chart from the open set $B \times A$ to F_f, which actually relates these two sets homeomorphically, and we obtain a manifold structure for F_f. As $B \times A$ is an open subset of $B \times B$, the dimension of F_f is therefore equal to $2\dim(A)$. The foliation structure of F_f is a straightforward consequence of its construction, where the leaves are given by F_x, $x \in B$, and their dimension is $\dim(B)$. ■

Example 5.1.7 (Pile for the sinusoidal example)**.** In our previous Example 5.1.3 of the function $f(x) = \sin(x), x \in \mathbb{T} = \mathbb{R}/\mathbb{Z}$ with $A = \{x \mod (2\pi), -\epsilon < x < \epsilon\}$, the pile F_f can be identified with a surface ($\dim(F_f) = 2$) described by the graph of the function $\phi : \mathbb{T}\times]-\epsilon, \epsilon[\to \mathbb{R}$, $\phi(x, y) = \sin(x + y)$, and for the corresponding leaves we have $\dim(F_x) = 1$.

Remark 5.1.3 (Relating F_f and M_f)**.** There is an obvious relation between a pile F_f and a functional cloud M_f. If we define an equivalence relation in F_f, as $R = \{(u, v) \in F_f \times F_f,\ d(p(u), p(v)) = 0\}$, for the projection map $p : F_f \to M_f$, $p((x, y, f_x(y)) = f_x$, and d is the metric induced by the uniform norm in $C(A, \mathbb{R})$, we have an identification (as sets) between F_f/R and M_f. This remark has important implications when using the pile F_f for studying the geometry and topology of M_f. Indeed, the relations between a space X and a quotient space X/R for an equivalence relation R (or more generally a groupoid G) is an important source of examples in the noncommutative geometry world. In this field, there is a very important machinery for studying quotients X/R using C^*-algebras defined on the spaces X and R. This framework provides important tools for studying pathological quotients, sometimes called "bad quotients" (e.g. X/R non Hausdorff while X being Hausdorff). A prototypical example is the noncommutative torus, defined as the quotient of the 2-torus $\mathbb{T}^2 = \mathbb{R}^2/\mathbb{Z}^2$ with the Kronecker foliation constructed from the differential equation $dy = \theta dx$ [21]. But it is very important to remark that the tools from noncommutative geometry are also useful for studying objects in the commutative world.

Remark 5.1.4 (Relation to Modulated Spaces)**.** Before using the noncommutative strategy for studing functional clouds and piles, as described in the previous Remark 5.1.3, we notice an important connection with modulated spaces which makes more explicit the interaction of these problems with modern tools from manifold learning and dimensionality reduction. Recall that in Definition 4.2.1, we introduced the concept of a modulated space using $\{\phi_k\}_{k=1}^d \subset \mathcal{H}$ a set of vectors in an Euclidean space $\mathcal{H}$, and $\{s_k : \Omega \to \mathcal{C}_{\mathcal{H}}(\mathcal{H})\}_{k=1}^d$ a family of continuous maps from a space Ω to $\mathcal{C}_{\mathcal{H}}(\mathcal{H})$. We recall that we say that $\mathcal{M} \subset \mathcal{H}$ is a $\{\phi_k\}_{k=1}^d$-*modulated space* if $\mathcal{M} = \left\{\sum_{k=1}^d s_k(\alpha)\phi_k,\ \alpha \in \Omega\right\}$. In this case, the map $\mathcal{A} : \Omega \to \mathcal{M}$, $\alpha \mapsto \sum_{k=1}^d s_k(\alpha)\phi_k$, is denoted *modulation map*. The idea of a *modulation*

map, summarizes the well-known concept of modulation in signal processing, using a geometrical and topological language. The fundamental objective of a modulation map is to construct spaces $\mathcal{M}$ using generating functions $\{\phi_k\}$ and a parametrization space Ω. This concept is a related, but different component in the machinery of a functional cloud and piles. An explicit example of this concept is given by a *frequency modulation map*, which considers $\phi(t) = \sin(t)$ and a modulation using the coordinates of points in a space Ω [43, 45, 46]. We now review our previous example of the cloud of a sinusoid that also fits in this setting.

Example 5.1.8 (Cloud of a sinusoid as a modulated space)**.** We use again our previous example for the cloud of a sinusoid to show a modulated space with $f(x) = \sin(x), x \in \mathbb{T} = \mathbb{R}/2\pi\mathbb{Z}$ and $B =]-\epsilon, \epsilon[\mod (\mathbb{T})$. Here, the map ϕ is a modulation map when $0 < \epsilon < 2\pi$, and for this case, the functional cloud M_f is homeomorphic to a circle.

5.1.2 Basics on Groupoids Crossed Products and C^*-Dynamical Systems

In noncommutative geometry, the fundamental interplay between locally compact Hausdorff topological spaces and (commutative) C^*-algebras as explained in the Gelfand-Naimark theory [36, 89] has been extended to an important framework using noncommutative C^*-algebras [21, 41, 56]. The multiple conceptual and application developments over the last decades is a evident indication of its breath and increasing importance in mathematics. A basic example of a noncommutative space, is the noncommutative torus [21, 22], which can be defined as a crossed product C^*-algebra $\mathcal{A}_\theta = C^1(S^1) \rtimes_{R_\theta} \mathbb{Z}$, for a rotation $R_\theta(x) = (x + \theta) \bmod 1$, $x \in \mathbb{T}$. In this construction, the algebra $C^1(S^1)$ can be replaced with other algebras depending on the type of analysis and resolution required: for geometrical, topological and measure theoretical properties, the spaces that can be used are $C^\infty(S^1) \subset C^1(S^1) \subset L^1(S^1)$, respectively. The noncommutative torus is just one particular example in the world of noncommutative geometry, and it belongs to the general theory of spaces of leaves of foliations. But an even more general setting can be described with the powerful theory of groupoids. The important application of groupoids in noncommutative geometry is given by the concept of noncommutative quotients, and a particular example is the analysis of quotient spaces $X = Y/\sim$ of an equivalence relation $\sim$ in Y. We remark that there is an important family of C^*-algebras (the AF-algebras) particularly useful for studying finite structures, as required in applications of signal processing and data analysis. We now introduce some basic tools from groupoid theory we need for our setting.

Groupoids C^*-algebras

A groupoid G can be defined as a small category where each morphism has an inverse [21, 24]. More explicitly, we say that a groupoid over a set X is a set G together with two maps $r, s : G \to X$, called the *range and source maps*, and a composition law (or product) $\circ : G^{(2)} \to G$ denoted $\gamma \circ \eta = \gamma\eta$, where

$$G^{(2)} = \{(\gamma, \eta) \in G \times G, r(\gamma) = s(\eta)\},$$

and $r(\gamma\eta) = r(\gamma), s(\gamma\eta) = s(\eta)$, $\gamma(\eta\xi) = (\gamma\eta)\xi$. We additionally have an embedding $e : X \to G$ and an inversion map $i : G \to G$ with $e(r(\gamma)) = \gamma = \gamma e(s(\gamma))$, and $i(\gamma)\gamma = e(s(\gamma))$, $\gamma i(\gamma) = e(r(\gamma))$. We have an hierarchy of sets defined as $G^{(0)} = e(X) \simeq X$ (the *unit space*), $G^{(1)} = G$, and $G^{(2)}$ as previously defined. For $u \in G^{(0)}$ we define $G_u = s^{-1}(u)$ and $G^u = r^{-1}(u)$.

An alternative way to introduce a groupoid is to start with a subset $G^{(2)}$ of $G \times G$ as the set of composable pairs, an inverse operation $G \to G, \gamma \mapsto \gamma^{-1}$ for each $\gamma \in G$, and define the maps r and s with $r(\gamma) = \gamma\gamma^{-1}$, $s(\gamma) = \gamma^{-1}\gamma$. From the axioms, the maps r, s have a common image $G^{(0)}$ as the unit space, meaning that $\gamma s(\gamma) = r(\gamma)\gamma = \gamma$, for each $\gamma \in G$ [13, Section 2.1].

The *isotropy group* for a unit $u \in X$ is defined as

$$G_u^u = \{\gamma \in G, s(\gamma) = r(\gamma) = u\} = s^{-1}(u) \cap r^{-1}(u),$$

and in general, we define $G_v^u = r^{-1}(u) \cap s^{-1}(v)$. The *isotropy group bundle* is defined as $G' = \{\gamma \in G, s(\gamma) = r(\gamma)\}$. When the groupoid is seen as a category, the set of objects is $\mathrm{Ob}(G) = G^{(0)}$, and the morphisms are identified with G itself [54, Definition 2.1].

A *homomorphism of groupoids* G and Γ is a map $\phi : G \to \Gamma$, such that $(\gamma, \eta) \in G^{(2)}$, then $(\phi(\gamma), \phi(\eta)) \in \Gamma^{(2)}$, and $\phi(xy) = \phi(x)\phi(y)$. We have, in particular, $\phi(\gamma^{-1}) = (\phi(\gamma))^{-1}$, and $\phi(G^{(0)}) \subset \Gamma^{(0)}$ [13, p73].

We will consider groupoids where both $G^{(0)}$ and $G^{(1)}$ have topologies such that the maps $(\gamma, \eta) \mapsto \gamma\eta$ from $G^{(2)} \to G$, and $\gamma \mapsto \gamma^{-1}$ from G to G are continuous [39, Definition 1.8]. In the following, we denote by G a second countable locally compact Hausdorff groupoid.

Important examples of groupoids are equivalence relations, groups, and group actions. For instance, with an equivalence relation $R \subset X \times X$, we define a groupoid $G = G^{(1)} = R$, $G^{(0)} = X$, $r(x, y) = x, s(x, y) = y$. For a group Γ, we can define the groupoid $G = \Gamma$, $G^{(0)} = \{e\}$ (the unit of Γ), and the groupoid composition is the group product. For a group Γ acting on a set X, we can define $G = X \times \Gamma$, $G^{(0)} = X$, $r(x, g) := x, s(x, g) := xg$, for all $(x, g) \in X \times \Gamma$, and the product is defined as $(x, g)(xg, h) = (x, gh)$. Another important example of groupoid is a *group bundle* defined as a disjoint union of groups $\{\Gamma_i\}_{i\in U}$ indexed by a set U. The composition between two elements is defined by the corresponding group composition if the elements are in the same group. A groupoid is a group bundle if $s(x) = r(x)$ for all $x \in G$, and for this case, the groupoid G equals its isotropy group bundle G' (see [13, 2.3 p76]).

Definition 5.1.2 (Haar Systems for Groupoids [13, Section 2.4])**.** The concept of a Haar system generalizes, to groupoids, the notion of a Haar measure for locally compact groups. A Haar system is family $\{\lambda^u\}_{u\in G^{(0)}}$ of Radon Measures on G with $\text{supp}(\lambda^u) = G^u$, and $u \mapsto \int f(\gamma)d\lambda^u(\gamma)$ is a continuous function from $G^{(0)}$ to $\mathbb{C}$ for all $f \in C_c(G)$ (the space of complex-valued continuous functions with compact support). Additionally, we require

$$\int f(\eta)d\lambda^{r(\gamma)}(\eta) = \int f(\gamma\eta)d\lambda^{s(\gamma)}(\eta),$$

for all $f \in C_c(G)$, and all $\gamma \in G$.

Remark 5.1.5 (Hilbert bundles and direct integrals)**.** In groupoid theory and groupoid representations, the concept of Hilbert bundles has the same fundamental role as the concept of Hilbert space in group representations [13, Section 2.6]. A Hilbert bundle is constructed with a family of Hilbert spaces $\mathcal{H} = \{H(x)\}_{x\in X}$ indexed by X, which can be more precisely denoted as a disjoint family $X * \mathcal{H} := \{(x, \chi), \chi \in H(x)\}$ (see [72, Chapter 3]). In general, for X_1, X_2, two spaces with maps $\tau_i : X_i \to T, i = 1, 2$, one defines [10]

$$X_1 * X_2 := \{(x, y) \in X_1 \times X_2 : \tau_1(x) = \tau_2(y)\}.$$

If X is an analytic Borel space, then $X * \mathcal{H}$ is denominated a *analytic Borel Hilbert bundle* with the natural projection $\pi : X * \mathcal{H} \to X$, and the corresponding set of Borel sections is denoted as $B(X * \mathcal{H})$ [10, Definition 3.61 p109].

The concept of a *direct integral* of the spaces $\{H(x)\}_{x\in X}$ is defined for an analytic Borel Hilbert bundle $X * \mathcal{H}$, and μ a measure in X, as (see [10, Definition 3.80 p118], [13, p83])

$$\mathcal{L}^2(X * \mathcal{H}, \mu) = \{f \in B(X * \mathcal{H}), \int_X ||f(x)||^2_{H(x)}d\mu(x) < \infty\}.$$

The space $\mathcal{L}^2(X * \mathcal{H}, \mu)$, denoted also as $\int_X^{\oplus} H(x)d\mu(x)$, is a Hilbert space with the product $\langle f, g\rangle = \int \langle f(x), g(x)\rangle_{H(x)}d\mu(x)$. When X is a discrete space $\int_X^{\oplus} H(x)d\mu(x)$ is

just $\bigoplus_{x\in X} H(x)$, and in general case, if the $H(x)$'s are the fibers of the vector bundle $\mathcal{H}$, the direct integral $\int_X^{\oplus} H(x)d\mu(x)$ is the space of sections that are square integrable with respect to μ [36, p223].

Given a Borel bundle $X*\mathcal{H}$ are constructed with a *Borel field of operators* defined with a family of bounded linear maps $T(x) : H(x) \to H(x)$, which can be used to define the operator $\int_X^{\oplus} T(x)d\mu(x)$, also denoted as $T \in B(L^2(X*\mathcal{H},\mu))$, and denominated the *direct integral* of $T(x)$ (see [10, Definition 3.88 p120, Proposition 3.91]). Recall that in harmonic analysis, the direct integral is a basic concept in the decomposition of representations of groups. For instance, in the case of locally compact Abelian groups, a unitary representation is equivalent to a direct integral of irreducible representations, and in more general situations, as locally compact groups, a similar mechanism (the Plancherel theorem) is implemented for the regular representation [36, Theorem 7.36, Section 7.5].

Remark 5.1.6 (Isomorphism groupoid for a Borel Hilbert bundle and groupoid representations)**.** Given a Borel Hilbert bundle, its fibred structure gives rise to an isomorphism groupoid that will be used to define unitary groupoid representations. The *isomorphism groupoid* for an analytic Hilbert bundle $X * \mathcal{H}$ is $\mathrm{Iso}(X * \mathcal{H}) = \{(x, V, y), V : H(y) \to H(x)\,\text{unitary}\}$, with composable pairs $\mathrm{Iso}(X * \mathcal{H})^{(2)} = \{((x, V, y), (w, U, z)) \in \mathrm{Iso}(X * \mathcal{H}) \times \mathrm{Iso}(X * \mathcal{H}), y = w\}$, and the composition is defined as $(x, V, y)(y, U, z) = (x, VU, z)$, $(x, V, y)^{-1} = (y, V^*, z)$ [10, Definition 3.67 p111], [13, p83].

Definition 5.1.3 (Groupoid representation)**.** A *groupoid representation* of a locally compact Hausdorff groupoid G is a triple $(\mu, G^{(0)} * \mathcal{H}, L)$ with μ a quasi invariant measure in $G^{(0)}$, $G^{(0)} * H$ is an analytic Borel Hilbert bundle, and $L : G \to \mathrm{Iso}(G^{(0)} * \mathcal{H})$ a Borel groupoid homomorphism with $L(\gamma) = (r(\gamma), L_\gamma, s(\gamma))$, for a unitary $L_\gamma : H(y) \to H(x)$ [10, Definition 3.76 p117], [13, p83].

Definition 5.1.4 (Groupoid C^*-algebra)**.** Given a Haar system $\{\lambda^u\}_{u\in G^{(0)}}$ of a locally compact Hausdorff groupoid G, we define, for $f, g \in C_c(G)$, the convolution as

$$(f * g)(\gamma) = \int f(\gamma\eta)g(\eta^{-1})\, d\lambda^{s(\gamma)}(\eta) = \int f(\eta)g(\eta^{-1}\gamma)\, d\lambda^{r(\gamma)}(\eta)$$

and the involution by $f^*(x) = \overline{f(x^{-1})}$. With these operations, $C_c(G)$ is a topological $*$-algebra (see [13, Section 3.1] and [78]). In order to define a C^*-algebra with $C_c(G)$, we can select several norms giving rise to the full and reduced C^*-algebras for the groupoid G. The basic step for constructing these norms, is to consider a *representation* of $C_c(G)$, defined as a $*$-homomorphism from $C_c(G)$ into $B(H)$, the bounded operators for some Hilbert space H. Every groupoid representation $(\mu, G^{(0)} * \mathcal{H}, L)$ can be related to a representation of $C_c(G)$ with $H = \int_{G^{(0)}}^{\oplus} H(x)d\mu(x)$, for $\mathcal{H} = \{H(x)\}_{x\in G^{(0)}}$ [13, p87].

The analogue in groupoid theory of the regular representation of a group is a representation of $C_c(G)$ given by an operator $\mathrm{Ind}\mu$ in $L^2(G)$ with $\mathrm{Ind}\mu(f)\xi(x) = (f * \xi)(x)$. The *reduced norm* is constructed as $\|f\|_{red} = \|\mathrm{Ind}\mu(f)\|$, making $C_c(G)$ into a C^*-algebra (see [13, p87] for details).

Groupoids actions and orbit spaces

The concept of a groupoid action G on X generalizes the concept of a group action by considering partially defined maps on pairs $(\gamma, x) \in G \times X$. This is a natural consequence of the partially defined multiplication in a groupoid [39, Section 1.2].

Definition 5.1.5 (Groupoid action)**.** A (left) action of a groupoid G in a set X is a surjection $r_X : X \to G^{(0)}$, together with a map

$$G * X = \{(\gamma, x) \in G \times X, s(\gamma) = r_X(x)\} \to X, \quad (\gamma, x) \mapsto \gamma x,$$

with the following three properties (see [72, Chapter 2] and [39, Definition 1.55]):

1- $r(\gamma x) = r(\gamma)$ for $(\gamma, x) \in G * X$.

2- If $(\gamma_1, x) \in G * X$ and $(\gamma_2, \gamma_1) \in G^{(2)}$, then $(\gamma_2\gamma_1, x), (\gamma_2, \gamma_1 x) \in G * X$ and

$$\gamma_2(\gamma_1 x) = (\gamma_2\gamma_1)x.$$

3- $r_X(x)x = x$ for all $x \in X$.

With these conditions, we say that X is a (left) G-space. We can define in a similar way right actions and right G-spaces by denoting with s_X the map from X to $G^{(0)}$, and using $X * G = \{(x, \gamma) \in X \times G : s_X(x) = r(\gamma)\}$ instead of $G * X$.

The action of a groupoid in a set defines an equivalence relation that can be used to construct the *orbit space*, which represents a main object to study.

Definition 5.1.6 (Orbit space for groupoid actions)**.** Given a left G-space X, we define the *orbit equivalence relation* on X defined by G with $x \sim y$ if and only if there exist a $\gamma \in G$, with $\gamma \cdot x = y$, and the corresponding quotient space is the *orbit space*, and denoted by X/G with elements $G \cdot x$ or $[x]$. The same notation is used for right G-spaces, but in situations where X is both a left G-space and right H-space, the orbit space with respect to the G-action is denoted $G\backslash X$ and the orbit space with respect to the H-action is denoted by X/H [39, Definition 1.67].

In the particular case where $X = G^{(0)}$, the equivalence relation can be defined as $u \sim v$ iff $G_v^u \neq \emptyset$. The orbits $[u]$ for $u \in G^{(0)}$ are the corresponding equivalence classes and the orbit space is denoted by $G^{(0)}/G$. The graph of the equivalence relation can be described as $R = \{(r(\gamma), s(\gamma)), \gamma \in G\}$. We say that the subset $A \subset G^{(0)}$ is *saturated* if it contains the orbits of its elements, and we say that the groupoid G is *transitive* or *connected* if it has a single orbit. Alternatively, we say that G is *transitive* or *connected* if there is a morphism between any pair of elements in $G^{(0)}$ [54, Example 2.2.2, p50] [68, p20] For each orbit $[u]$ of a groupoid G, the set $G|_{[u]}$ is a transitive groupoid denominated *transitive component* of G. An important property is that each groupoid is a disjoint union of its transitive components (see [13, p73] for details). In a similar topic we also mention that, seen as a category, each groupoid is equivalent (but not isomorphic) to a category of disjoint union of groups (see [25, Appendix A] for a very short but nice survey on this topic).

We can now state some basic results we need on the characterization of a C^*-algebra of a transitive groupoid:

Theorem 5.1.1 (Muhly-Renault-Williams: Transitive Groupoids and their C^*-algebras [13,73])**.** *Let G be a transitive, locally compact, second countable and Hausdorff groupoid, then the (full) C^*-algebra of G is isomorphic to $C^*(H) \otimes K(L^2(\mu))$, where H is the isotropy group G_u^u at any unit $u \in G^{(0)}$, and μ a measure on $G^{(0)}$, $C^*(H)$ denotes the group C^*-algebra of H, and $K(L^2(\mu))$ denotes the compact operators on $L^2(\mu)$.*

Definition 5.1.7 (Free and proper groupoid actions)**.** The action of a groupoid G in a set X is *free* if the map $\Phi : G*X \to X \times X$, $(\gamma, x) \mapsto (\gamma x, x)$, is injective [10, Conventions 1.1]. This can also be rephrased by saying that $\gamma x = x$ implies γ is a unit ($\gamma \in G^{(0)}$) [39, Definition 1.83]. The action is *proper* if the map Φ is proper (meaning that the inverse images of compact sets are compact). A main property for proper actions is that the orbit space X/G is locally compact and Hausdorff if G acts property on the locally compact space Hausdorff space X [39, Proposition 1.85].

Groupoid dynamical systems and groupoid crossed products

A natural consequence of the fibred properties of a groupoid is the usage of fibred C^*-algebras when generalizing the concept of dynamical systems to the groupoid language.

Remark 5.1.7 ($C_0(X)$-algebras and C^*-bundles)**.** A $C_0(X)$-*algebra* is a C^*-algebra with a nondegenerate homomorphism Φ_A from $C_0(X)$ (the space of continuous functions vanishing at infinity on X) into $Z(M(A))$, where $M(A)$ denotes the multiplier algebra of A, and $Z(A)$ denotes the center of A. Here, Φ_A is nondegenerate when $\Phi_A(C_0(X)) \cdot A = \text{span}\{\Phi_A(f)a, f \in C_0(X), a \in A\}$ is dense in A (see [93] for details).

Remember that the multiplier algebra $M(A)$ of A is the maximal C^*-algebra containing A as an essential ideal (see [6, Chapter 4]). For instance, if A is unital, $M(A) = A$. If $A = C_0(X)$, the continuous functions with compact support in a locally compact Hausdorff space, then $M(A) = C_b(X)$, the continuous functions bounded on X. If A is the space of compact operators on a separable Hilbert space H, $M(A) = B(H)$, the C^*-algebra of all bounded operators on H. Recall also that the *center* of an algebra A is the commutative algebra $Z(A) = \{x \in A, xa = ax \ \forall a \in A\}$. This concept plays a crucial role as, for instance, in the theory of Von Neumann algebras (algebras of bounded operators on a Hilbert space). Von Neumann algebras with a trivial center are called *factors*, and these are basic building blocks for general Von Neumann algebras via direct integral decompositions.

An *upper semicontinuous C^*-bundle* over X, a locally compact Hausdorff space, is a topological space $\mathscr{A}$ with a continuous open surjection $p_{\mathscr{A}} = p : \mathscr{A} \to X$ such that the fiber $A(x) = p^{-1}(x)$ is a C^*-algebra with the following conditions. First, the map $a \mapsto \|a\|$ is upper-continuous from $\mathscr{A}$ to $\mathbb{R}^+$ (i.e. for all $\epsilon > 0$, the set $\{a \in \mathscr{A}, \|a\| < \epsilon\}$ is open). The operations sum, multiplication, scalar multiplication, and involution in the algebra $\mathscr{A}$ are continuous. Finally, if $\{a_i\}$ is a net in $\mathscr{A}$ with $p(a_i) \to x$, and $\|a_i\| \to 0$, then $a_i \to 0_x$, with 0_x the zero element of $A(x)$.

Two fundamental properties of $C_0(X)$-algebras are the fact that there is a one to one correspondence between $C_0(X)$-algebras and upper-semicontinuous bundles C^*-bundles [10, Definition 3.12 p91], and that the primitive ideal space of a $C_0(X)$-algebra is fibred over X [10, p93].

The interaction between $C_0(X)$-algebras and upper-semicontinuous bundles C^*-bundles is given by the fact that the C^*-algebra $A = \Gamma_0(X, \mathscr{A})$ of continuous sections of $\mathscr{A}$ vanishing at infinity, is a $C_0(X)$-algebra, as we now explicitly rephrase in the following example.

Example 5.1.9 ($C_0(X)$-algebras)**.** A basic example of a $C_0(X)$-algebra is given by $A = C_0(X, D)$, where D is any C^*-algebra, X is a locally compact Hausdorff space, and $\Phi_A(f)(a)(x) = f(x)a(x)$, for $f \in C_0(X)$, $a \in A$. For this example, each fiber $A(x)$ is identified with D. [39, Example 3.16, p91]

As previously mentioned, a fundamental example of a $C_0(X)$-algebra is $A = \Gamma_0(X, \mathscr{A})$, for a $\mathscr{A}$ upper-semicontinuous C^*-bundle, with $\Phi_A(\phi)f(x) = \phi \cdot f(x) = \phi(x)f(x)$, for $\phi \in C_0(X)$, and $f \in A$. [39, Example 3.18, p91]

Definition 5.1.8 ($(\mathscr{A}, G, \alpha)$ Groupoid dynamical system)**.** Let G be a groupoid with Haar system $\{\mu^u\}_{u\in G^{(0)}}$, and $\mathscr{A}$ is an upper-semicontinuous C^*-bundle over $G^{(0)}$. An action α of G on $A = \Gamma_0(X, \mathscr{A})$ is a family of $*$-isomorphisms $\{\alpha_\gamma\}_{\gamma\in G}$ with $\alpha_\gamma : A(s(\gamma)) \to A(r(\gamma))$, for all $\gamma \in G$, $\alpha_{\gamma\eta} = \alpha_\gamma\alpha_\eta$ for all $(\gamma, \eta) \in G^{(2)}$, and the map $G * \mathscr{A} \to \mathscr{A}$, $(\gamma, a) \mapsto \alpha_\gamma(a)$ is continuous. With these conditions, the triple $(\mathscr{A}, G, \alpha)$ is a *groupoid dynamical system* (see [10, Definition 2.2]).

Example 5.1.10 ($(\mathscr{C}_X, G, \mathrm{lt})$ Groupoid dynamical system)**.** A basic example of a groupoid dynamical system is $(\mathscr{C}_X, G, \mathrm{lt})$, where G is a groupoid acting on a second countable locally compact Hausdorff space X, and the upper semi-continuous C^*-bundle $\mathscr{C}_X = G^{(0)} * \{C_0(r_X^{-1}(u))\}_{u\in G^{(0)}}$ is associated with the $C_0(G^{(0)})$-algebra $C_0(X)$. The action of G on X induces an action of G on $\mathscr{C}_X$ by left translation [11, Example 3.30, Proposition 3.31, p25],

$$\mathrm{lt}_\gamma(f) : C_0(r_X^{-1}(s(\gamma))) \to C_0(r_X^{-1}(r(\gamma))), \quad x \mapsto f(\gamma^{-1} \cdot x).$$

Remark 5.1.8 (Reduced crossed product of a groupoid dynamical system)**.** With a groupoid dynamical system $(\mathscr{A}, G, \alpha)$, we can construct a convolution algebra that can be completed to the reduced crossed product, which is one possible generalization of the concept of a crossed product. An important tool for this task is the *pullback bundle* $r^*\mathscr{A}$ of a bundle $\mathscr{A}$ over X, with bundle map $p_{\mathscr{A}} : \mathscr{A} \to X$. The pullback bundle is defined as

$$r^*\mathscr{A} := \{(\gamma, a), r(\gamma) = p_{\mathscr{A}}(a)\},$$

for $r : G \to X$. The corresponding bundle map for $r^*\mathscr{A}$ is $q : r^*\mathscr{A} \to G$, with $q(\gamma, a) = \gamma$ [39, Definition 3.33 p97].

The first step for constructing the groupoid crossed product is a property [10, Proposition 2.4] ensuring that, given a groupoid G with Haar system $\{\lambda^u\}_{u\in G^{(0)}}$, the set of continuous compactly supported sections of $r^*\mathscr{A}$, denoted by $\Gamma_c(G, r^*\mathscr{A})$, is a $*$-algebra with respect to the operations

$$(f * g)(\gamma) := \int_G f(\eta)\alpha_\eta(g(\eta^{-1}\gamma))d\lambda^{r(\lambda)}(\eta), \quad f^*(\gamma) := \alpha_\gamma(f(\gamma^{(-1)})^*).$$

The second step we consider here is to complete $\Gamma_c(G, r^*\mathscr{A})$ with the *reduced norm* $\|f\|_r = \sup\{\|\mathrm{Ind}\pi(f)\|, \pi \text{ is a } C_0(G^{(0)}) \text{ linear representation of } A\}$ (see [10, p4] for details). We define the completion of $\Gamma_c(G, r^*\mathscr{A})$ with the norm $\|\|_r$ as the *reduced crossed product* of the dynamical system $(\mathscr{A}, G, \alpha)$, and we denoted it with $\mathscr{A} \rtimes_{\alpha,r} G$. Notice that this procedure is the important strategy of using representations of an algebra in order to construct a meaningful norm that leads to a C^*-algebra construction denominated *enveloping C^*-algebra* (see [41, Definition 12.2, p523]).

Remark 5.1.9 (Morita equivalence)**.** Representation theory plays a crucial role in the interplay between topological spaces and algebraic structures. The Gelfand-Naimark theorem identifies a locally compact Hausdorff space X with a commutative C^*-algebra

$A = C_0(X)$ (continuous functions vanishing at infinity) by considering an homeomorphism between X and the set of *characters* $\hat{A}$ identified with the set of unitary equivalence classes of irreducible $*$-representations [56, 89]. The set $\hat{A}$ is also known as the *structure space* and, for commutative C^*-algebras, it coincides with the *primitive spectrum* $\mathrm{Prim}(A)$, defined as the space of kernels of irreducible $*$-representations of A [56, Section 2.3]. The set of characters of a Banach algebra A is also known as the *Gelfand spectrum*, also denoted by $\mathrm{sp}(A)$ (see [41, Definition 1.3, p5]).

This conceptual interaction between representation theory, commutative C^*-algebras and topological spaces has its origins in the Morita theory, as described in the context of representation theory of rings [2, Chapter 6] [77]. Recall that modules are intimately related to representations of rings, and this fact motivates the concept of Morita equivalence relation between two rings R and S, defined as an equivalence of categories between ${}_RM$ and ${}_SM$, (the categories of modules over R and S, respectively).

These ideas can be extended to the context of C^*-algebras, but for this task, we require more subtle procedures, and a crucial role is played by the landmark ideas of M. Rieffel who introduced the concept of *strong* Morita equivalence. Given two C^*-algebras, A and B, the basic concept behind a Morita equivalence is the notion of a $A-B$ *equivalence bimodule* M (also known as *imprimitivity bimodule*), defined as a $A-B$ bimodule such that M is a full left Hilbert A-module and full right Hilbert B-module, and we have an associativity formula ${}_A\langle x, y\rangle z = x\langle y, z\rangle_B$, for $x, y, z \in M$ (see [54, Definition 2.4.3], [77, Chapter 3]). A *right Hilbert B-module* for a C^*-algebra B is a right B-module M with a B-valued inner product $\langle \cdot, \cdot \rangle : M \times M \to B$, with corresponding generalizations of the standard notion of inner product (see [54, Definition 2.4.1]). With these notions, we say that two C^*-algebras A and B, are *(strongly) Morita equivalent* ($A \overset{\mathrm{m}}{\sim} B$) if there exist an equivalence $A-B$ bimodule (see also [41, Definition 4.9, p162]). We follow the explanations of [77, Remark 3.15], and we will usually omit the word *strongly* for this Morita equivalence concept. Many important properties are conserved under this equivalence relation. In particular, a crucial fact is that the structure space $\hat{A}$ is homeomorphic to the structure space $\hat{B}$ when A and B are (strong) Morita equivalent (see [41, p167]).

Remark 5.1.10 (Open covers of manifolds)**.** A basic example in noncommutative geometry is given by the *open covers of manifolds* (see [21, Chap 2, Example 2α] and [54, Example 2.5.3, p81]). Here, a Morita equivalence relation is established between the (noncommutative) C^*-algebra $C^*(R)$ and the (commutative) C^*-algebra $C_0(\mathcal{M})$, for a locally compact manifold $\mathcal{M}$, where the equivalence relation R is defined in the set $V = \bigsqcup U_i$ for a finite covering $\bigcup U_i = \mathcal{M}$, with $z \overset{\mathrm{R}}{\sim} z'$ iff $p(z) = p(z')$, using the canonical projection $p : V \to \mathcal{M}$. This example will be fundamental in our framework, as this Morita equivalence will be used to exploit the configuration introduced by an open cover in order to analyze the particular type of manifolds (the piles F_f) we are interested in.

Proper groupoid dynamical systems

A fundamental result used in noncommutative geometry is a property proposed by Green [42], which constructs a Morita equivalence relation between the C^*-algebra $C_0(H\backslash X)$ on the quotient space $H\backslash X$ of a group H acting on X, and the corresponding crossed product $C_0(X) \rtimes_{\mathrm{lt}} H$.

Theorem 5.1.2 (Green 1977 [42, Corollary 15], [11, Theorem 4.1, p61]). *If H is a locally compact Hausdorff group acting freely and properly on a locally compact Hausdorff space X, then $C_0(X) \rtimes_{lt} H$ is Morita equivalent to $C_0(H\backslash X)$.*

An important generalization of this property has been prepared by Rieffel [80] who considers the action of a group G in a (noncommutative) C^*-algebra. We describe now a generalization of this machinery in the setting of groupoid actions as prepared by Brown in [10].

Definition 5.1.9 (Proper dynamical system [10, Definition 3.1]). Let $(\mathscr{A}, G, \alpha)$ be a groupoid dynamical system and $A = \Gamma_0(G^{(0)}, \mathscr{A})$ its associated $C_0(G^{(0)})$-algebra. We say that $(\mathscr{A}, G, \alpha)$ a *proper dynamical system* if there exist a dense $*$-subalgebra $A_0 \subset A$ with the following two conditions.

1- we construct functions ${}_E\langle a, b\rangle$ that will generate a dense subspace E of $\mathscr{A} \rtimes_{\alpha,r} G$ (see Theorem 5.1.3). For this step, we require that, for each $a, b \in A_0$, the function ${}_E\langle a, b\rangle : \gamma \to a(r(\gamma))\alpha_\gamma(b(s(\gamma))^*)$, $\gamma \in G$, is integrable (see also [11, Section 4.1.1, p62]). Notice that with this requirement we use the sections a, b (in $\Gamma_0(G^{(0)}, \mathscr{A})$) to construct sections ${}_E\langle a, b\rangle$ defined in the groupoid G and considered in $\Gamma_c(G, r^*\mathscr{A})$.

2- We set a requirement for constructing the fixed point algebra A^α (see Theorem 5.1.3) by defining

$$M(A_0)^\alpha = \{d \in M(A), A_0 d \subset A_0, \overline{\alpha_\gamma}(d(s(\gamma))) = d(r(\gamma))\}.$$

We define now $\langle a, b\rangle_D \in M(A_0)^\alpha$ such that for all $c \in A_0$, $(c \cdot \langle a, b\rangle_D)(u) = \int_G c(r(\gamma))\alpha_\gamma(a^* b(s(\gamma)))d\lambda^u(\gamma)$.

We can now state the main result in [10, Theorem 3.9], generalizing to the groupoid language the property of Rieffel [80, Section 2] which generalizes to (non necessarily commutative) C^*-algebras the result of Green [42, Corollary 15].

Theorem 5.1.3 (Morita equivalence in proper dynamical systems [10, Theorem 3.9]). *Let $(\mathscr{A}, G, \alpha)$ be a proper dynamical system with respect to A_0, and let $D_0 = \mathrm{span}\{\langle a, b\rangle_D, a, b \in A_0\}$ is a dense subalgebra of $A^\alpha = \overline{D_0}$, the fixed point algebra which is the completion of D_0 in $M(A)$. Let also $E_0 = \mathrm{span}\{{}_E\langle a, b\rangle, a, b \in A_0\}$ be a dense subalgebra of $E = \overline{E_0}$, the completion of E_0 in $\mathscr{A} \rtimes_{\alpha,r} G$.*

With these conditions, A_0 is a $E_0 - D_0$ pre-imprimitivity bimodule, which can be completed to a $E - A^\alpha$ imprimitivity bimodule. As a consequence, the generalized fixed point algebra A^α is Morita equivalent to a subalgebra E of the reduced crossed product $\mathscr{A} \rtimes_{\alpha,r} G$.

Saturated groupoid dynamical systems

We now present a basic tool we need, as developed by J.H. Brown [10,11], generalizing to the setting of groupoid theory, the results of Rieffel [80]. The core concept is the notion of saturated groupoid dynamical systems (Definition 5.1.10), whose requirements can be ensured when considering principal and proper groupoids (Definition 5.1.11). The main Theorem 5.1.4 considers the case of a general groupoid dynamical system $(\mathscr{A}, G, \alpha)$, but our main current interest is the particular case where $\mathscr{A} = C_0(G^{(0)})$, as described in the Theorem 5.1.5.

Definition 5.1.10 (Saturated Groupoid Dynamical System [10, Definition 5.1])**.** A dynamical system $(\mathscr{A}, G, \alpha)$, is saturated if ${}_{E_0}A_{0D_0}$ completes to a $\mathscr{A} \rtimes_{\alpha,r} G - A^{\alpha}$ imprimitivity bimodule.

Definition 5.1.11 (Principal groupoid and proper groupoid)**.** Given a groupoid G with its unit space $G^{(0)} = X$, if the natural action of G in X, $\gamma s(\gamma) = r(\gamma)$, is free (see Definition 5.1.7), we say that G is *principal*, and we say that G is *proper* if this action is proper (see Definition 5.1.7 and [10, Conventions 1.1]).

Theorem 5.1.4 (Principal and proper groupoids, saturated actions, and Morita Equivalence [10, Theorem 5.2])**.** *Let $(\mathscr{A}, G, \alpha)$ be a groupoid dynamical system and $A = \Gamma_0(G^{(0)}, \mathscr{A})$ the associated $C_0(G^{(0)})$-algebra. Then, if G is principal and proper, the action of G on A is saturated with respect to the dense subalgebra $C_c(G^{(0)}) \cdot A$. Therefore, A^{α} is Morita equivalent to $\mathscr{A} \rtimes_{\alpha,r} G$.*

Theorem 5.1.5 (Case $\mathscr{A} = C_0(G^{(0)})$ [10, Theorem 5.9])**.** *If the groupoid G is principal and proper, then, the dynamical system $(C_0(G^{(0)}), G, lt)$ is saturated with respect to the dense subalgebra $C_c(G^{(0)})$. As a consequence, we have the following Morita equivalence:*

$$C_0(G\backslash G^{(0)}) \overset{\text{m}}{\sim} C_r^*(G) \quad \textit{for} \quad C_r^*(G) := C_0(G^{(0)}) \rtimes_{lt,r} G.$$

Renault's equivalence for groupoid crossed products

A fundamental additional property we need in our framework is the concept of Morita equivalent dynamical systems which is helpful to ensure when two groupoid crossed products are Morita equivalent. Two dynamical systems $(\mathscr{A}, G, \alpha)$, $(\mathscr{B}, G, \beta)$ are *Morita equivalent* if there is a $\mathscr{A} - \mathscr{B}$ imprimitivity bimodule $\mathscr{H}$ over $G^{(0)}$ and a G action on $\mathscr{H}$ with adequate compatibility conditions (see [74, Definition 9.1, p54]).

Remark 5.1.11 (Renault's equivalence of groupoid crossed products)**.** An important consequence of the Renault's equivalence for groupoid crossed products (see [74, Theorem 5.5, p27], [79]) is the fact that a Morita equivalence between dynamical systems $(\mathscr{A}, G, \alpha)$, and $(\mathscr{B}, G, \beta)$ implies that the corresponding crossed products are Morita equivalent:

$$\mathscr{A} \rtimes_{\alpha,r} G \overset{\text{m}}{\sim} \mathscr{B} \rtimes_{\beta,r} G.$$

5.1.3 Functional Clouds and Some Basic Properties

The concept of a functional cloud M_f can be described as the set of possible *local* states of a signal $f : B \to \mathbb{R}$, where the *local* properties are measured with respect to a set $A \subset B$ as a basic analysis unit. We now want to study the topology of M_f in order to analyze the different types of local components present in f. An important scenario is to consider the case where f is a combination of different signals $f = \sum f_i$. Here, the objective is to use tools from C^*-algebras and their K-theory in order to study how the topology of M_f is assembled from the pieces $\{M_{f_i}\}_i$. A very simplified scenario for this situation is presented in Proposition 5.1.3. The strategy we use for the analysis of the spaces M_f and F_f is to study the C^*-algebras of spaces $M_f^G = F_f/G$, using groupoids G with $G^{(0)} = F_f$. We use the Theorem 5.1.1 to describe simple geometrical relationships between F_f and M_f.

Notice that the space $M_f^G = F_f/G$ considers a generalization of the equivalence relation used to define M_f. A main advantage of this strategy is that we can directly apply the large body of work already available in groupoid theory and operator algebras. Additionally, this method prepares the terrain for addressing more complex problems crucial in concrete applications of signal processing.

The groupoid C^*-algebra of G contains information related to M_f, and the space $M_f^G = F_f/G$ is in relation to $\mathrm{Prim}(C^*(G))$, the primitive spectrum of the algebra $\mathcal{A}$, used as a basic tool in the Gelfand-Naimark theory [36, 56]. The following property includes these ideas, and it is inspired by the basic strategy presented in [54, Example 2.2.2].

Proposition 5.1.2. *Let M_f be a functional cloud, F_f the related pile, and G a groupoid with $G^{(0)} = F_f$. If G is as a finite disjoint union $G = \bigsqcup_{i=1}^k G_i$, for G_i transitive groupoids, and $M_f^G := F_f/G$ is locally compact and Hausdorff, then by denoting with H_i the isotropy group at any unit $u \in G_i^{(0)}$, we have for the K-theory of M_f^G:*

$$K^0(M_f^G) \simeq K_0(C_0(F_f) \rtimes_{lt,r} G) \quad \textit{with} \quad K_0(C^*(G)) \simeq \bigoplus_{i=1}^{k} K_0(C^*(H_i)).$$

Proof. This is a direct application of the characterization of the C^*-algebra of a transitive groupoid in Theorem 5.1.1. For each transitive groupoid G_i we have the isomorphism $C^*(G_i) \simeq C^*(H_i) \otimes K(L^2(\mu_i))$, for a measure μ_i on H_i, and $C^*(G_i)$, $C^*(H_i)$, the C^*-algebras of G_i and H_i, respectively. Therefore, given $G = \bigsqcup_{i=1}^k G_i$, we have

$$C^*(G) \simeq \bigoplus_{i=1}^{k} C^*(G_i)) \simeq \bigoplus_{i=1}^{k} C^*(H_i) \otimes K(L^2(\mu_i)).$$

The K-theory can now be computed using the stability of the functor K_0, that is $K_0(C^*(H_i) \otimes K(L^2(\mu_i))) \simeq K_0(C^*(H_i))$ (see [6, Corollary 6.2.11 p118]). With the relation between the topological and algebraic K-theory we can conclude that $K^0(M_f^G) \simeq K_0(C_0(M_f^G))$ (see [41, Corollary 3.21, p101] and the corresponding generalization to locally compact spaces in [41, p103]). Now, as

$$C_0(M_f^G) \overset{\mathrm{m}}{\sim} C_r^*(G) \quad \text{for} \quad C_r^*(G) := C_0(F_f) \rtimes_{\mathrm{lt},r} G$$

(due to the Theorem 5.1.5), and using the result from Exel [41, Theorem 4.30, p165], [31, Theorem 5.3] (ensuring that Morita equivalent C^*-algebras have isomorphic K-theory groups) we have

$$K^0(M_f^G) \simeq K_0(C_0(M_f^G)) \simeq K_0(C_0(F_f) \rtimes_{\mathrm{lt},r} G).$$

■

Remark 5.1.12 (The discrete setting for groupoid algebras)**.** The Proposition 5.1.2 is partially inspired by the description of a groupoid algebra in a discrete setting (see [54, Example 2.2.2]). By denoting with $\mathbb{C}G$ the $*$-algebra with multiplication and $*$ operation as declared in Definition 5.1.4 (and ignoring for now its C^* properties), we can describe its structure using a canonical decomposition $G = \bigsqcup_i G_i$ for G_i transitive groupoids as:

$$\mathbb{C}G \simeq \bigoplus_i \mathbb{C}H_i \otimes M_{n_i}(\mathbb{C}),$$

where H_i is the isotropy group of a unit in $G_i^{(0)}$ (whose isomorphism class is independent of the chosen unit), and $M_{n_i}(\mathbb{C})$ is the noncommutative algebra of $n_i \times n_i$ matrices with complex entries. Each transitive groupoids G_i is assumed to be finite, and its cardinality is denoted by n_i.

Remark 5.1.13 (Relations to Persistent Homology)**.** In the previous constructions, we considered the groupoid as a generalized equivalence relation, but with these constructions in groupoid theory we can include more complex situations as required by applications. An important additional aspect to consider is the generalization of the groupoid construction used in the previous Remark 5.1.12. If we consider the groupoid $G_\epsilon = \{(u, v) \in F_f \times F_f,\ d(p(u), p(v)) < \epsilon\}$, we can study the family $\{M_{f,A}^{G_\epsilon}\}_{\epsilon>0}$ as a filtration in the context of persistent homology (see Section 3). As we will see in the following Section, the framework of persistent homology can also be adapted to handle C^*-algebra structures.

Function decompositions, clouds and their K-theory

We now present a basic property where we study how the topology of the functional cloud of $f = \sum_{i=1}^n f_i$ interacts with the topology of the functional clouds of f_i. The long term objective is to design signal analysis and separation algorithms using topological or geometrical invariants of the functional clouds of f_i.

The next Proposition 5.1.3 represents just a first glance on how to study the topological interactions between M_f and $\{M_{f_i}\}_i$. Here, the mechanism is based on the simplified assumption that a group G is acting in F_f, and the study of the quotient F_f/G represents an approximation for M_f. There are two different, but interrelated aspects occurring. On the one hand, we have the group G acting on F_f, and on the other hand we have the decomposition of F_f with an open cover originated from the consideration of the function decomposition $f = \sum f_i$.

Remark 5.1.14 (noncommutative algebra $M_k(A)$)**.** In the following we use the standard notation $M_k(A)$ for the noncommutative algebra of $k \times k$ matrices with entries in an algebra A. Recall also that $M_k(A) = M_k(\mathbb{C}) \otimes A$.

We start with very simple propositions to get some familiarity with the concepts and their properties.

Proposition 5.1.3. *Let $f : B \to \mathbb{R}$ be a continuous function, M_f a functional cloud and F_f its related pile. Let $f = \sum_{i=1}^{k} f_i$ with $\text{supp}(f_i) \subset U_i$, for $\{U_i\}_{i=1}^{k}$ an open cover of a locally compact group B, and define*

$$V_i := \bigsqcup_{x \in U_i} F_x, \quad F_x = \{(y, f_x(y)), y \in A\},$$

for $f_x : A \to \mathbb{R}$ with $f_x(y) = f(x+y), x \in B, y \in A$, for A a measurable compact set with $0 \in A \subset B$. If a locally compact group G is acting on F_f then for the K-theory of $M_f^G := F_f/G$ we have:

$$K^0(M_f^G) \simeq K_0(\mathcal{A} \otimes C^*(G)), \quad \mathcal{A} := \Big\{ [h_{ij}] \in M_k(C_0(F_f)),\ h_{ij} \in C_0(V_i \cap V_j) \Big\}.$$

Proof. The proof is a simple application of two basic facts concerning the C^*-algebra of a quotient space given by a group action and the mechanism for studying quotients of *open covers of a manifold* (see Remark 5.1.10). First, recall that a group action $\alpha : G \times F_f \to F_f$ induces an action in the algebra $C_0(F_f)$, and the resulting dynamical system can be encoded in a cross product denoted as $C_0(F_f) \rtimes_\alpha G$, and, seen as a vector space, it can be written as

$$C_0(F_f) \rtimes_\alpha G = C_0(F_f) \otimes C^*(G).$$

The corresponding product defined for this algebra is given by $(a \otimes g)(b \otimes h) = ag(b) \otimes gh$ (see [54, Example 2.2.7]). As a consequence of Theorem 5.1.2 (see also [54, Theorem 2.5.1, p78]), we have $C_0(M_f^G) \overset{\text{m}}{\sim} C_0(F_f) \rtimes_\alpha G$. On the other hand, the open cover property (see Remark 5.1.10) ensures that the C^*-algebra $C_0(F_f)$ is Morita equivalent to $\mathcal{A}$ when considering the open cover $\{V_i\}_{i=1}^{k}$ of F_f. By combining these two properties, together with the result from Exel in [41, Theorem 4.30, p165], [31, Theorem 5.3] ensuring that Morita equivalent C^*-algebras have isomorphic K-theory groups, we have

$$K^0(M_f^G) \simeq K_0(C_0(M_{f,A}^G)) \simeq K_0(C_0(F_f) \otimes C^*(G)) \simeq K_0(\mathcal{A} \otimes C^*(G)).$$

■

The simplified scenario of this proposition is just a first step where more general situations should consider not just a group G acting on F_f but a groupoid (see the Remark 5.1.13) for capturing more accurately the interactions between the components f_i. This is particularly important in applications, as illustrated in Example 5.1.4, where M_f is actually just an intermediate structure, and the principal goal is to understand the geometry and topology of the underlying parameter set Ω (see the Example 5.1.4).

Example 5.1.11 (Image Segmentation)**.** A typical application which illustrates the objectives in Proposition 5.1.3 is to consider an grayscale image $f : [0,1]^2 \to [0,1]$, where different areas $U_i \subset [0,1]^2$ correspond to different regions in the image. The main task is to understand how the topology of M_f is assembled from the different regions $f(U_i)$ and the corresponding clouds M_{f_i}, for f_i a function equal to f in U_i, and zero otherwise. This

requires not only to study the regions themselves, but also their contours or edges represented by $f(U_i \cap U_j), i \neq j$. The combination and interaction between these topologies is encoded in the algebra $\mathcal{A}$ together with the partition of F_f with the group G (in a more general setting, crucial for applications, a groupoid structure G defined in F_f should be considered, as explained in the previous paragraph). We remark that the consideration of patches of images is currently an important research direction in image processing, with significant results in denoising, classification (see e.g. [69]).

Voice transforms and groupoids crossed products

We now consider a more general situation using the abstract machinery of time-frequency analysis represented by the theory of voice transforms. A crucial advantage of this setting is the fact that multiple time-frequency transforms (e.g. wavelets, Gabor analysis, etc) are represented in a single abstract environment. Additionally, we consider signals as vectors in an abstract Hilbert space, allowing a clean, general, and powerful environment for expressing our problems and the solutions strategies.

Given a mixture of signals $f = \sum_{i=1}^{k} f_i \in H$, for a Hilbert space H, the following property is an initial step in understanding the interaction between the functional clouds $M^G_{V_\psi f}$ and the components f_i of the signal f. One possible analogy for this scenario is to consider each signal f_i as a measurement originated from a particular physical event i, and f is the mixture of signals encoding the interactions of all k events.

Theorem 5.1.6. *Let $f = \sum_{i=1}^{k} f_i \in H$, for a Hilbert space H and $V_\psi : H \to C(\mathcal{G})$, a voice transform for a locally compact group $\mathcal{G}$. Let G be a principal and proper groupoid with unit space $G^{(0)} = F_{V_\psi f} := \mathrm{graph}(V_\psi f|_{suppV_\psi f})$, and consider an open cover $\{U_i\}_{i=1}^{k}$ of $\mathcal{G}$. If $\mathrm{supp}(V_\psi f_i) \subset U_i$, for $i = 1, \ldots, k$, then the following Morita equivalence holds for $M^G_{V_\psi f} := F_{V_\psi f}/G$,*

$$C_0(M^G_{V_\psi f}) \overset{\mathrm{m}}{\sim} \mathcal{A} \rtimes_{lt,r} G, \quad \mathcal{A} := \Big\{ [h_{ij}] \in M_k(C_0(F_{V_\psi f})),\ h_{ij} \in C_0(F_{V_\psi f_i} \cap F_{V_\psi f_j}) \Big\}.$$

Proof. This follows directly from a combination of properties on Morita equivalence for groupoid C^*-algebras as discussed in the previous sections. First, notice that for a proper and principal groupoid G with $G^0 = F_{V_\psi f}$ we have a Morita equivalence

$$C_0(F_{V_\psi f}/G) \overset{\mathrm{m}}{\sim} C^*_r(G) \quad \text{for} \quad C^*_r(G) := C_0(F_{V_\psi f}) \rtimes_{\mathrm{lt},r} G,$$

using the Theorem 5.1.5. We have also a Morita equivalence $C_0(F_{V_\psi f}) \overset{\mathrm{m}}{\sim} \mathcal{A}$ for an open cover of the manifold $F_{V_\psi f}$, as explained in Remark 5.1.10. Notice that for any $f \in H$, $F_{V_\psi f}$ is indeed a manifold as defined for a voice transform (see Example 5.1.6 and Proposition 5.1.1). These two relations can be combined with the Renault's equivalence property, as discussed in Remark 5.1.11, in the following computation:

$$\begin{aligned} C_0(M^G_{V_\psi f}) &= C_0(F_{V_\psi f}/G) \\ &\overset{\mathrm{m}}{\sim} C_0(F_{V_\psi f}) \rtimes_{\mathrm{lt},r} G \qquad \text{(Morita equivalence: Theorem 5.1.5)} \\ &\overset{\mathrm{m}}{\sim} \mathcal{A} \rtimes_{\mathrm{lt}} G, \qquad \text{(Renault's equivalence: Remark 5.1.11)} \end{aligned}$$

$$\text{using} \quad C_0(F_{V_\psi f}) \overset{\mathrm{m}}{\sim} \mathcal{A} \qquad \text{(Open cover property: Remark 5.1.10).}$$

■

Remark 5.1.15 (Interpreting the Theorem 5.1.6)**.** There are several ways in which the Theorem 5.1.6 can be interpreted. Broadly speaking, one can see this property as an initial step for understanding how one can analyze and encode, with the noncommutative C^*-algebra $\mathcal{A} \rtimes_{lt,r} G$, the interaction of different phenomena, measured with the signals f_i, and occurring at different time-frequency regions $F_{V_\psi f_i}$. In special cases, the signals f_i can be seen as measurements from different dynamical systems whose phase spaces contain the sets $M_{V_\psi f_i}$, as explained in the setting of the Taken's theorem (see the Example 5.1.5). With the rule $f = \sum_{i=1}^{k} f_i$, the spaces $M_{V_\psi f_i}$ are combined in a single structure $M_{V_\psi f}$ whose construction depends on two main properties encoded in the C^*-algebra $\mathcal{A} \rtimes_{lt,r} G$. As we will now explain, these properties are clearly visible in the noncommutative C^*-algebra $\mathcal{A} \rtimes_{lt,r} G$, but they are completely ignored in the commutative C^*-algebra $C_0(M^G_{V_\psi f})$. This feature illustrates the usefulness of the Morita equivalence property as a new analysis layer (constructed on top of the time-frequency machinery) for studying hidden features of a signal.

In order to explain the previous remark, we consider the particular case of Gabor analysis $V_g f(b,w) = \int_{\mathbb{R}} f(t)g(t-b)e^{-2\pi i t w}dt$, $f \in L^2(\mathbb{R})$, and the cloud $M_f = \{x_b\}_b$ with chunks $x_b = fg_b$ using $g_b(t) = g(t-b)$ for a window function g. We consider also the cloud $M_{V_g f} = \{V_g f(b,.)\}_b$ (isometric to M_f) in the corresponding Fourier view (see the Example 5.1.6).

Now, the two main properties encoded in the C^*-algebra $\mathcal{A} \rtimes_{lt,r} G$, can be described as the time-domain pattern for the function f represented with an adequate groupoid G, and the time-frequency relations between the signals f_i encoded with the C^*-algebra $\mathcal{A}$. A time-domain pattern encoded in a groupoid G takes into account the way different vectors $x_b = fg_b$ are repeated at different time positions $b \in \mathbb{R}$. Recall that the cloud M_f is the quotient $M_f = F_f/R$, for an adequate equivalence relation $R = \{(u,v) \in F_f \times F_f,\ d(p(u),p(v)) = 0\}$ and the projection map $p : F_f \to M_f$, $p((x,y,f_x(y)) = f_x$. (see Remark 5.1.3). We use the important generalization $M^G_{V_\psi f} = F_{V_\psi f}/G$ for a groupoid G with $G^{(0)} = F_{V_\psi f}$, and the groupoid G can be used to encode the similarities and repetitions between the vectors x_b as the time parameter b changes, in order to construct a meaningful quotient space $M^G_{V_\psi f}$. The second important property encoded in the C^*-algebra $\mathcal{A} \rtimes_{lt,r} G$ is the relationship between the time-frequency regions corresponding to each signal f_i, captured by the algebra $\mathcal{A} = \left\{[h_{ij}] \in M_k(C_0(F_{V_\psi f})),\ h_{ij} \in C_0(F_{V_\psi f_i} \cap F_{V_\psi f_j})\right\}$. The influence of each signal f_i in the whole system is encoded in a C^*-algebra $C_0(F_{V_\psi f_i})$ stored in a diagonal entry of $\mathcal{A}$. The time-frequency interference between different phenomena measured with f_i and f_j is encoded in a C^*-algebra $C_0(F_{V_\psi f_i} \cap F_{V_\psi f_j})$ located in the off-diagonal entries of the noncommutative C^*-algebra $\mathcal{A}$.

Remember that the time-frequency analysis machinery "unfolds" the information of a function f in order to understand its internal properties. In this context, in contrast to the usage of $C_0(M^G_{V_\psi f})$, the consideration of the (larger) Morita equivalent C^*-algebra $\mathcal{A} \rtimes_{lt,r} G$, can be used as a further analysis level for understanding the features of the function f and its internal structure.

Remark 5.1.16 (Towards an application example of the Theorem 5.1.6)**.** In the Example 5.1.4, we have defined a *cloud of a modulated path* M_f constructed with an embedded manifold $\Omega \subset [-1,1]^d$, a continuous path $\phi : [0,1] \to \Omega$, and the construction of a

real function $f(x) = \sum_{i=1}^{d} \sin\left(\int_0^x (\alpha_c^i + \gamma\phi_i(t))\, dt \right)$, for a fixed center frequency vector $\alpha_c = (\alpha_c^i)_{i=1}^d \in \mathbb{R}^d$, bandwidth parameter γ, and the i-th coordinate of $\phi(x)$ denoted as $\phi_i(x)$. Given the function f, the main problem is to use a functional cloud $M_{f,A}$ in order to estimate geometrical and topological features of Ω. Notice that in this example, $M_f = M_{f,A}$ is just a curve in $C(A, \mathbb{R})$, when using A as a closed interval in $[0, 1]$, due to the fact that $M_{f,A} = \bigcup_{x\in[0,1]} \{\mathcal{F}_x : A \to \mathbb{R}\}$ is parametrized by $x \in [0, 1]$, and $[0, 1]$ set as a torus group (see the Definition 5.1.1). It is therefore not immediate how to obtain topological information of Ω using $M_{f,A}$. However, under adequate conditions, we can construct a groupoid G with $G^{(0)} = F_{V_\psi f} = \text{graph}(V_\psi f|_{\text{supp}V_\psi f})$, such that the quotient space $M^G_{V_\psi f} = F_{V_\psi f}/G$ can be used to compute topological features of Ω.

More precisely, one strategy is to consider a *topological approximation scheme* as explained in [56, Section 3.1, p23], where a covering $\mathcal{U} = \{U_i\}$ of Ω is used to construct an equivalence relation R, defined as

$$x \overset{\text{R}}{\sim} y \quad \text{if and only if} \quad x \in U_i \Leftrightarrow y \in U_i, \quad \forall\, U_i \in \mathcal{U}.$$

As explained in [56, Section 3.2, p27], topological features of the space Ω can computed with the approximation $P_{\mathcal{U}}(\Omega) = \Omega/R$, and in the limit, using finer coverings, the whole space Ω can be approximated [56, Section 3.3, p30]. Now, broadly speaking, by designing a groupoid G (with $G^{(0)} = F_{V_\psi f} = \text{graph}(V_\psi f|_{\text{supp}V_\psi f})$) mirroring the properties of a covering $\mathcal{U} = \{U_i\}$ of Ω, we can construct an approximation space $M^G_{V_\psi f}$ with similar topological features as $P_{\mathcal{U}}(\Omega) = \Omega/R$. With this scenario, we can now conjecture the feasibility of using $M^G_{V_\psi f} = F_{V_\psi f}/G$ for estimating topological features of Ω together with an adequate groupoid G with $G^{(0)} = F_{V_\psi f}$, and adequate conditions on the density of Image$(\phi) \subset \Omega$. We also notice that a main motivation for studying the topological features of the cloud $M^G_{V_\psi f}$ is to understand the parameter space Ω seen in the dimensionality reduction context. The Theorem 5.1.6 delivers a strategy for this task using the C^*-algebra $\mathcal{A} \rtimes_{lt} C(G)$ in order to study the properties of $M^G_{V_\psi f}$ with respect to the components f_i and Ω_i.

Now, given a family of manifolds $\{\Omega_i\}_{i=1}^k$, $\Omega_i \subset [-1, 1]^d$, and paths $\phi_i : [0, 1] \to \Omega$ with corresponding functions f_i (defined as in the previous paragraph), the sum $f = \sum_{i=1}^k f_i$ leads to the study of a space M_f (resp. F_f) resulting from a particular type of combination of the spaces M_{f_i} (resp. F_{f_i}). The analysis of M_f can be performed with the Theorem 5.1.6, which provides an explicit understanding of the assembling process of the spaces $F_{V_\psi f_i}$ into a single structure $M^G_{V_\psi f}$, and whose topological properties can be studied with $\mathcal{A} \rtimes_{lt,r} G$. We will see very preliminary initial steps for such an setting in the toy example presented in section 5.2.

Schematic diagram for the Theorem 5.1.6

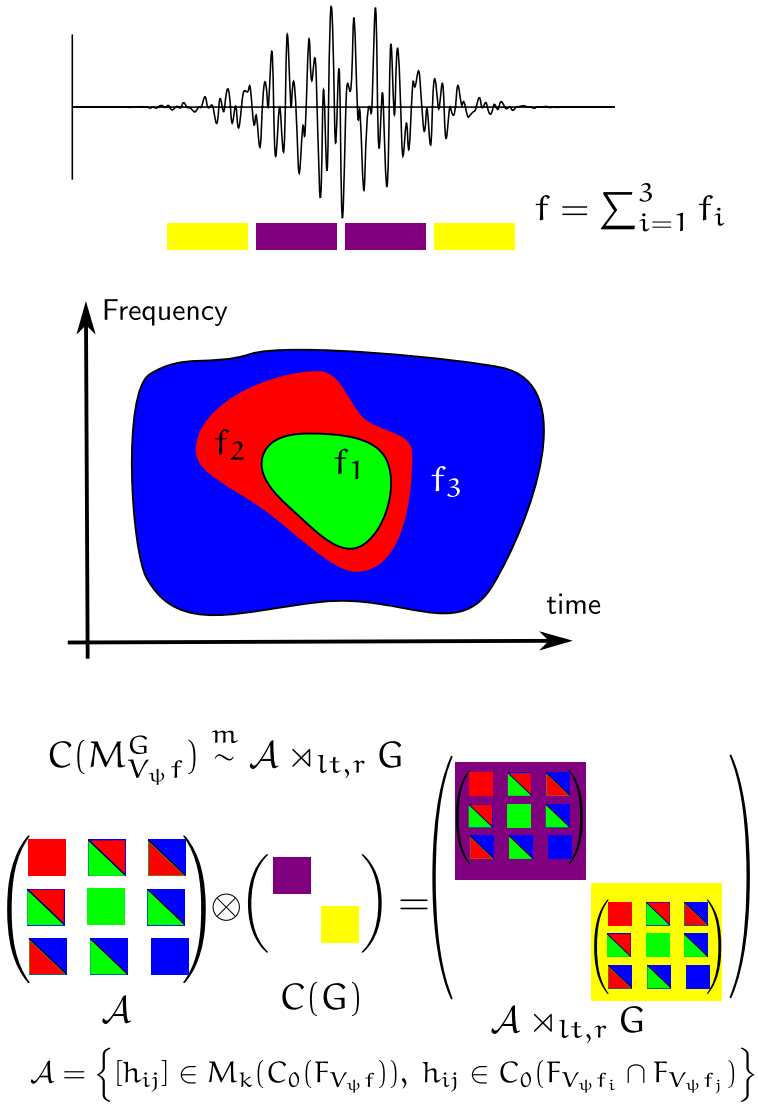

Figure 5.1: Schematic illustration of Theorem 5.1.6

The diagram of Figure 5.1 illustrates a schematic view of the results in Theorem 5.1.6. Given a signal $f = \sum_{i=1}^{3} f_i$ with three components whose time-frequency regions are illustrated in the green (f_1), red (f_2), and blue (f_3) areas, we can see the crossed product $\mathcal{A} \rtimes_{lt,r} G$, from an algebraic point of view, as a tensor product $\mathcal{A} \otimes C(G)$. Similarities in the waveform of the function f are encoded in the groupoid algebra $C(G)$ (yellow, violet), and the time-frequency interference is encoded in the algebra $\mathcal{A}$. The resulting algebra $\mathcal{A} \rtimes_{lt,r} G$ integrates this information in a single algebraic entity that represents the interaction of the signal components f_1, f_2 and f_3.

5.1.4 AF-Algebras in the Persistent Homology Framework

We need to study now the problem of implementing, in a practical and computationally feasible environment, the concepts we have developed for signal analysis with groupoid crossed products. For this task, we need to apply basic ideas of C^*-algebras for the analysis of finite structures. As we will see, we consider for this problem, the theory of AF-algebras, which has a rich and well developed theoretical framework. Another basic component in our strategy is persistent homology (as introduced in Section 3), which will be another crucial theoretical and algorithmic tool, with a readily available efficient computational setting.

The objective now is to use some basic ideas on C^*-algebras discussed in Section 5.1 in combination with the framework of persistent homology. The main task is to use the basic input of persistent homology, a filtration $K_1 \subset K_2 \subset \cdots \subset K_r$, and construct an associated sequence of C^*-algebras. Given a simplicial complex, there are several strategies for constructing an associated C^*-algebra. We follow the method, presented in [56,85], which consists of building a poset structure, together with its associated Bratelli diagram and AF-algebra. We remark that other alternatives are available, for instance, the concept of noncommutative simplicial complex has been introduced in [23].

There are two basic steps for implementing this program. First, we remark that there is a close interaction between the concept of simplicial complex and a poset [91]. Given a poset P, a simplicial complex $K(P)$ (the *order complex*), is constructed by considering the set of vertices as the elements of P, and its faces as the totally ordered subsets (chains) of P. Inversely, given a simplicial complex K, we can build a poset $P(K)$ (the *face poset*) by considering the nonempty faces ordered by inclusion (see [91] for additional details). The second step is to construct a Bratelli diagram from a poset, as discussed in [56], which represents an AF-algebra containing all information from a topological space encoded in an algebraic structure.

The framework of AF-algebras and posets describes in a finite setting basic ideas in noncommutative geometry [56]. Recall that $\mathcal{A}$ is an approximately finite (AF) dimensional algebra if there exist an increasing sequence

$$\mathcal{A}_0 \overset{I_0}{\hookrightarrow} \mathcal{A}_1 \overset{I_1}{\hookrightarrow} \dots \overset{I_{n-1}}{\hookrightarrow} \mathcal{A}_n \overset{I_n}{\hookrightarrow} \dots$$

of finite dimensional C^*-subalgebras of $\mathcal{A}$, with I_k injective $*$-morphisms and $\mathcal{A} = \overline{\bigcup_n \mathcal{A}_n}$. Any finite dimensional C^*-algebras is of the form $\oplus_i M_{n_i}$, where M_{n_i} is the full $n_i \times n_i$ matrix algebra. The complete structure of an AF-algebra includes the matrix algebras $\mathcal{A}_k$ and the injective morphisms I_k, and can be encoded in a representation denominated Bratelli diagram (see [56]). We can now describe the interaction between simplicial complexes, posets, and their Bratelli diagrams in the framework of persistent homology. The following diagram is a summary of the three basic components:

$$\begin{array}{lccccccc}
\text{Simplicial Complexes:} & K_0 & \longrightarrow & K_1 & \longrightarrow & \dots & \longrightarrow & K_n \\
& \downarrow & & \downarrow & & & & \downarrow \\
\text{Face Posets:} & P(K_0) & \longrightarrow & P(K_1) & \longrightarrow & \dots & \longrightarrow & P(K_n) \\
& \downarrow & & \downarrow & & & & \downarrow \\
\text{AF-Algebras:} & \mathcal{A}^0 & \longrightarrow & \mathcal{A}^1 & \longrightarrow & \dots & \longrightarrow & \mathcal{A}^n
\end{array}$$

Each horizontal arrow is an injective inclusion, and the vertical arrows represent the two main constructions: first we build posets from simplicial complexes, and then AF-algebras are computed from posets (using Bratelli diagrams as a main tool). Each AF-algebra $\mathcal{A}^k$, has its own decomposition with finite dimensional matrix algebras $\mathcal{A}_i^k$, and injective $*$-morphisms I_i^k:

$$\mathcal{A}_0^k \overset{I_0^k}{\hookrightarrow} \mathcal{A}_1^k \overset{I_1^k}{\hookrightarrow} \ldots \overset{I_{n-1}^k}{\hookrightarrow} \mathcal{A}_n^k \overset{I_n^k}{\hookrightarrow} \ldots$$

Further Remarks

Our main property, described in Theorem 5.1.6, explains basic conceptual interactions between a functional cloud $M_{V_\psi f}^G = F_{V_\psi f}/G$ for an element f in a Hilbert space H, and its components f_i. In this property, we use a groupoid G with $G^{(0)} = F_{V_\psi f} := \text{graph}(V_\psi f|_{\text{supp}V_\psi f})$, and $V_\psi f$ the voice transform of f. These results are a first step in our strategy for using noncommutative C^*-algebras in time-frequency analysis. Among the many questions to analyze, an important issue is the consideration of other algebras, besides $C_0(F_{V_\psi f_i})$, for capturing different type of features. Recall that the spaces $C^\infty(F_{V_\psi f_i}) \subset C_0(F_{V_\psi f_i}) \subset L^1(F_{V_\psi f_i})$ can be used to encode geometrical, topological, and measure theoretical properties, respectively. The general framework prepared in the Theorem 5.1.4 could be a way to address these possibilities. We remark that new results have been recently achieved in the setting of AF-algebras and *spectral triples*, which is a fundamental tool for accessing geometrical data using C^*-algebras (see [21] for the concept of spectral triples, and [17] for its interaction with AF-algebras).

We also notice that related developments have been recently achieved in the integration of time-frequency analysis and noncommutative geometry as explained in [65–67]. These novel research directions are complementary to the ones we follow, but the same tools from noncommutative geometry and noncommutative topology are considered. We notice also that modern developments in pattern classification are investigating new type of invariants based on algebraic criteria (see e.g. [70]). Our framework is designed to consider these research directions, and the basic tool is to exploit the flexibility of C^*-algebras for representing interactions between geometrical/topological and algebraic structures.

We finally remark that the fundamental domain of time-frequency transforms in harmonic analysis, and the new developments in persistent homology and dimensionality reduction, have shown powerful perspectives in their own domains. However, an adequate integration of these tools is necessary in order to resolve modern application and theoretical problems in signal processing and data analysis. We argue that concepts based on noncommutative C^*-algebras can play a role in this interaction.

5.2 Computational Toy Examples

We present now an illustrative example of a filtering procedure and its interaction with topological measurements of a dataset X_f [45]. This toy example only shows a limited view of our conceptual developments, but the goal is to provide an initial sketch illustrating basic features of our setting. We consider the function $f = (1-\alpha)g + \alpha h$, $\alpha \in [0,1]$ to be a sum of two functions g and h, where the datasets X_g and X_h are sampled from spaces homeomorphic to a sphere $\mathbb{S}^2$ and a torus $\mathbb{T}^2$, respectively. We construct g and h with the design described in Example 5.1.4, where Ω is a sphere and a torus, respectively.

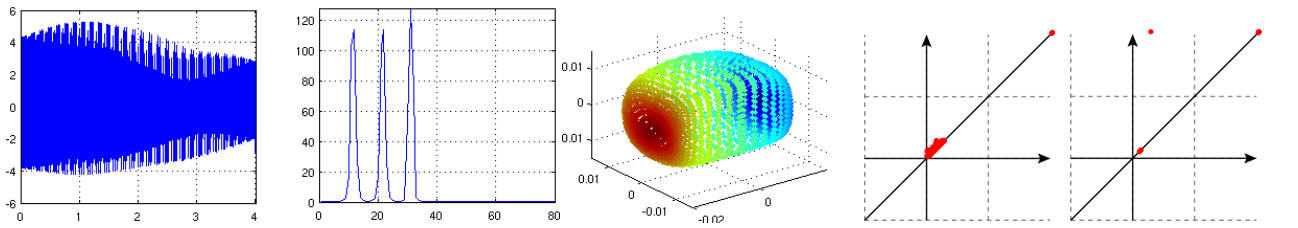

$f = (1-\alpha)g + \alpha h$
$\alpha = 0.00$

Frequency Bands

Cloud $P(X_f)$

1rst Homology Level

2nd Homology Level

Figure 5.2: $f = g$, and $X_f \subset \mathcal{M}$ with $\mathcal{M}$ homeomorphic to $\mathbb{S}^2$

We construct X_g and X_h, as described in our examples on modulation maps in Section 2.3. For instance, in Fig. 5.2, each element x of the point cloud data X_f is a signal whose main frequency content is located in three frequency bands depicted in the second plot in the Fig. 5.2. We additionally design each element $x \in X_g$ and $y \in X_h$ such that their frequency content do not overlap. For example, in Fig. 5.3, the second diagram shows the six different frequency bands for the signal $x + y$: the first three bands corresponding to a typical element $x \in X_g$, and the other bands correspond to elements $y \in X_h$.

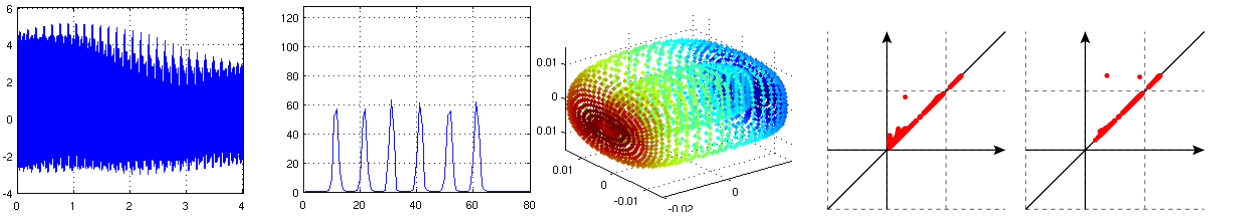

$f = (1-\alpha)g + \alpha h$
$\alpha = 0.50$

Frequency Bands

Cloud $P(X_f)$

1rst Homology Level

2nd Homology Level

Figure 5.3: $f = (g+h)/2$, and X_f as an intermediate structure

For these examples, the variations of the parameter α correspond to a filtering process, where we selectively remove (or add) the component g (or h) from the signal f. The topological effects can be seen by studying the persistent homology diagrams of X_f. For each Figure 5.2, 5.3, and 5.4, we have diagrams representing the first and second homology level. With this information we have an estimation for the number of one and two dimensional holes in X_f.

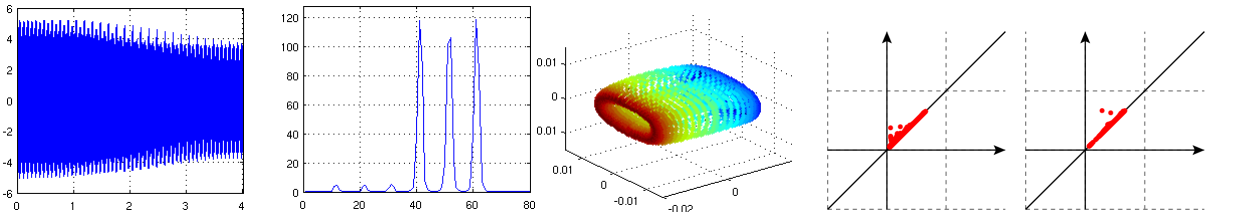

Figure 5.4: $f = h$, and $X_f \subset \mathcal{M}$ with $\mathcal{M}$ homeomorphic to $\mathbb{T}^2$

In Fig. 5.2, the persistent diagram for X_f shows a clear stable two dimensional hole, and only noise like one dimensional holes. As previously mentioned, this corresponds to a spherical structure for X_f. For the Fig. 5.4, we have two, closely related, one dimensional holes, and additionally two 2-dimensional holes, which (approximately) corresponds to a torus structure. The persistent homology diagrams for the intermediate structure $X_{(g+h)/2}$ is depicted in Fig. 5.3, where several two dimensional holes are present.

Example 5.2.1 (Champignon Example)**.** With similar ideas as in the previous sphere-torus toy example, we consider now a champignon image with two major components: the champignon (signal g) and its surroundings (signal h). We use a simple color based segmentation algorithm to split the image in these two parts, and we study the signal $f_\alpha = (1-\alpha)g + \alpha h$ for $\alpha \in [0,1]$, using the same mechanism as in the previous setting. We compute the persistent homology of the different point cloud data constructed from patches of the images f_α for each $\alpha \in [0,1]$. We show the images f_α and the corresponding persistent diagrams for $\alpha = 0, \alpha = 0.5$, and $\alpha = 1$ in Figure 5.5.

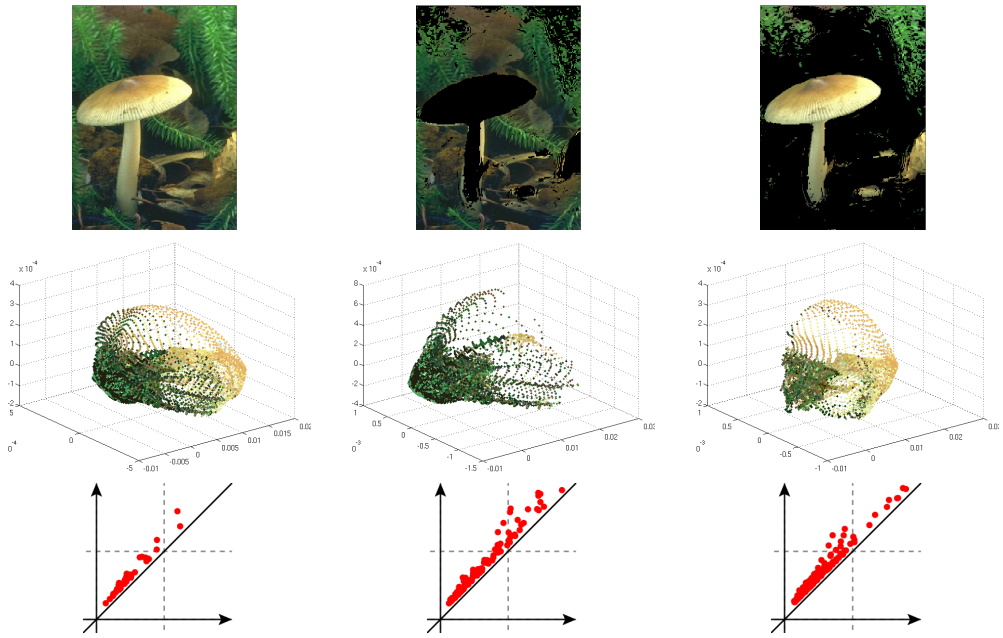

Figure 5.5: Champignon image, point cloud data of patches, and the persistent diagrams

6 Some Geometric Tools for Signal Analysis

The challenging task of extracting or detecting components from a signal has multiple applications for the study of biomedical signals, audio analysis or image processing. In the first part of this chapter, we propose a strategy for signal analysis combining standard signal processing tools with geometric algebra and dimensionality reduction. Our concept relies on geometrical transformations, defined in the context of Clifford algebras, for modifying the geometric characteristics of a point cloud data. The objective is to design geometric transformations for time-frequency data and improve the quality of classification, detection, and filtering procedures. This new framework is an addition to the manifold learning and dimensionality reduction toolbox, combining ideas from Clifford algebras, dimensionality reduction, and filtering procedures in signal analysis. Some computational experiments [1] are presented indicating the potential and shortcomings of this framework. The second part of this Chapter presents an overview of a basic engineering strategy for signal separation using time-frequency data, dimensionalty reduction, and independent component analysis (ICA). This technique, known as independent subspace analysis ISA, has been originally proposed in [15], and discussed in recent developments (e.g. [86]).

6.1 Geometric Transformations of Time-Frequency Data

In the field of signal separation, a fundamental strategy is the usage of Fourier transforms or wavelet analysis for filtering particular components of a signal. These concepts provide a powerful framework used in multiple theoretical and application fields. But the ever increasing complexity of signal data requires more sophisticated analysis tools. An important source of ideas for addressing these modern challenges is the new set of tools from dimensionality reduction and manifold learning based on geometrical and topological concepts. Inspired by these developments, we propose a framework based on Clifford geometry for signal analysis, as an addition to the manifold learning and dimensionality reduction toolbox.

We recall that, in our setting, we consider a bandlimited signal $f \in L^2(\mathbb{R})$ and a segmentation of its domain in such a way that small consecutive signal patches are analyzed, as routinely performed in STFT or wavelet analysis. For instance, the set of signal patches can be defined as a dataset

$$X_f = \{x_i^f\}_{i=1}^m, \quad x_i^f = (f(t_{k(i-1)+j}))_{j=0}^{n-1} \in \mathbb{R}^n,$$

for $k \in \mathbb{N}$ a fixed hop-size. Here, the regular sampling grid $\{t_\ell\}_{\ell=0}^{km-k+n-1} \subset [0,1]$ is constructed when considering the Nyquist-Shannon theorem for f. Now, a standard signal separation problem is to remove from f a component x_σ that appears at different time positions t, with varying frequency characteristics. Note that many relevant application problems dealing with a mixture of signals can be considered in this setting. For instance, in *noise reduction* we have a perturbation of a signal f by nonstationary noise σ. A typical non-blind solution scenario is to select a patch x_σ of sufficient noise characteristics such that an adequate removal can be performed (for instance using spectral subtraction

[1] Available at `www.math.uni-hamburg.de/home/guillemard/`

methods). A more complex situation are *cocktail party effect* problems, where $f = g + h$ is a mixture of two signals g and h, and the objective is to separate g and h from f (classically addressed with independent component analysis in multichannel signals). For the sake of simplicity, we restrict ourselves to the situation where some knowledge of X_g and X_h is given (e.g. in form of representative patches $x_g \in X_g, x_h \in X_h$). Moreover, for a signal transformation T (identity, Fourier, power spectrum, wavelet, etc), and $T(X) := \{T(x_i)\}_{i=1}^m$, we consider the case where $T(X_g)$ or $T(X_h)$ are localized in small regions of $\mathbb{R}^n$ and the size of $T(X_g) \cap T(X_h)$ is negligible. A concrete acoustical example is a one-channel signal f composed of two different percussion instruments (g and h). It is reasonable to obtain sample patches $x_g \in X_g$ and $x_h \in X_h$, but due to their complex frequency characteristics, an accurate separation of f, specially when g and h are played simultaneously, is a challenging problem. In the particular case of noise reduction, *power spectral subtraction* is a fundamental strategy which removes the noise signal g from $f = g + h$ by subtracting the frequency content $\|\hat{f}_k\| - \|\hat{h}_k\|$ at each frequency bin k [63]. A basic hypothesis is that the noise and clear signal vectors are orthogonal to each other. But this assumption is usually wrong, and a generalized approach takes into account a more accurate geometrical relation between the noise and signal vectors [64]. In our framework we use this generalized scenario but considering point cloud data structures instead of single frequency bins.

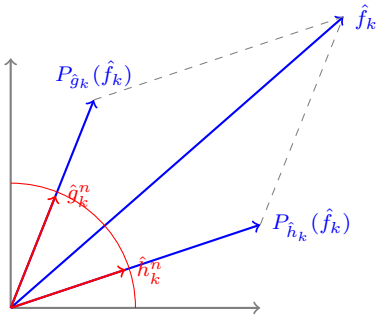

Diagram 1: Power Spectral Subtraction ($P_g(f)$: projection of f in the direction of g)

General Algorithm Framework

In this section, we describe the basic ingredients of our framework. We assume we are given the dataset $X_f = \{x_i^f\}_{i=1}^m \subset \mathbb{R}^n$ sampled from a bandlimited signal $f = g + h$. We consider a signal transformation T (power spectrum, wavelet transforms, etc). Our main objective is to use the point cloud data $T(X_f)$ in order to extract the signal g from f. A fundamental component is a dimensionality reduction map R which reduces the dimension of $T(X_f)$, and provides an initial simplification of its geometry. The resulting set, $R(T(X_f)) = \Omega_f$, is further manipulated with a Möbius map $\mathfrak{f}$ that rotates and shrinks a particular cluster (X_h or X_g). With these geometrical manipulations a filtering procedure $\mathbb{T}$ is now implemented, extracting the signal of interest.

The crucial preprocessing step of this algorithm, is the *learning phase* which constructs the Möbius map $\mathfrak{f}$ by considering the low dimensional representation $R(T(X_g) \cup T(X_h))$. The objective of $\mathfrak{f}$ is to map the elements of Ω_g close to an element e_g of an orthogonal basis, while the elements of Ω_h are transformed to another region. The second component

delivered by the learning phase is the filtering procedure $\mathbb{T}$, which depends on e_g and the geometrical modifications of $\mathfrak{f}$.

$$\begin{array}{ccccccc} X_g & \xrightarrow{T} & T(X_g) & & & & \\ & & & \searrow & & & \\ & & & & T(X_g) \cup T(X_h) & \xrightarrow{R} & \Omega_{g\cup h} \longrightarrow (\mathfrak{f}, \mathbb{T}) \\ & & & \nearrow & & & \\ X_h & \xrightarrow{T} & T(X_h) & & & & \end{array}$$

Diagram 2: Learning phase

With the resulting set $\mathfrak{f}(\Omega_{g+h})$, we can extract the contents of $g+h$ with the filter $\mathbb{T}$. The final step is the reconstruction of the high-dimensional data with the inverse R^{-1} in order to recover $T(X_g)$, and so g.

$$\begin{array}{ccccccc} X_{g+h} & \xrightarrow{T} & T(X_{g+h}) & \xrightarrow{R} & \Omega_{g+h} & \overset{\mathfrak{f}}{\searrow} & \\ & & & & & & \mathfrak{f}(\Omega_{g+h}) \\ X_g & \xleftarrow[T^{-1}]{} & T(X_g) & \xleftarrow[R^{-1}]{} & \Omega_g & \underset{\mathbb{T}}{\swarrow} & \end{array}$$

Diagram 3: Separation phase

As it can be seen from this description, any gain in understanding the geometry of X_f is useful for improving the quality of the algorithm. This is particularly important since X_f may be embedded in a very high-dimensional space $\mathbb{R}^n$, although the dimension of X_f itself may be small (in audio analysis, for 44kHz signals, $n = 1024$ is commonly used). In such situations, customized dimensionality reduction methods are of vital interest. For instance, if $X_f \subset \mathcal{M}$, with $\mathcal{M}$ being a manifold (or a topological space), a suitable dimensionality reduction map $R : \mathcal{M} \subset \mathbb{R}^n \to \mathcal{M}_R \subset \mathbb{R}^d$ outputs by $\mathcal{M}_R$ a low-dimensional diffeomorphic (or homeomorphic) version of $\mathcal{M}$, where $d < n$. If the map R^{-1} is computationally not too expensive, then the Möbius transforms and filtering procedures in the low dimensional space $R(X_f)$ will improve the algorithmic performance.

The remainder of this chapter is structured as follows. First, we present a short description of radial basis functions as a tool for transforming data from low to high dimensions. In Section 6.1.1, we describe basic ideas of Clifford algebras as a setting for defining Möbius transforms in high dimensions. In Section 6.1.2, we discuss the potential relevance of cluster analysis with persistent homology. Finally, in Section 6.1.3, we present several computational experiments illustrating the separation and classification of signals.

Radial Basis Function Interpolation

An important ingredient in our framework are radial basis functions (RBF) and their interpolation methods for high-dimensional data. As previously described in our framework (Section 6.1), our usage of dimensionality reduction requires to map data between high and low dimensional spaces. Some dimensionality reduction methods have intrinsic interpolation strategies, but in general, the reconstruction of high-dimensional data from

the low-dimensional representation is a non trivial problem. In order to consider a flexible framework that embraces different reduction methods, we consider the multi-purpose features of RBFs as already suggested, for instance, in [9].

The inputs of the RBF interpolation methods are the datasets $X = \{x_i\}_{i=1}^m \subset \mathbb{R}^n$ and $Y = \{y_i\}_{i=1}^m \subset \mathbb{R}^d$. The RBF interpolant requires a family of centers $\{c_j\}_{j=1}^N$ (simply chosen randomly from the datasets in our experiments), and can be written as:

$$y_k = w_0 + \sum_{j=1}^{N} w_j \phi(\|x_k - c_j\|), \quad k = 1, \ldots, m,$$

or in matrix form, this can be described as:

$$Y = W\Phi^T,$$

with the $m \times (N+1)$ matrix $\Phi = (\mathbf{1}_m, \Phi_1, \ldots, \Phi_N)$, $(\Phi_j)_k = \phi(\|x_k - c_j\|)$, the $d \times (N+1)$ coefficient matrix $W = (w_0, \ldots, w_N)$, and the $d \times m$ matrix $Y = (y_1, \ldots, y_m)$. A solution can be constructed with the *pseudo-inverse* $\Phi^\dagger$: $W^T = \Phi^\dagger Y^T$. In our computational experiment we use the Gaussian RBF $\phi(r) = \exp(-r^2/\alpha)$, for some fixed $\alpha > 0$.

6.1.1 The Clifford Algebra Toolbox

Another ingredient in our framework is a mechanism for manipulating the geometry of a point cloud data. For this purpose a basic building block is given by the conceptual interplay between Clifford algebras, exterior algebras, and geometric algebra. These tools can be particularly important in the design of signal separation and classification algorithms. In fact they provide efficient algebraic methods for manipulating geometrical data, and they lead to flexible nonlinear functions in high dimensional spaces. Here, we focus on the construction of a fundamental nonlinear map, the Möbius transformation in $\mathbb{R}^n$.

A Clifford algebra is a generalization of the complex numbers defining a product in the vector space $V = \mathbb{R}^n$ with similar properties as the complex multiplication. More precisely, let q_n be the standard Euclidean inner product in $\mathbb{R}^n$. Then, the Clifford algebra $\mathrm{Cl}_n = \mathrm{Cl}(\mathbb{R}^n, q_n)$ is an associative algebra generated by the elements of $\mathbb{R}^n$ subject (only) to the relation $v^2 = -q_n(v, v)1, v \in \mathbb{R}^n$. More general bilinear forms q_n are of relevance in many fields (e.g. differential geometry or noncommutative geometry [57]), but here we restrict ourselves to the case of the standard inner product. An explicit construction is given by considering Cl_n to be the associative algebra over the reals generated by elements $e_1, \ldots, e_n$ subject to the relations $e_i^2 = -1$, $e_i e_j = -e_j e_i, i \neq j$ (anti-commutativity). Every element $a \in \mathrm{Cl}_n$, can be represented as

$$a = \sum_J a_J e_J, \quad e_J := e_{j_1} \ldots e_{j_k},$$

where each a_J is real, and the sum ranges over all multi-indices $J = \{j_i\}_{i=1}^k \subseteq \{1, \ldots, n\}$ with $0 < j_1 < \cdots < j_k \leq n$. Sometimes we will abuse the notation $e_\emptyset = e_0 = 1$ for the unit of the algebra Cl_n, but it is important not to confuse the unit of Cl_n, $e_0 = 1$, with the unit of the field $\mathbb{R}$. With this construction it is clear that $\dim(\mathrm{Cl}_n) = 2^n$. We follow

the (non standard) selection of Vahlen and Ahlfors [1], by identifying the *vectors* of $\mathbb{R}^n$ with the elements spanned by $e_0, \ldots, e_{n-1}$. There are three important involutions in Cl_n similar to the complex conjugation. The *main involution* defined as $a \to a'$ which replaces each e_J by $-e_J$, the *reversion* $a \to a^*$, which reverses the order of each multi-index in e_J, and their combination, the *Clifford conjugation*, $a \to \bar{a} := a'^* = a^{*\prime}$. An important subgroup of the Clifford algebra is Γ_n, the *Clifford group*, which is the set of invertible elements in Cl_n that can be represented as products of non-zero vectors in $\mathbb{R}^n$.

With our particular identification of vectors $\mathbb{R}^n$ in Cl_n, the Clifford product xy between two vectors $x, y \in \mathbb{R}^n$, $x = \sum_{i=0}^{n-1} x_i e_i$, $y = \sum_{i=0}^{n-1} y_i e_i$, can be written as

$$\begin{aligned} xy = &\Big(x_0 y_0 - \sum_{i=1}^{n-1} x_i y_i\Big) e_0 + \sum_{i=1}^{n-1} (x_0 y_i + x_i y_0) e_i \\ &+ \sum_{i=1}^{n-1} \sum_{i<j} (x_i y_j - x_j y_i) e_{ij}. \end{aligned}$$

Remark 6.1.1. (Geometric Algebra) An algebraic structure closely related to the Clifford algebra is the *exterior algebra* (or *Grassmann algebra*), $\Lambda(V)$, generated by the elements $e_1, \ldots, e_n$ with the *wedge product* (or *exterior product*) defined by the relations $e_i \wedge e_i = 0$ and $e_i \wedge e_j = -e_j \wedge e_i, i \neq j$. Basic building blocks are the exterior products of k-vectors $\{v_i\}_{i=1}^k$, also referred as *k-blades* $v_1 \wedge \cdots \wedge v_k$, and linear combinations of blades, called *multi-vectors*. A useful property of the exterior product is the efficient algebraic representation of basic geometrical entities. More precisely, if we have a k-dimensional homogeneous subspace W spanned by k vectors $\{w_i\}_{i=1}^k$, the k-blade $w = w_1 \wedge \cdots \wedge w_k$ can be used to represent W as

$$x \in W \iff x \wedge w = 0.$$

For instance, if x is an element of the line spanned by $v \in V$, we have $x = \lambda v$ iff $x \wedge v = 0$. If x lies in a plane spanned by v and u, then $x = \lambda v + \gamma u$ iff $x \wedge v \wedge u = 0$. But this framework is not only restricted to homogeneous subspaces: further generalizations can be considered with the same algebraic efficiency for more elaborate geometrical objects [26]. Particularly important tools in this field are efficient algorithms (the `join` and `meet` operations) for constructing the intersection and union of subspaces.

Möbius Transforms in $\mathbb{R}^n$

Möbius transformations, and the general concept of conformal maps, have appeared in a wide range of theoretical and practical applications, ranging from airfoil design in aerodynamics to modern problems in brain surface conformal mapping. In this chapter, we are interested in their flexible geometrical properties for designing invertible nonlinear maps with computationally efficient algebraic characteristics. Recall that a Möbius transformation is a function $\mathfrak{f} : \hat{\mathbb{C}} \to \hat{\mathbb{C}}$, with $\hat{\mathbb{C}} = \mathbb{C} \cup \{\infty\}$, of the form

$$\mathfrak{f}(z) := \frac{az + b}{cz + d},$$

where $\left(\begin{smallmatrix} a & b \\ c & d \end{smallmatrix}\right) \in \mathrm{Mat}(2, \mathbb{C})$, with $ad - bc \neq 0$. During the last century, Möbius transforms were generalized by Vahlen, Maass, and Ahlfors to arbitrary vector spaces using Clifford algebras and Clifford groups [1]:

Definition 6.1.1. For the vector space $V = \mathbb{R}^n$, a Möbius transform $\mathfrak{f} : \hat{\mathbb{R}}^n \to \hat{\mathbb{R}}^n$, with $\hat{\mathbb{R}}^n := \mathbb{R}^n \cup \{\infty\}$, is defined as $\mathfrak{f}(v) = (av + b)/(cv + d)$, where the *Clifford matrix* $H_{\mathfrak{f}} := \left(\begin{smallmatrix} a & b \\ c & d \end{smallmatrix}\right) \in \mathrm{Mat}(2, \mathrm{Cl}_n)$ is required to satisfy the following three conditions.

1) $a, b, c, d \in \Gamma_n \cup \{0\}$,

2) $ab^*, cd^* \in \mathbb{R}^n$,

3) $\Delta(\mathfrak{f}) := ad^* - bc^* \in \mathbb{R}^*$.

Remark 6.1.2. (The Vahlen-Maass Theorem) The *Vahlen-Maass Theorem* states that the set of Clifford matrices, denoted by $\mathrm{SL}_2(\Gamma_n)$, forms a group under the matrix multiplication. Moreover, the product $H_{\mathfrak{f}}H_{\mathfrak{g}}$ corresponds to composition of Möbius transforms $\mathfrak{f} \circ \mathfrak{g}$. The Vahlen-Maass Theorem also relates the concept of Möbius maps as composition of *similarities* and *inversions over the unit sphere* with the Clifford matrices. The expression $\Delta(\mathfrak{f})$ is sometimes denominated *pseudo determinant*.

An Explicit Construction

In this section, we provide a simple and explicit construction of a Möbius transform in $\mathbb{R}^n$, satisfying the three conditions in Definition 6.1.1. This yields an algorithm for designing Möbius transformations matching our specific needs, as for instance, the construction of hyperbolic transformations from two given fixed points.

Remark 6.1.3. (Constructing Möbius transforms in $\hat{\mathbb{C}}$) For designing a Möbius transform in $\hat{\mathbb{C}}$ such that $\mathfrak{f}(x) = u, \mathfrak{f}(y) = v, \mathfrak{f}(z) = w$ we can use the following standard construction which consist of first mapping the points x, y, z to $0, 1$ and ∞ using $\mathfrak{f}_1(x) = 0$, $\mathfrak{f}_1(y) = 1$, and $\mathfrak{f}_1(z) = \infty$, with

$$\mathfrak{f}_1(t) := \frac{(t-x)(y-z)}{(t-z)(y-x)},\ H_{\mathfrak{f}_1} := \begin{pmatrix} y-z & x(z-y) \\ y-x & z(x-y) \end{pmatrix}.$$

If we consider also a second map $\mathfrak{f}_2$ with $\mathfrak{f}_2(u) = 0, \mathfrak{f}_2(v) = 1, \mathfrak{f}_2(w) = \infty$, we can now construct $\mathfrak{f} := \mathfrak{f}_2^{-1} \circ \mathfrak{f}_1$ with $\mathfrak{f}(x) = u$, $\mathfrak{f}(y) = v$, $\mathfrak{f}(z) = w$, using $H_{\mathfrak{f}} := H_{\mathfrak{f}_2}^{-1} H_{\mathfrak{f}_1}$.

The general idea of this construction can be extended to $\mathbb{R}^n$, but some constraints need to be considered. The following is a particular strategy that can be used in our framework.

Lemma 6.1.1. *Given a vector $x \in \mathbb{R}^n$, $n > 1$, we can construct a Möbius transform $\mathfrak{f}$ such that $\mathfrak{f}(x) = 0$, $\mathfrak{f}(y) = 1$ and $\mathfrak{f}(z) = \infty$, for $y, z \in \mathbb{R}^n$ provided that the following three conditions are fulfilled:*

1) $z_i = kx_i,\ i = 1, \ldots, n-1, \quad$ *for* $\ k \in \mathbb{R}^*$,

2) $y = \alpha x + \beta z, \quad$ *for* $\quad \alpha, \beta \in \mathbb{R}, \quad \alpha + \beta = 1$,

3) $3(x_0 - z_0)^2 = \sum_{i=1}^{n-1} (x_i - z_i)^2$.

Proof: Using the ideas of Remark 6.1.3, we analyze the three conditions in Definition 6.1.1. Recall that with our particular identification of $\mathbb{R}^n$ in Cl_n we have $x = \sum_{i=0}^{n-1} x_i e_i$, $y = \sum_{i=0}^{n-1} y_i e_i$, and $z = \sum_{i=0}^{n-1} z_i e_i$. For an arbitrary triple x, y, z, the coefficients

$$\begin{aligned} a &= y - z, \quad b = x(z - y), \\ c &= y - x, \quad d = z(x - y), \end{aligned}$$

fulfill the first requirement in Definition 6.1.1. As for the second condition in Definition 6.1.1, we have

$$\begin{aligned} ab^* &= (y - z)(z - y)^* x^* = -(y - z)^2 x, \\ cd^* &= (y - x)(x - y)^* z^* = -(y - x)^2 z, \end{aligned}$$

and the *pseudo determinant* is given by

$$\Delta(\mathfrak{f}) = ad^* - bc^* = (y - z)(x - y)(z - x).$$

Now, $(y - z)^2 x \in \mathbb{R}^n$ and $(y - x)^2 z \in \mathbb{R}^n$, if

$$\begin{aligned} (\mathbf{y} - \mathbf{z})^2 \wedge \mathbf{x} &= 0, \\ (\mathbf{y} - \mathbf{x})^2 \wedge \mathbf{z} &= 0, \end{aligned}$$

where $\mathbf{x}$ is the non-real part of x i.e. $\mathbf{x} = \sum_{i=1}^{n-1} x_i e_i$. These two conditions can be fulfilled if we require (as described in Remark 6.1.1) the vector $\mathbf{y} - \mathbf{z}$ to be an element of the line spanned by $\mathbf{x}$, and the vector $\mathbf{y} - \mathbf{x}$ to be an element spanned by $\mathbf{z}$. Therefore we have $\mathbf{z} = k\mathbf{x}$, $k \in \mathbb{R}$. If we select a vector $y = \alpha x + \beta z$, $\alpha + \beta = 1$, we have

$$ad^* - bc^* = (y - z)(x - y)(z - x) = \alpha\beta(z - x)^3.$$

Now, for a vector $v = \sum_{i=0}^{n-1} v_i e_i \in \mathbb{R}^n$ we have

$$v^3 = \left(v_0^2 - \textstyle\sum_{i=1}^{n-1} v_i^2\right) e_0 + \displaystyle\sum_{i=1}^{n-1} \left(3v_0^2 - \textstyle\sum_{i=1}^{n-1} v_i^2\right) v_i e_i.$$

Therefore $v^3 \in \mathbb{R}$ if and only if $3v_0^2 = \sum_{i=1}^{n-1} v_i^2$, which implies that $(z - x)^3 \in \mathbb{R}$ if and only if $3(x_0 - z_0)^2 = \sum_{i=1}^{n-1} (x_i - z_i)^2$. We finally notice that by combining these conditions we also need $\mathbf{z} = k\mathbf{x}$, for $k \in \mathbb{R}^*$. ■

Note that we can relax our above conditions on $y - z$ (resp. $y - x$). But the statement on Lemma 6.1.1 is sufficient for our next objective. In particular, we can now construct a variety of useful linear or nonlinear maps in $\mathbb{R}^n$ as hyperbolic Möbius transforms based on the next proposition.

Proposition 6.1.1. *For a pair $u, v \in \mathbb{R}^n$, $n > 1$, and two vectors $w_i = \alpha_i u + \beta_i v$, $i = 1, 2$, with $\alpha_i + \beta_i = 1$, $\alpha_i, \beta_i \in \mathbb{R}$, there exists a Möbius transform $\mathfrak{f} : \hat{\mathbb{R}}^n \to \hat{\mathbb{R}}^n$ satisfying $\mathfrak{f}(u) = u$, $\mathfrak{f}(v) = v$, and $\mathfrak{f}(w_1) = w_2$.*

Proof: This follows as a straightforward consequence of Lemma 6.1.1 and the Vahlen-Maass Theorem which relates the group structure of $\mathrm{SL}_2(\Gamma_n)$ with the composition of

Möbius transforms in $\mathbb{R}^n$ (see Remark 6.1.2). More precisely, following the lines of Remark 6.1.3, we first consider the translation $\mathfrak{t}$, with $\mathfrak{t}((u+v)/2) = 0$, followed by a rotation $\mathfrak{r}$, such that the third condition of Lemma 6.1.1 is fullfilled. Now we can use Lemma 6.1.1 for constructing two Möbius maps $\mathfrak{f}_1, \mathfrak{f}_2$ with $\mathfrak{f}_1(\mathfrak{r}(\mathfrak{t}(u))) = 0, \mathfrak{f}_1(\mathfrak{r}(\mathfrak{t}(w_1))) = 1, \mathfrak{f}_1(\mathfrak{r}(\mathfrak{t}(v))) = \infty$, and $\mathfrak{f}_2(\mathfrak{r}(\mathfrak{t}(u))) = 0, \mathfrak{f}_2(\mathfrak{r}(\mathfrak{t}(w_2))) = 1, \mathfrak{f}_2(\mathfrak{r}(\mathfrak{t}(v))) = \infty$. Using now the Vahlen-Maass Theorem the composition $\mathfrak{f} := \mathfrak{t}^{-1}\mathfrak{r}^{-1}\mathfrak{f}_2^{-1}\mathfrak{f}_1\mathfrak{r}\mathfrak{t}$ is a Möbius transform and its Clifford matrix is given by $H_{\mathfrak{f}} = H_{\mathfrak{t}}^{-1}H_{\mathfrak{r}}^{-1}H_{\mathfrak{f}_2}^{-1}H_{\mathfrak{f}_1}H_{\mathfrak{r}}H_{\mathfrak{t}}$. ■

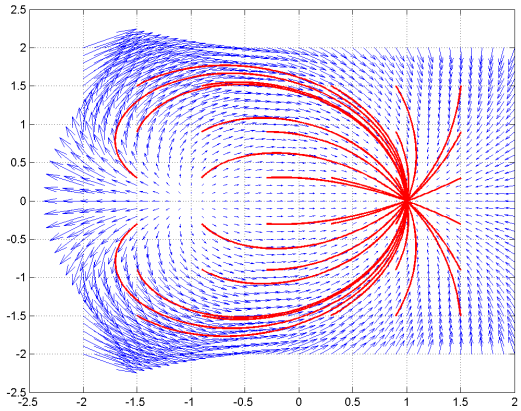

Figure 6.1: Hyperbolic Möbius transform with two fixed points (one attractive and one repulsive).

By Proposition 6.1.1, we can now construct hyperbolic Möbius transforms by calibrating its vector field (see Fig. 6.1) with the vectors w_1 and w_2. These kind of maps have useful properties for shrinking or separating clusters. In general, with Lemma 6.1.1 we can also design other maps, as rotations in $\mathbb{R}^n$, with alternative constructions to more classical strategies as the well known *Procrustes problem*.

6.1.2 Persistent Homology and Clusters

Cluster analysis is a fundamental component in the analysis of point cloud data (PCD). Recent developments in applied topology have provided robust computational and conceptual mechanisms for topological analysis of PCD [14]. For instance, the persistent homology algorithm provides qualitative information as the numbers of components, holes or voids of a PCD. This information is codified in the concept of *Betti numbers*, an algebraic topological construct characterizing a topological space by the number of unconnected components, two and three dimensional holes, (voids, circular holes), etc. Another important task we require is a hierarchical cluster analysis (dendrogram) of a PCD, together with a detection of its center components. Recent developments from applied topology have made first progress with addressing these issues, both from a conceptual and computational point of view. [14]. A basic concept relating a given point cloud data $X = \{x_i\}_{i=1}^m$ with its topological structure is the notion of an ϵ-covering, denoted $\mathbb{X}_\epsilon$, and defined as the union of balls $B_\epsilon(x)$ of radius $\epsilon > 0$ centered around each $x \in X$,

$$\mathbb{X}_\epsilon = \bigcup_{x \in X} B_\epsilon(x).$$

The output of the persistent homology algorithm is a barcode of intervals representing a summary of the topological information, in the form of Betti numbers, for each $\mathbb{X}_\epsilon$, where $\epsilon \in [0, \epsilon_{\max}]$. As a straightforward application, we present in Fig. 6.2 the persistent barcodes for the PCD generated with the spectrogram of a corrupted speech signal. The correct interpretation and usage of persistent homology for analyzing frequency representation of signals is still work in progress, but the robust conceptual machinery of this framework is a strong motivation for a better understanding of its properties.

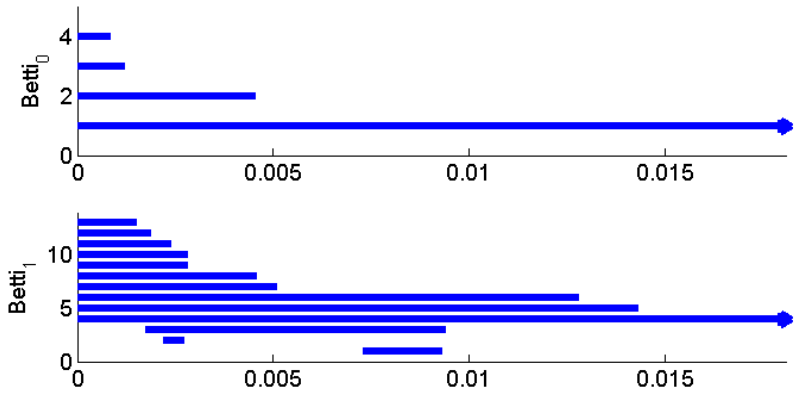

Figure 6.2: Betti barcodes of a PCD spectrogram of the corrupted speech signal in the experiment of Fig. 6.5b.

6.1.3 Computational Experiments

In this section we present numerical examples concerning the dimensionality reduction problem using synthetic signals, based on modulation maps, and the separation and classification of speech signals.

Frequency Modulated Manifolds

The analysis based on the Clifford algebra machinery is applied to a low dimensional representation $P(X_f)$ of a dataset X_f for a signal f, and a dimensionality reduction map P. This example quickly reintroduces the problems of combining the dimensionality reduction map P with signal manipulations (e.g. modulation maps). We first show a basic phenomenon occurring when using dimensionality reduction methods in time domain signals and their frequency representations. We first rephrase the concept of *frequency modulated manifold* (see the Example 4.2.2) based on the standard notion of modulation techniques, but here placed in a more geometrical setting. Modulation techniques are well-known engineering procedures used to transmit data by varying the frequency content of a carrier signal. We analyze, from a dimensionality reduction viewpoint, a *frequency modulation map* $\mathcal{A} : \Omega \to \mathcal{M} \subset \mathbb{R}^n, \Omega \subset \mathbb{R}^d$, where $\mathcal{M}$ contains the carrier signals modulated by Ω. We define $\mathcal{A}_\alpha(t_i) = \sum_{k=1}^{d} \sin((\alpha_k^0 + \gamma\alpha_k)t_i)$, $\alpha = (\alpha_1, \alpha_2, \alpha_3) \in \Omega$, $\{t_i\}_{i=1}^n \subset [0, 1]$. The bandwidth parameter γ controls each frequency band centered at α_k^0. The dataset to analyze (the modulated manifold) is $\mathcal{M} = \{\mathcal{A}_\alpha\}_{\alpha\in\Omega}$, and for a Torus example $\Omega = \mathbb{T}^2, d = 3$, we notice the difficulty of recovering Ω with PCA, both

in time and frequency domains (Figs. 6.3b, 6.4a). Isomap improves the reconstruction but still with a significant distortion (Fig. 6.4b). These examples were generated with $\alpha_1^0 = 1000\text{Hz}, \alpha_2^0 = 1200\text{Hz}, \alpha_3^0 = 1400\text{Hz}$, and a bandwidth of 180Hz.

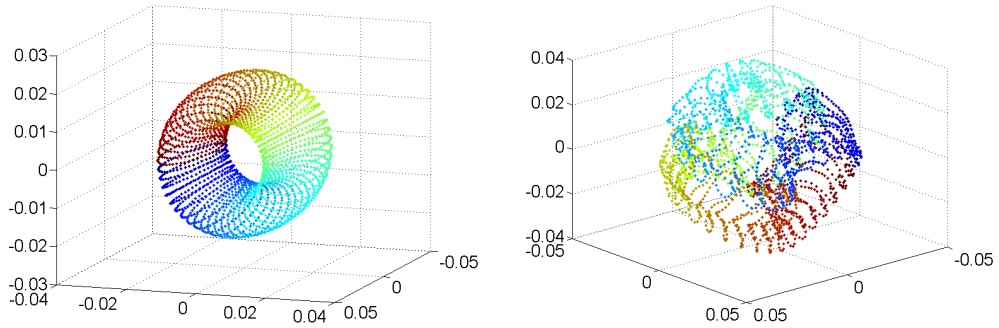

(a) **(b)**

Figure 6.3: **(a)** The torus $\Omega = \mathbb{T}^2 \subset \mathbb{R}^3$; **(b)** The PCA 3D projection of $\mathcal{M} = \{\mathcal{A}_\alpha\}_{\alpha \in \Omega}$.

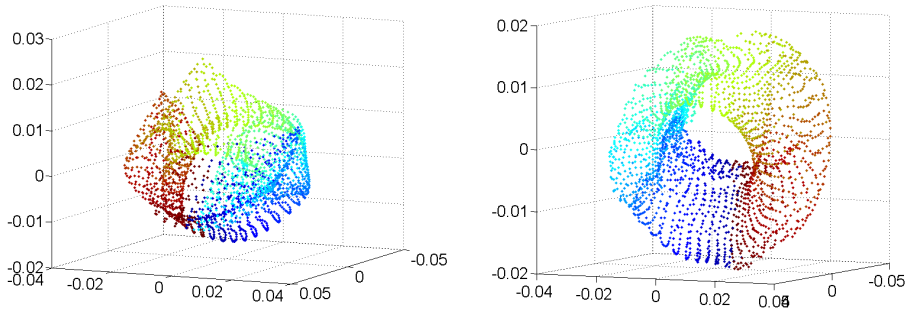

(a) **(b)**

Figure 6.4: **(a)** The PCA 3D projection of the frequency content of $\mathcal{M}$. **(b)** The Isomap 3D projection of the frequency content of $\mathcal{M}$.

Separation of Speech Signals

In this second set of examples, we now separate speech signals distorted with transient phenomena represented by regular clicks. Recall that we use a non-blind strategy, and a preliminary learning phase is required for storing low-dimensional clusters for the speech and click components. In the learning phase, we reduce the dimensionality of the spectrogram data (from $\mathbb{R}^{128}$ to $\mathbb{R}^8$), and we design a hyperbolic Möbius transform in $\mathbb{R}^8$, together with a rotational map that moves and shrinks the click cluster close to an element of the standard basis. In this case filtering procedures and projection maps can be applied. The main transformations involved are invertible, and we can then reconstruct signal data with RBF interpolation (Figs. 6.5,6.6). Despite the acoustical artifacts still

present in the current prototype, these preliminary results indicates the feasibility of this method, especially since no particular calibration has been included.

In Figure 6.5(a) we see the spectrogram of the mixture speech signals and clicks, where the frequency content of the corrupting clicks are clearly visible in a regular pattern in the lower frequency area. In Figure 6.5(b) we see a two dimensional projection of the point cloud data whose elements are constructed from the FFT vectors in the spectrogram (i.e. each column in the spectrogram corresponds to a element in the point cloud data). In Figure 6.5(b) we see the two clusters (speech in red and clicks in blue) in the learning phase. In Figure 6.6 we see the resulting spectrograms of the separated signals, where in Figure 6.6(a) we have the spectrogram of the signal with prominent speech component, and in Figure 6.6(b) we have the spectrogram with prominent click component.

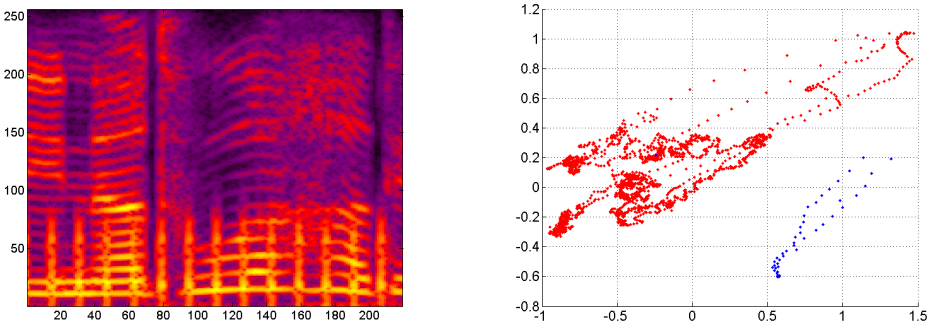

(a) **(b)**

Figure 6.5: **(a)** The spectrogram of the speech signal corrupted by regular clicks **(b)** The point cloud data of the speech and click signal in the learning phase.

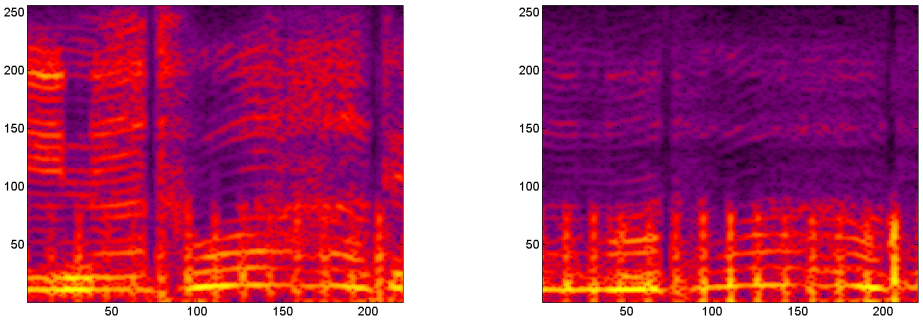

(a) **(b)**

Figure 6.6: **(a)** Extracting the speech signal **(b)** Extracting the clicks signal

Classification of Speech Components

Another example for application of this framework is the classification or identification of consonants in a speech signal. The analysis procedures are similar as in the previous

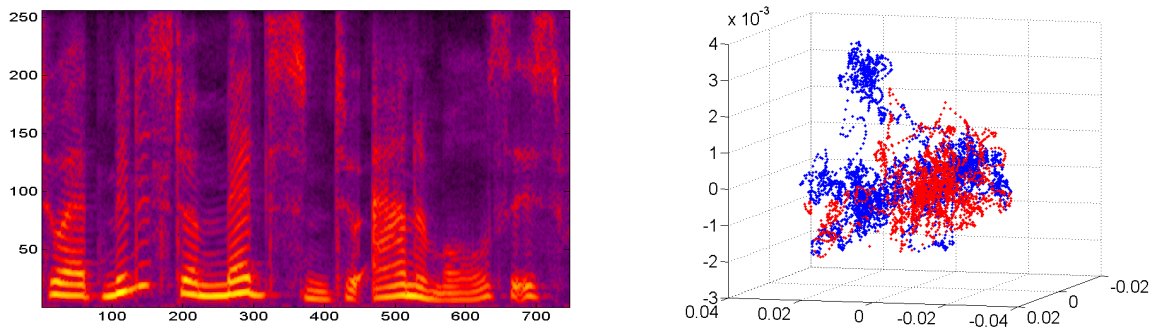

(a) **(b)**

Figure 6.7: **(a)** Spectrogram of speech signal **(b)** PCA projection with consonants (red) vs vocals (blue).

example, but here, no reconstruction step is required. In Figure 6.7, we have the spectrogram of the speech signal, and the corresponing point cloud data (similarly, as explained in the setting of the Figure 6.5). The 3D projection of the point cloud data presented in Figure 6.7(a) is implemented with PCA, but the alternatives using Isomap and our Isomap with Möbius projection is shown in Figure 6.8(a) and Figure 6.8(b) respectively.

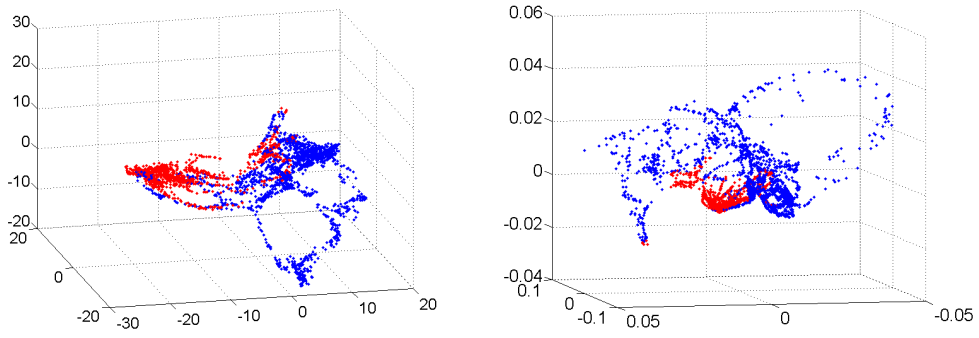

(a) **(b)**

Figure 6.8: **(a)** Isomap projection and consonants (red) vs vocal (blue) components **(b)** Isomap-Möbius projection.

With PCA, an identification of the consonant cluster can be achieved, but Isomap slightly improves the separation of vocal and consonant clusters, which can then be further improved with a Möbius map, designed with an attractive fixed point located in the center of the consonant cluster (Figs. 6.7, 6.8).

6.2 Dimensionality Reduction and ISA for Signal Detection

We now explain a basic engineering strategy ([15]) for the separation of a signal $f = \sum_i f_i$, based on a combination of dimensionality reduction tools with time-frequency representations. In this context, recent developments for (single-channel) signal separation have been proposed using time-frequency data and a combination of independet component analysis (ICA) and principal component analysis (PCA). Given a mixture of signals $f = \sum_i f_i$, the task is to estimate the components f_i given some characteristics on their time-frequency or statistical properties. An important strategy, known as *independent subspace analysis* (ISA), is to reduce the embedding dimension of the time-frequency representation of f, prior to the application of independent component analysis (ICA). In these methods, a standard strategy for dimensionality reduction is principal component analysis (PCA), but nonlinear methods have also being proposed for this task [35]. In this Section, we compare different dimensionality reduction methods for single channel signal separation in the context of ISA. Our focus is on signals with transitory components, and the objective is to detect the locations in time where each individual signal f_i is activated.

6.2.1 Preliminaries

Signal separation is a crucial task in many application fields, and its modern development depends on experimental breakthroughs supported by a correct understanding of the underlying mathematical framework. In the last decade, several approaches have been proposed for the problem of blind source separation of single channel signals. A fundamental strategy proposed in [15, 35] combines independent component analysis (ICA) methods with time-frequency transforms. These ideas have been extended by considering other types of matrix decompositions in addition to the statistically oriented strategy of ICA. In particular, methods using non-negative matrix factorization techniques have gained significant attention in recent years.

A crucial step in many of these strategies is to reduce the dimension of the Euclidean space where the time frequency representation is embedded. New methods for dimensionality reduction of point cloud data $X = \{x_i\}_{i=1}^m \subset \mathbb{R}^n$ have actively been developed using geometrical and topological concepts [58]. Novel algorithms based on concepts from differential geometry are Whitney embedding based methods, isomap, local tangent space alignment (LTSA), Laplacian eigenmaps, Riemannian normal coordinates (RNC), to mention but a few.

The objective of this Section is to evaluate the usage of new dimensionality reduction tools in signal detection and separation algorithms. Recent developments on this topic were presented in [35], but further investigations on the signal processing and mathematical framework of these algorithms are essentially required. This Section discusses various important aspects concerning the application of dimensionality reduction methods in the context of ISA. In particular, we focus on the signal detection problem in a complex mixture of transitory acoustic sounds. A better mathematical understanding of these procedures, and additional empirical insights, are fundamental for improving current strategies and designing new methods for signal separation.

The outline of this Section is as follows. We first present briefly some basic ideas

on ICA and its relation to dimensionality reduction strategies. In Section 6.2.2, we briefly review current techniques proposed in the literature for independent subspace analysis. Finally, in Section 6.2.3, we present computational experiments illustrating the signal detection capabilities of the ISA and dimensionality reduction framework using two different methods, the linear PCA method and nonlinear Laplacian eigenmaps.

Independent Component Analysis (ICA)

The ICA algorithm is a separation algorithm based on statistical principles for unmixing a linear combination of signals. The ICA procedure is not, in a strict sens, a dimensionality reduction method, but it is frequently used in combination with classical dimensionality reduction methods such as PCA. The input of the ICA algorithm is the point cloud data $X = \{x_i\}_{i=1}^m \subset \mathbb{R}^n$ written in matrix form as $X = (x_1 \dots x_m) \in \mathbb{R}^{n\times m}$. The objective is to find a matrix of source signals $S = (s_1 \dots s_m) \in \mathbb{R}^{n\times m}$, assuming a linear dependence between X and S. By denoting the *mixing matrix* as $W \in \mathbb{R}^{n\times n}$, this can be expressed as:

$$X = WS, \quad X, S \in \mathbb{R}^{n\times m}, W \in \mathbb{R}^{n\times n}.$$

In this equation, the mixing matrix W and the source signals S are unknown variables, and ICA estimates these matrices using some assumptions on the statistical independence of the signals $\{s_i\}_{i=1}^n$. The general strategy uses the following measure for a set of random variables $Y = \{y_i\}_{i=1}^n$:

$$I(Y) = D(P_Y, \prod_i P_{Y_i}), \quad D(p,q) = \int_{\mathbb{R}} p(x) \log\left(\frac{p(x)}{q(x)}\right) dx.$$

The measure I allows us to compute the degree of statistical independence by comparing the joint distribution P_Y, and the marginal distributions P_{Y_i}. The comparison function D, used in the measure I, is the *Kullback-Leibler distance*, also known as *relative entropy*. This allows us to formulate the ICA algorithm as an optimization problem, where the solution space is the *general linear group*, defined as the set of $n \times n$ invertible matrices, $\mathrm{GL}(n,\mathbb{R}) = \{A \in \mathbb{R}^{n\times n},\ \det(A) \neq 0\}$, with $p(A) := I(A^{-1}X)$:

$$W = \underset{A\in \mathrm{GL}(n,\mathbb{R})}{\operatorname{argmin}}\ p(A).$$

6.2.2 ISA and Time-Frequency data

With the previous background on dimensionality reduction and unmixing methods based on ICA, we now describe ISA as an important strategy for single-channel signal separation. We recast the concepts with following along the lines of [15, 35, 88, 90].

The original meaning of the term *independent subspace analysis* (ISA) is related to a generalization of independent component analysis by considering a multidimensional version of ICA. In very general terms, the main idea is to group the source vectors $\{s_i\}$ in subfamilies or linear subspaces, where the elements within each subgroup are statistically dependent, but elements of different groups are statistically independent (see e.g. [52]). Due to the work of Casey and Westner [15], the term ISA has frequently been used to denote methods using ICA to decompose power spectrograms of single channel signals for sound separation (see [90]).

The concept of ISA for single channel signal separation consist of decomposing a signal $f = \sum f_i$, by applying ICA to a dimensionality reduced representation of the power spectrogram. More precisely, given the function f, we compute the power spectrogram by considering $T(x_i)$ as the magnitude of the discrete Fourier transform FT of each element of the point cloud data $X_f = \{x_i\}_{i=1}^m$. Namely, $T(x_i)_k = \|\mathrm{FT}(x_i)_k\|$, for $k = 1, \ldots, m$. The following step is to use the power spectrogram $T(X_f)$ for constructing its low-dimensional representation $P(T(X_f))$ using a linear or nonlinear method P (e.g. PCA, Laplacian eigenmaps, LTSA, etc). We then apply ICA to the dataset $P(T(X_f))$ for unmixing the resulting signals, to obtain estimations of the components f_i. We briefly explain these steps as follows (cf. [15, 88, 90]).

1- Construct a dimensionality reduced power spectrogram using principal component analysis, (i.e. $P = \mathrm{PCA}$),

$$X_f \xrightarrow{T} T(X_f) \xrightarrow{P} P(T(X_f))$$

2- Unmix the resulting matrix $P(T(X_f))$ using ICA,

$$P(T(X_f)) \xrightarrow{\text{ICA}} \{\tilde{f}_i\}$$

3- Group different components $\{\tilde{f}_i\}$ to estimate the signals f_i in $f = \sum_i f_i$.

In order to reconstruct the spectrogram for each f_i, we apply the inverse short term Fourier transform with the phase information of the original mixture signal f (see [15, 88, 90] for details). We consider using different dimensionality reduction methods P, with focussing on Laplacian eigenmaps and isomap. We finally remark that in recent developments new types of unmixing methods have been used in step 2 for replacing the statistically oriented ICA strategy. In particular, non-negative matrix factorizations have gained increasing attention (see [90]).

6.2.3 Computational Experiments

To compare the signal detection quality for different dimensionality reduction methods, we construct a mixture of acoustic transient signals. We consider $f = f_1 + f_2$, where f_1 is a sequence of *castanets* and f_2 a *cymbal* signal, as depicted in Figure 6.9.

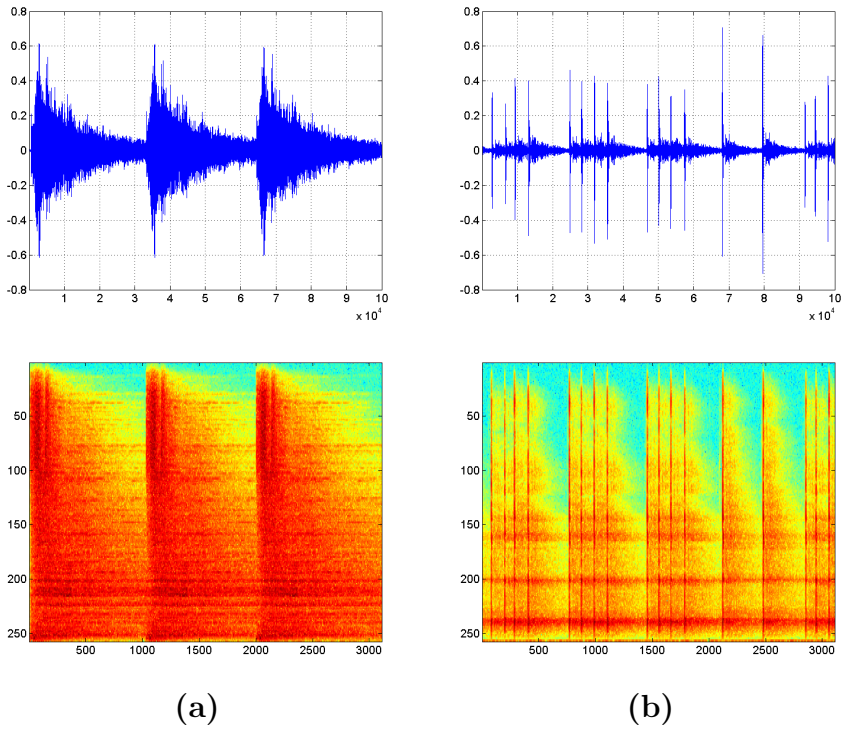

(a) (b)

Figure 6.9: (a) Cymbal signal f_1; (b) castanets signal f_2.

The combination $f = f_1 + f_2$ of the cymbal and castanets is depicted in Figure 6.10. The power spectrogram in this figure represents the point cloud data $T(X_f)$, where each column represents the FT of a segment x_i of the signal f. Due to the complex frequency characteristics of f, identifying and extracting the castanets signals is a very challenging task.

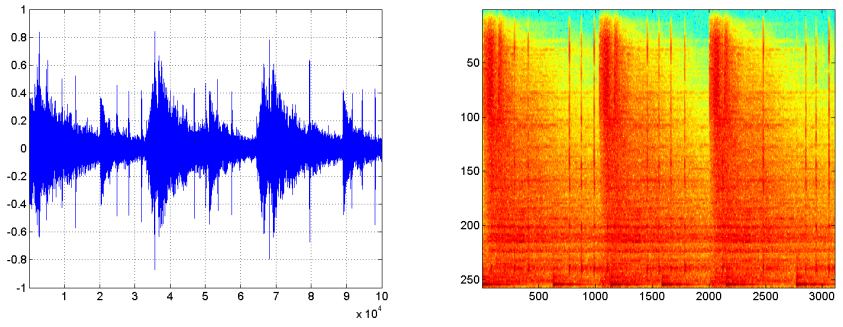

(a) (b)

Figure 6.10: Signal $f = f_1 + f_2$ and its power spectrogram $T(X_f)$.

In Figures 6.11-6.13, we present detection results for identifying the positions of the castanets and cymbal signals. To this end, we use the dimensionality reduction methods P = PCA, P = LE (Laplacian eigenmaps), and P = isomap. In the case of the two nonlinear methods (P = LE, P = isomap), a suitable nearest neighbor parameter k

can be selected [2]. We have manually identified some values for k that we display in Figures 6.12,6.13.

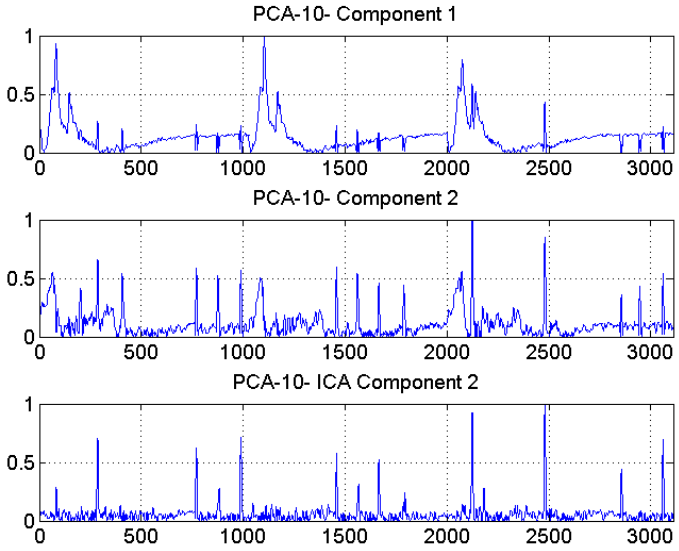

Figure 6.11: **PCA.** (a) cymbal (b) castanets (c) castanets (ICA).

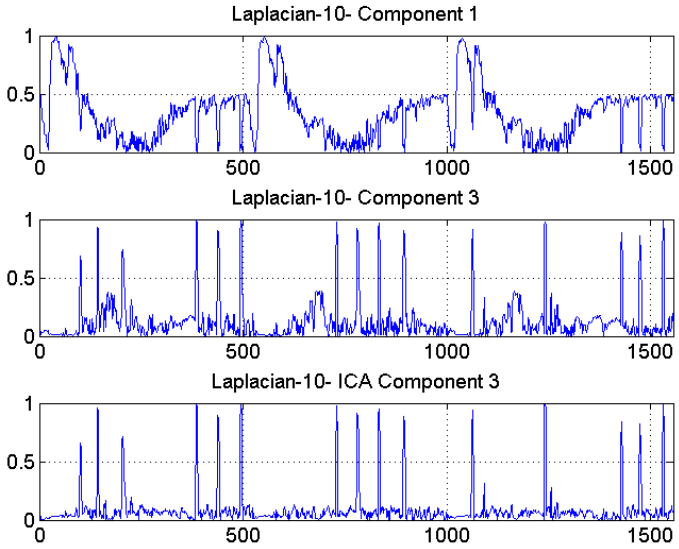

Figure 6.12: **LE.** (a) cymbal (b) castanets (c) castanets (ICA).

[2]Code available at `www.math.uni-hamburg.de/home/guillemard/`

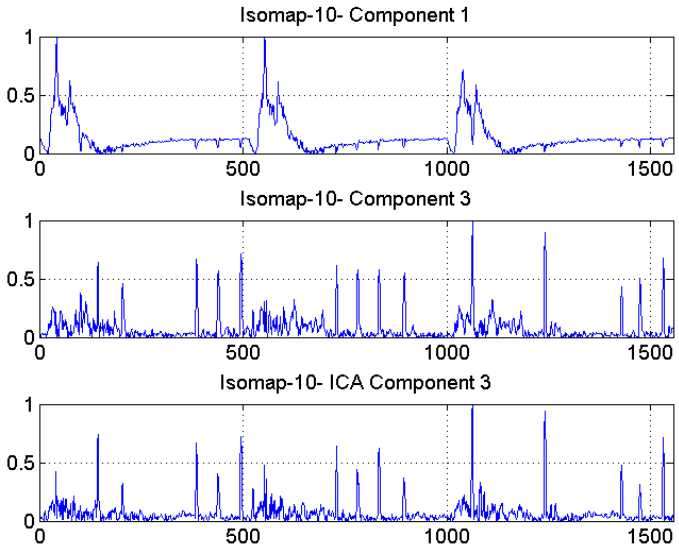

Figure 6.13: **Isomap.** (a) cymbal (b) castanets (c) castanets (ICA).

In Figures 6.11-6.13, (a) shows a component f_i that matches the cymbal signal, and the two plots (b) and (c) correspond to the components related to the castanet signal. Moreover, plots (a) and (b) are obtained from the detection algorithm without the ICA procedure, whereas in plot (c), the ICA procedure is activated. Note that the unmixing ICA algorithm slightly improves the quality of the castanets detection by decreasing some background signal in the case of PCA and Laplacian eigenmaps. In conclusion, these dimensional reduction strategies are able to detect the relevant signals for this particular example up to some degree, but further steps are required to improve the detection quality and the analysis of resynthesis algorithms.

Bibliography

[1] L.V. Ahlfors. Möbius transformations in $\mathbb{R}^n$ expressed through $2\times$ 2 matrices of Clifford numbers. *Complex Variables and Elliptic Equations*, 5(2):215–224, 1986.

[2] F.W. Anderson and K.R. Fuller. *Rings and categories of modules*, volume 13. Springer, 1992.

[3] AP Balachandran, G. Bimonte, E. Ercolessi, G. Landi, F. Lizzi, G. Sparano, and P. Teotonio-Sobrinho. Noncommutative lattices as finite approximations. *Journal of Geometry and Physics*, 18(2):163–194, 1996.

[4] M. Belkin and P. Niyogi. Laplacian Eigenmaps for Dimensionality Reduction and Data Representation, 2003.

[5] M. Belkin, J. Sun, and Y. Wang. Discrete Laplace operator on meshed surfaces. In *Proceedings of the twenty-fourth annual symposium on Computational geometry*, pages 278–287. ACM, 2008.

[6] B. Blackadar. *K-theory for operator algebras*, volume 5. Cambridge Univ Pr, 1998.

[7] E.D. Bloch. A Characterization of the Angle Defect and the Euler Characteristic in Dimension 2. *Discrete and Computational Geometry*, 43(1):100–120, 2010.

[8] A.I. Bobenko and Y.B. Suris. *Discrete Differential Geometry: Integrable Structure*. Amer Mathematical Society, 2008.

[9] DS Broomhead and M. Kirby. A New Approach to Dimensionality Reduction: Theory and Algorithms. *SIAM Journal on Applied Mathematics*, 60:2114, 2000.

[10] J. H. Brown. Proper Actions of Groupoids on C^*-Algebras. *to appear in Journal of Operator Theory arXiv:0907.5570*, 2009.

[11] J.H. Brown. *Proper Actions of Groupoids on C^*-Algebras*. PhD thesis, Darthmouth College, 2009.

[12] A. Brun, C.-F. Westin, M. Herberthson, and H. Knutsson. Fast manifold learning based on riemannian normal coordinates. In *Proceedings of the SCIA;05*, pages 920–929, Joensuu, Finland, June 2005.

[13] M.R. Buneci. Groupoid C^*-Algebras. *Surveys in Mathematics and its Applications*, 1:71–98, 2006.

[14] G. Carlsson. Topology and data. *American Mathematical Society*, 46(2):255–308, 2009.

[15] M.A. Casey and A. Westner. Separation of mixed audio sources by independent subspace analysis. In *Proceedings of the International Computer Music Conference*, 2000.

[16] J. Cheeger, W. Müller, and R. Schrader. On the curvature of piecewise flat spaces. *Communications in mathematical Physics*, 92(3):405–454, 1984.

[17] E. Christensen and C. Ivan. Spectral triples for AF C^*-algebras and metrics on the Cantor set. *Journal of Operator Theory*, 56(1):17–46, 2006.

[18] Ole Christensen. *An Introduction to Frames and Riesz Bases.* Applied and Numerical Harmonic Analysis. Birkhäuser, Boston, 2003.

[19] C. K. Chui. *An Introduction to Wavelets.* Academic Press, 1992.

[20] D. Cohen-Steiner, H. Edelsbrunner, and J. Harer. Stability of persistence diagrams. *Discrete and Computational Geometry*, 37(1):103–120, 2007.

[21] A. Connes. *Noncommutative Geometry.* Academic Press, 1994.

[22] A. Connes and M. Marcolli. A walk in the noncommutative garden. In *An invitation to noncommutative geometry*, pages 1–128. World Scientific Publishing, Hackensack, NJ, 2008.

[23] J. Cuntz. Noncommutative simplicial complexes and the Baum−Connes conjecture. *Geometric And Functional Analysis*, 12(2):307–329, 2002.

[24] A.C. Da Silva and A. Weinstein. *Geometric Models for Noncommutative Algebras.* Amer Mathematical Society, 1999.

[25] R.E. DeVille and E. Lerman. Dynamics on networks I. combinatorial categories of modular continuous-time systems. *Arxiv preprint arXiv:1008.5359*, 2010.

[26] L. Dorst, D. Fontijne, and S. Mann. *Geometric algebra for computer science: an object-oriented approach to geometry.* Morgan Kaufmann, 2009.

[27] H. Edelsbrunner and J. Harer. Persistent homology - a survey. In *Surveys on discrete and computational geometry: twenty years later: AMS-IMS-SIAM Joint Summer Research Conference, June 18-22, 2006, Snowbird, Utah*, volume 453, page 257. American Mathematical Society, 2008.

[28] H. Edelsbrunner, D. Letscher, and A. Zomorodian. Topological persistence and simplification. In *Proc. 41st Ann. IEEE Sympos. Found Comput. Sci.*, pages 454–463, 2000.

[29] E. Ercolessi and G. Landi. K-theory of noncommutative lattices. *K-Theory*, 18:339–362, 1999.

[30] E. Ercolessi, G. Landi, and P. Teotonio-Sobrinho. Noncommutative lattices and the algebras of their continuous functions. *Reviews in Mathematical Physics*, 10:439–466, 1998.

[31] R. Exel. A Fredholm operator approach to Morita equivalence. *K-theory*, 7(3):285–308, 1993.

[32] Hans G. Feichtinger and Karlheinz Gröchenig. A unified approach to atomic decompositions via integrable group representations. *Lect. Notes in Math.*, 1302:52–73, 1988.

[33] Hans G. Feichtinger and Karlheinz Gröchenig. Gabor wavelets and the Heisenberg group: Gabor expansions and short time Fourier transform from the group theoretical point of view. In *Wavelets: a tutorial in theory and applications*, volume 2 of *Wavelet Anal. Appl.*, pages 359–397. Academic Press, Boston, 1992.

[34] Hans G. Feichtinger and Karlheinz Gröchenig. Non-orthogonal wavelet and Gabor expansions, and group representations. In *Wavelets and their Applications*, pages 353–376. Jones and Bartlett, 20 Park Plaza, Boston, MA 02116, USA, 1992.

[35] D. FitzGerald, E. Coyle, and B. Lawlor. Independent subspace analysis using locally linear embedding. In *Proc. DAFx*, pages 13–17, 2003.

[36] G. B. Folland. *A Course in Abstract Harmonic Analysis*. CRC Press, Boca Ratón, 1995.

[37] R. Forman. A users guide to discrete Morse theory. *Seminaire Lotharingien de Combinatoire*, 48:B48c, 2002.

[38] R. Forman. Bochner's method for cell complexes and combinatorial Ricci curvature. *Discrete and Computational Geometry*, 29(3):323–374, 2003.

[39] G. Goehle. *Groupoid crossed products*. PhD thesis, Darthmouth College, Arxiv preprint arXiv:0905.4681, 2009.

[40] J. González and M. Guillemard. Algunas aplicaciones de la topología algebráica. *In Aportaciones Matemáticas, Sociedad Matemática Mexicana*, 42:153–170, 2011.

[41] J.M. Gracia-Bondía, J.C. Várilly, and H. Figueroa. *Elements of Noncommutative Geometry*. Birkhäuser, 2001.

[42] P. Green. C^*-algebras of transformation groups with smooth orbit space. *Pacific J. Math*, 72(1):71–97, 1977.

[43] M. Guillemard and A. Iske. Curvature analysis of frequency modulated manifolds in dimensionality reduction. *Calcolo*, 48(1):107–125, 2011.

[44] M. Guillemard and A. Iske. On groupoid C^*-algebras, persistent homology and time-frequency analysis. *Preprint*, 2011.

[45] M. Guillemard and A. Iske. Signal filtering and persistent homology: an illustrative example. *Proc. Sampling Theory and Applications (SampTA'11)*, 2011.

[46] M. Guillemard and A. Iske. Analysis of high-dimensional signal data by manifold learning and convolutions. *Sampling Theory and Applications (SampTA'09) Laurent Fesquet and Bruno Torrésani (eds.), Marseille (France)*, pages 287–290, May 2009.

[47] M. Guillemard, A. Iske, and S. Krause-Solberg. Dimensionality reduction methods in independent subspace analysis for signal detection. *Proc. Sampling Theory and Applications (SampTA'11)*, 2011.

[48] M. Guillemard, A. Iske, and Zoelzer U. Clifford Algebras and Dimensionality Reduction for Signal Separation and Classification. *Preprint*, 2010.

[49] A. Hatcher. *Algebraic Topology*. Cambridge University Press, 2002.

[50] H.C. Hege and K. Polthier. *Visualization and Mathematics III*. Springer Verlag, 2003.

[51] M. Holschneider. *Wavelets An Analysis Tool*. Clarendon Press Oxford, 1995.

[52] A. Ilin. Independent dynamics subspace analysis. In *Proc. ESANN 2006*, 2006.

[53] H. Kantz and T. Schreiber. *Nonlinear Time Series Analysis*. Cambridge Univ Pr, 2004.

[54] M. Khalkhali. *Basic Noncommutative Geometry*. European Mathematical Society, 2009.

[55] V. Kwatra, A. Schodl, I. Essa, G. Turk, and A. Bobick. Graphcut textures: Image and video synthesis using graph cuts. *ACM Transactions on Graphics*, 22(3):277–286, 2003.

[56] G. Landi. *An Introduction to Noncommutative Spaces and their Geometries*. Springer, Heidelberg, 1997.

[57] H.B. Lawson and M.L. Michelson. *Spin Geometry*. Princeton University Press, Princeton, New Jersey, 1989.

[58] J.A. Lee and M. Verleysen. *Nonlinear Dimensionality Reduction*. Springer, 2007.

[59] J.M. Lee. *Riemannian Manifolds: an Introduction to Curvature*. Springer Verlag, 1997.

[60] J.M. Lee. *Introduction to Smooth Manifolds*. Springer Verlag, 2003.

[61] T. Lin and H. Zha. Riemannian manifold learning. *IEEE Transactions on Pattern Analysis and Machine Intelligence*, 30(5):796, 2008.

[62] T. Lin, H. Zha, and S.U. Lee. Riemannian Manifold Learning for Nonlinear Dimensionality Reduction. *Lecture Notes in Computer Science*, 3951:44, 2006.

[63] P.C. Loizou. *Speech enhancement: theory and practice*. CRC press Boca Raton, FL, 2007.

[64] Y. Lu and P.C. Loizou. A geometric approach to spectral subtraction. *Speech communication*, 50(6):453–466, 2008.

[65] Franz Luef. On spectral invariance of non-commutative tori. In *Operator Theory, Operator Algebras, and Applications*, volume 414 of *Contemp. Math.*, pages 131–146. Amer. Math. Soc., Providence, RI, 2006.

[66] Franz Luef. Projective modules over non-commutative tori are multi-window Gabor frames for modulation spaces. *J. Funct. Anal.*, 257(6):1921–1946, 2009.

[67] Franz Luef. Projections in noncommutative tori and Gabor frames. *Proc. Amer. Math. Soc.*, 139(2):571–582, 2011.

[68] S. Mac Lane. *Categories for the working mathematician*, volume 5. Springer verlag, 1998.

[69] J. Mairal, M. Elad, and G. Sapiro. Sparse representation for color image restoration. *Image Processing, IEEE Transactions*, 17(1):53–69, 2008.

[70] S. Mallat. Group invariant scattering. *Arxiv preprint arXiv:1101.2286*, 2011.

[71] M. Meyer, M. Desbrun, P. Schröder, and A.H. Barr. Discrete differential-geometry operators for triangulated 2-manifolds. *Visualization and mathematics*, 3:35–57, 2002.

[72] Paul Muhly. *Coordinates in Operator Algebras*. Amer Mathematical Society, to appear.

[73] P.S. Muhly, J. Renault, and D.P. Williams. Equivalence and isomorphism for groupoid C^*-algebras. *J. Operator Theory*, 17(1):3–22, 1987.

[74] P.S. Muhly and D.P. Williams. Renaults equivalence theorem for groupoid crossed products. *New York Journal of Mathematics Monographs*, 3:1–83, 2008.

[75] P. Niyogi, S. Smale, and S. Weinberger. Finding the homology of submanifolds with high confidence from random samples. *Discrete and Computational Geometry*, 39(1):419–441, 2008.

[76] Y. Otsu and T. Shioya. The Riemannian structure of Alexandrov spaces. *J. Differential Geom*, 39(3):629–658, 1994.

[77] I. Raeburn and D.P. Williams. *Morita equivalence and continuous-trace C^*-algebras*, volume 60. Amer Mathematical Society, 1998.

[78] J. Renault. *A Groupoid Approach to C^*-Algebras*. Springer-Verlag, 1980.

[79] J. Renault. Représentation des produits croisés dalgebres de groupoides. *J. Operator Theory*, 18:67–97, 1987.

[80] M.A. Rieffel. Proper actions of groups on C^*-algebras. In *Mappings of operator algebras: proceedings of the Japan-US joint seminar, University of Pennsylvania, 1988*, volume 84, page 141. Birkhauser, 1991.

[81] S.T. Roweis and L.K. Saul. Nonlinear dimensionality reduction by locally linear embedding. *Science*, 290(5500):2323–2326, 2000.

[82] E. Saucan, E. Appleboim, and Y.Y Zeevi. Geometric sampling of manifolds for image representation and processing. *Lecture notes in Computer Science*, 4485:907, 2007.

[83] E. Saucan, E. Appleboim, and Y.Y. Zeevi. Sampling and Reconstruction of Surfaces and Higher Dimensional Manifolds. *Journal of Mathematical Imaging and Vision*, 30(1):105–123, 2008.

[84] T. Sauer, J.A. Yorke, and M. Casdagli. Embedology. *Journal of Statistical Physics*, 65(3):579–616, 1991.

[85] R.D. Sorkin. Finitary substitute for continuous topology. *International Journal of Theoretical Physics*, 30(7):923–947, 1991.

[86] S.T. Spencer and M.A. Casey. Elementary sources: Latent component analysis for music composition. In *Proc. 12th Intern. Conf. on Music Information Retrieval (ISMIR)*, 2011.

[87] J.B. Tenenbaum, V. de Silva, , and J.C. Langford. A global geometric framework for nonlinear dimensionality Reduction. *Science*, 290(5500):2319–2323, 2000.

[88] C. Uhle, C. Dittmar, and T. Sporer. Extraction of drum tracks from polyphonic music using independent subspace analysis. In *Proc. ICA*, pages 843–847, 2003.

[89] J.C. Várilly. *An Introduction to Noncommutative Geometry*. American Mathematical Society, 2006.

[90] T. Virtanen. Monaural sound source separation by nonnegative matrix factorization with temporal continuity and sparseness criteria. *Audio, Speech, and Language Processing, IEEE Transactions on*, 15(3):1066–1074, 2007.

[91] M.L. Wachs. Poset topology: tools and applications. *Geometric combinatorics, IAS/Park City Math. Ser*, 13:497–615, 2007.

[92] G. Walschap. *Metric Structures in Differential Geometry*. Springer, 2004.

[93] D.P. Williams. *Crossed products of C*-algebras*, volume 134. Amer Mathematical Society, 2007.

[94] H. Zha and Z. Zhang. Continuum Isomap for manifold learnings. *Computational Statistics and Data Analysis*, 52(1):184–200, 2007.

[95] A. Zomorodian and G. Carlsson. Computing persistent homology. In *Proc. 20th Ann. ACM Sympos. Comput. Geom.*, pages 347–356, 2004.

[96] A. Zomorodian and G. Carlsson. Computing persistent homology. *Discrete Comput. Geom.*, 33(2):249–274, 2005.

Zusammenfassung

In dieser Arbeit werden Dateien aus der Signalanalyse unter geometrischen Aspekten bezüglich Dimensionsreduktion und "Manifold Learning" studiert. Signale und Messungen sind grundlegende Instrumente für die Untersuchung von Interaktionen komplexer Phänomene. Ein Beispiel ist ein polyphones Audiosignal $f = \sum_\ell f_\ell$ bestehend aus verschiedenen sich überlegenden Sounds f_ℓ. Die Extraktion des Komponenten f_ℓ aus f kann unter realistische Bedingungen sehr kompliziert sein, und moderne Methoden aus der harmonischen Analysis wie etwa Wavelet oder Frame-Theorie sind oft nicht ausreichend. In diesen Projekt bearbeiten wir dieses Problem mithilfe einer bestimmter Kombination von Zeit-Frequenz-Analyse und modernen Entwicklungen in Geometrie und Computational Topology.

CV December 2011

- **Name:** Mijail Antonio Guillemard
- **Birth:** November 17, 1971, Moscow, Russia
- **Citizenship:** Costa Rican and French
- **Languages:** English, French (native), German, Spanish (native)

- **Education:**

Mathematics PhD. Sep 2008 - Nov 2011, Universität Hamburg.
Mathematics Diplom. Oct 2005 - June 2008, Universität Hamburg.
Mathematics Bach. Mar 1989 - Mar 1994, Universidad de Costa Rica.
Primary/Secondary: 1978-1988, Lycée Franco Costaricien, Costa Rica.

- **Work Experience:**

11/2011-present	Postdoc, Technische Universität Berlin
09/2008-09/2011	Research Assistant (DFG), University of Hamburg
11/2004-10/2010	Research Assistant, Helmut Schmidt University Hamburg
03/2001-09/2004	Programmer/Researcher, TC-Works Hamburg, TC-Electronic Denmark
10/1999-02/2001	Programmer/Researcher, Absolute Software GmbH Hamburg
06/1999-09/1999	Programmer, Dcon Software & Service GmbH Hamburg
1997-1998	Programmer/Researcher, IICA Institute, Costa Rica
1996	Researcher, Environmental Studies Program, Univ. de Costa Rica
1995-1998	Mathematics Instructor, University of Costa Rica
1994	Mathematics Instructor, Universidad Estatal a Distancia, Costa Rica
1989-1993	Mathematics Assistant, Universidad de Costa Rica